DECIPHERING AXL-DRIVEN MOLECULAR MECHANISMS OF EMT

APPROVED BY SUPERVISORY COMMITTEE

Rolf Brekken, PhD

Melanie Cobb, PhD

Ganesh Raj, MD PhD

James Kim, MD PhD

ACKNOWLEDGEMENTS

I would like to thank my parents for fostering my love of knowledge from the very beginning and trusting my crazy life decisions. Without your unwavering support I wouldn't have a shot at being here today. Thank you to Jonathan for always pushing me to be my very best and always being willing to provide anything and everything I need to be successful. Thank you for choosing this hectic and rewarding life with me. I would also like to thank the Brekken Lab for their thoughtful discussion and input. My dissertation is truly a collaboration of many great minds. Finally, I want to thank my mentor Dr. Brekken. You pushed me, guided me, challenged me, and made me the scientist I am today.

DECIPHERING AXL-DRIVEN MOLECULAR MECHANISMS OF EMT

by

EMILY NICOLE ARNER

DISSERTATION

Presented to the Faculty of the Graduate School of Biomedical Sciences

The University of Texas Southwestern Medical Center at Dallas

In Partial Fulfillment of the Requirements

For the Degree of

DOCTOR OF PHILOSOPHY

The University of Texas Southwestern Medical Center at Dallas

Dallas, Texas

December 2021

DECIPHERING AXL-DRIVEN MOLECULAR MECHANISMS OF EMT

Publication No. _____

Emily N Arner, PhD

The University of Texas Southwestern Medical Center at Dallas, 2021

Supervising Professor: Rolf Brekken, PhD

Cellular plasticity, a feature associated with epithelial-to-mesenchymal transition (EMT), contributes to tumor cell survival, migration, invasion, and therapy resistance. Across human cancer, tumors that are high grade, poorly differentiated, and have undergone EMT carry a worse prognosis with a high likelihood of metastasis and poor outcome. AXL, a receptor tyrosine kinase (RTK), drives EMT and is implicated in tumor progression, metastasis, and therapy resistance in multiple cancer types including pancreatic cancer (PDA) and breast cancer. We investigated the contribution of TANK-binding kinase 1 (TBK1) to PDA progression and report that TBK1 supports the growth and metastasis of KRAS-mutant PDA by driving an epithelial plasticity program in tumor cells that enhances invasive and metastatic capacity. We identified that the receptor tyrosine kinase AXL induces TBK1 activity in a Ras-RalB-dependent manner. Furthermore, we report that AXL activation stimulates TBK1 binding and phosphorylation of the specific AKT isoform, AKT3 at S472. Activation of AKT3 drives the binding of AKT3 to slug/snail, where the complex is translocated into the nucleus. The binding of AKT3 to slug/snail protects the EMT-TFs from proteasomal degradation thus leading to an increase in EMT. These data suggest that the

translocation of AKT3 to the nucleus is required for AXL-driven EMT and metastasis. Congruently, nuclear AKT3 expression correlates with worse outcome in aggressive breast. These results suggest that selective AKT3 targeting represents a novel therapeutic avenue for treating aggressive cancer that may avoid toxicity associated with pan-AKT inhibition. Additionally, our findings suggest that interruption of the AXL-TBK1-AKT3 cascade, has potential therapeutic efficacy in AXL positive metastatic cancer.

TABLE OF CONTENTS

PRIOR PUBLICATIONS

Nie M, **Arner E**, Prudden J, Schaffer L, Head S, Boddy MN (2016) Functional Crosstalk between the PP2A and SUMO Pathways Revealed by Analysis of STUbL Suppressor, *razor 1-1*. **PLoS Genet** 12(7): e1006165. doi:10.1371/journal.pgen.1006165

Cruz VH, **Arner EN**, Wynne KW, Scherer PE, Brekken RA (2018). Loss of Tbk1 kinase activity protects mice from diet-induced metabolic dysfunction. **Molecular Metabolism**, ISSN 2212-8778, doi:10.1016/j.molmet.2018.06.007.

Arner EN*, Cruz VH*, Du W, Bremauntz AE, Brekken RA (2019). AXL-mediated activation of TBK1 drives epithelial plasticity in pancreatic cancer. **JCI Insight,** 5. doi:10.1172/jci.insight.126117

Zhu D, Huang H, Pinkas D, Luo J, Ganguly D, Fox A, **Arner EN**, Tu ZC, Bullock A, Brekken RA, Ding K, Lu X (2019). Novel 2-Amino-2, 3-Dihydro-1H-Indene-5-Carboxamide-Based Discoidin Domain Receptors 1 (DDR1) Inhibitors: Design, Synthesis, and In Vivo Anti-pancreatic Cancer Efficacy. **Journal of Medicinal Chemistry**, doi: 10.1021/acs.jmedchem.9b00365.

Arner EN, Du W, Brekken RA (2019). Behind the Wheel of Epithelial Plasticity in KRAS Driven Cancers. **Frontiers in Oncology,** doi: 10.3389/fonc.2019.01049.

Arner EN*, Zhang Y*, Toombs JE, Huang H, Warner SL, Foulks JM, Brekken RA. AXL inhibitor TP-0903 reduces metastasis and therapy resistance in pancreatic cancer. **Accepted, Molecular Cancer Therapeutics**.

Arner EN, Tiron C, Hinz S, Phinney N, Westcott JM, Toombs JE, Gausdal G, Loren JB, Brekken RA. AXL-driven nuclear AKT3 stabilizes Snail/Slug to drive metastasis. **In review**.

LIST OF FIGURES

LIST OF TABLES

LIST OF DEFINITIONS

2D – two-dimensional

3D – three-dimensional

ADM – acinar-to-ductal metaplasia

AKT3i – AKT3 inhibitor

ATP – adenosine triphosphate

B-cat – β-Catenin

BGB324 – Bemcentinib

bHLH – basic helix-loop-helix

bp – base pair

BRCA – invasive breast carcinoma

BSA – bovine serum albumin

CHX – cycloheximide

CIN – chromosomal instability

CK19 – cytokeratin-19

CO_2 – carbon dioxide

DAB – 3,3'-Diaminobenzidine

DAPI – 4′,6-diamidino-2-phenylindole

DE – differentially expressed

DMEM – Gibco Dulbecco's Modified Eagle Medium

DMSO – dimethyl sulfoxide

DNA – deoxyribonucleic acid

ECM – extracellular matrix

EDTA – Ethylenediaminetetraacetic acid

EGA – European Genome-phenome Archive

EGF – epidermal growth factor

EGFR – epidermal growth factor receptor

EMT – epithelial-to-mesenchymal transition

ENT1 – equilibrative nucleoside transporter 1

ERα – estrogen receptor α

ERVs – endogenous retroviruses

EV – empty vector

FBS – fetal bovine serum

FC – flow cytometry

GAS6 – growth arrest-specific gene 6

GDP – Guanosine diphosphate

GEMMs – genetically engineered mouse models

GEO – gene expression profiling interactive analysis

GEPIA – gene expression profiling interactive analysis

GFP – green fluorescent protein

GTP – Guanosine-5'-triphosphate

H&E – Hematoxylin and eosin stain

HBP – hexosamine biosynthetic pathway

HCL – hydrochloric acid

HEPES – 4-(2-hydroxyethyl)-1-piperazineethanesulfonic acid

HGF – hepatocyte growth factor

HIF-1α – hypoxia-inducible factor 1α

HK1 – hexokinase 1

HK2 – hexokinase 2

HMECs – human mammary epithelial cells

HR – hazard ratio

HRP – horseradish peroxidase

IB – immune blot

IGF1 – insulin-like growth factor 1

IHC – immunohistochemistry

IRF3/7 – interferon regulatory factor 3/7

IV – intravenously

KIC – $Kras^{LSL\text{-}G12D}/+$; $Cdkn2a^{Lox/Lox}$; $Ptf1a^{Cre/+}$

KO – knock-out

KPC – $Kras^{LSL\text{-}G12D/+}$; LSL-$Trp53^{LSL\text{-}R172H/+}$; $Ptf1a^{Cre/+}$

KPfC – $KRAS^{LSLG12D/+}$; $Trp53^{Lox/Lox}$; $Pdx1^{Cre/+}$

LDHA – lactate dehydrogenase A

MAPKs – mitogen-activated protein kinases

MET – mesenchymal-to-epithelial transition

miRNA – micro-ribonucleic acid

MMP – matrix metallopeptidase

mRNA – messenger ribonucleic acid

MUT – mutant

myrAKT1 – myristoylated AKT1

myrAKT3 – myristoylated AKT3

NLS – nuclear localization sequence

NSCLC – non-small cell lung cancer

NSG – NOD SCID gamma

O-GlcNAcylation – O-linked N-acetylglucosamine

PanIN – pancreatic intraepithelial neoplasia

PBS – phosphate buffered saline

PCR – polymerase chain reaction

PDAC/ PDA/ PAAD – pancreatic ductal adenocarcinoma

PDGF – platelet-derived growth factor

PEI – polyethyleneimine

Pen/strep – Penicillin Streptomycin

PFK-1 – Phosphofructokinase 1

PI3K – phosphatidylinositol 3-kinase

pS – phospho-serine

PTM – post-translational modification

qPCR – quantitative polymerase chain reaction

RFP – red fluorescent protein

RIPA – Radioimmunoprecipitation assay

RTK – receptor tyrosine kinase

RNA – ribonucleic acid

SD – standard deviation

SDS-PAGE – sodium dodecyl sulphate–polyacrylamide gel electrophoresis

SEM – standard error of the mean

SFM – serum free media

Shh – sonic hedgehog

shRNA – short-hairpin ribonucleic acid

SI – staining index

siRNA – small interfering ribonucleic acid

tAKT – total AKT

TAM – Tyro3, AXL, MerTK

TBK1 – TANK-binding kinase 1

TBK1i – TBK1 inhibitor

TBS – tris buffered saline

TCGA – The Cancer Genome Atlas

TFs – transcription factors

TGFβ – transforming growth factor β

TIMP3 – tissue inhibitor of metalloproteinase 3

TNBC – triple negative breast carcinoma

TRITC – Tetramethyl rhodamine

UTR – untranslated region

VEGF – vascular endothelial growth factor

WT – wildtype

CHAPTER ONE
Introduction

BEHIND THE WHEEL OF EPITHELIAL PLASTICITY

Epithelial plasticity or an epithelial-to-mesenchymal transition (EMT) is a key cellular program that can be activated by KRAS. EMT contributes to tumor progression by enhancing tumor cell survival and therapy resistance and by facilitating success in the metastatic cascade. In this review, we will introduce cellular plasticity and its effect on cancer progression and therapy resistance and then summarize drivers of EMT with an emphasis on KRAS signaling. Lastly, we will discuss the contribution of cellular plasticity to metastasis and its potential clinical implications.

Cellular Plasticity and EMT

Cellular plasticity serves as a mechanism of tissue adaptation and regeneration in normal tissues and can also predispose tissue to cancer transformation (Yuan et al., 2019). In the pancreas, pancreatic epithelial and acinar cells display robust plasticity, enabling adaptation to metabolic and environmental stress. In pancreatic cancer, tumor cells alter their phenotype as a result of exposure to diverse metabolic conditions, signaling molecules, stromal elements, and therapeutic agents. This plastic state in tumor cells can facilitate tumor progression, including metastasis, chemoresistance, and immune evasion (Yuan et al., 2019).

Acinar-to-ductal metaplasia (ADM) (Reichert & Rustgi, 2011), describes a process where normal pancreatic acinar cells assume a duct-like state in the setting of chronic injury, such as pancreatitis. When pancreatitis resolves in normal/nonmalignant pancreatic tissue, ADM lesions revert to acinar morphology. However, if KRAS-transformed acinar cells are subjected to the stress of pancreatitis, precancerous pancreatic intraepithelial neoplasia often forms (De La et al., 2008; Grippo, Nowlin, Demeure, Longnecker, & Sandgren, 2003; Kopp et al., 2012; Strobel et al., 2007; Yamaguchi, Yokoyama, Kokuryo, Ebata, & Nagino, 2018). This suggests that pancreatic ductal adenocarcinomas (PDACs) may arise from acinar cells that have undergone transdifferentiation to a duct-like state. Normal pancreatic cells are sensitive to the transforming effects of mutant *KRAS* and the loss of phosphatase and tensin homolog (Kopp et al., 2018), indicating that the likelihood of tumor formation and eventual histologic tumor type depends on the specific drivers that are present as well as the cellular compartments in which they are expressed (Fan et al., 2012; Guest et al., 2014; M. A. Hill et al., 2018; Ikenoue et al., 2016; Sekiya & Suzuki, 2012).

EMT is another example of cellular plasticity program that is used by cells and tissues to adapt to cues or cellular stress. EMT classically defined is a developmental program that is instrumental in early embryo patterning during gastrulation (T. Brabletz, Kalluri, Nieto, & Weinberg, 2018; Thiery, Acloque, Huang, & Nieto, 2009) and is characterized by epithelial cells losing cell-to-cell adhesion, epithelial tight junctions and desmosomes. These changes are thought to occur through coordinated genetic reprogramming induced by EMT-transcription factors (EMT-TFs) that are activated in response to extracellular cues (Thiery et

al., 2009). These cues include growth factors such as transforming growth factor-β (TGF-β), epidermal growth factor (EGF), hepatocyte growth factor (HGF), and insulin-like growth factor 1 (IGF1) (Bryant, Wylie, & Stow, 2005; Kamei et al., 1999; Perrais, Chen, Perez-Moreno, & Gumbiner, 2007; Qian, Karpova, Sheppard, McNally, & Lowy, 2004; Thiery et al., 2009). This essential developmental program can be hijacked during tumorigenesis to promote increased cell migration and survival.

EMT in tumor cells can also be induced by cellular stress such as inflammation or nutrient/oxygen deprivation (Z. Wang et al., 2011), and transforming oncogenes including oncogenic *KRAS* (Shao et al., 2014; Singh et al., 2009). The genetic reprogramming associated with EMT in normal tissue or cancer leads to a shift from an epithelial to a mesenchymal phenotype. Epithelial cells often have polygonal shapes in monolayer culture, are polarized along their apical-basal axis and are tightly joined to one another laterally through adherens junctions. In contrast, mesenchymal cells exhibit spindle-like morphology and are loosely attached to the surrounding stroma through focal adhesions, which contributes to increased motility and invasive behavior (Ye & Weinberg, 2015) **(Figure 1)**.

In epithelial tumors, the manifestation of an EMT program is associated with tumor grade. High-grade cancer is aggressive and characterized by a loss of normal tissue structure and architecture. High-grade tumors are often described as poorly differentiated and mesenchymal, displaying tumor cells that have undergone EMT. In contrast, low-grade tumors are characterized as well-differentiated cancers that retain an epithelial phenotype.

Across human cancer, tumors that are high grade and poorly differentiated carry a worse prognosis with a high likelihood of metastasizing to distant organs (Yuan et al., 2019).

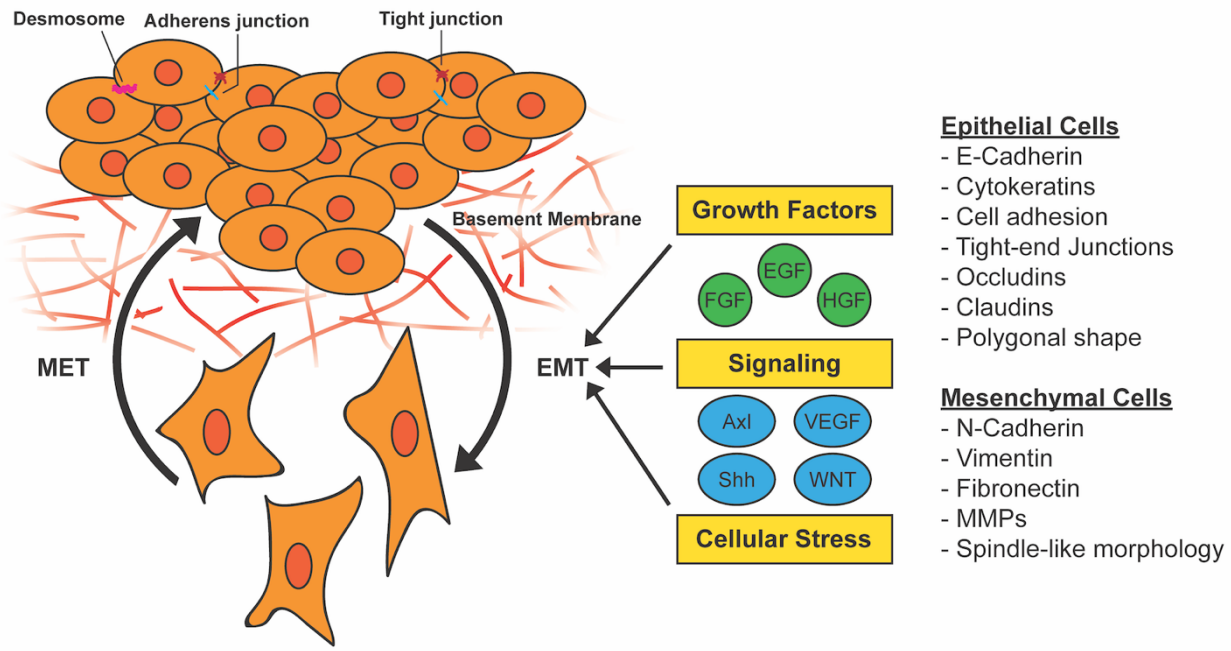

Figure 1. Activation of epithelial-to-mesenchymal transition (EMT). During EMT, epithelial cells lose their cell-to-cell adhesion and adopt a more spindle-like morphology due to the expression of mesenchymal markers. This morphology change results in the ability to escape the basement membrane and invade and survive stressful situations, including therapy. EMT can be induced by a variety of growth factors, signaling pathways, and cellular stress such as hypoxia and nutrient deprivation. Abbreviations: MET, mesenchymal-to-epithelial transition; MMP, matrix metallopeptidase.

EMT is a common feature associated with tumor progression and is thought to be critical to cancer cell dissemination in some tumors (Gaianigo, Melisi, & Carbone, 2017; Puls, Tan, Whittington, & Voytik-Harbin, 2017; S. Wang, Huang, & Sun, 2017). The metastasis of epithelial tumors, such as PDAC, requires the cancer cells to escape epithelial nests, invade

surrounding stroma, intravasate into blood or lymphatic vessels, survive circulation, and extravasate at the secondary site, where successful cells form micrometastases and eventually macrometastases (Seyfried & Huysentruyt, 2013). The escape of tumor cells from tumor cell nests encapsulated by a basement membrane can be facilitated by tumor cell epithelial plasticity, which results in epithelial tumor cells losing contact with the basement membrane and nearby cells while adopting mesenchymal-like features that enable cell migration and invasion. This is a common feature in mouse models of PDAC (Aiello et al., 2018; Mueller et al., 2018; Rhim et al., 2012). While epithelial plasticity alters morphology and cell-cell contact it also enhances tumor cell survival under stressful environmental conditions, such as chemotherapy and radiation (Cates et al., 2009; Kudo-Saito, Shirako, Takeuchi, & Kawakami, 2009; Larue & Bellacosa, 2005; Puls et al., 2017). EMT and metastasis are generally considered to be late events in tumorigenesis; however, EMT and the metastatic cascade has been shown to occur even in "preinvasive" stages of PDAC (Rhim et al., 2012). Thus the concept that EMT is driven by the oncogenotype of a tumor is worthy of consideration.

EMT and Therapy Resistance

Epithelial plasticity is a key chemoresistance and immune surveillance evasion strategy exploited by tumor cells (Dongre et al., 2017; Voon, Huang, Jackson, & Thiery, 2017). Plastic tumor cells exhibit increased rates of resistance to therapy including radio-, chemo-, targeted and immunotherapy (Cates et al., 2009; Creighton et al., 2009; Kudo-Saito et al., 2009; Ludwig et al., 2018; Singh & Settleman, 2010). Stress, such as inflammation,

nutrient/oxygen deprivation, and therapy can induce epithelial plasticity in cancer cells (Z. Wang et al., 2011). A common consequence of EMT is reduced drug uptake by tumor cells. For example, the expression of equilibrative nucleoside transporter 1 (ENT1), which can transport nucleoside analog chemotherapy into cells, is often reduced in tumor cells that have undergone EMT. However, tumors engineered to lack EMT transcription factors (EMT-TFs), such as Snail and Twist, showed elevated ENT1 expression and increased sensitivity to gemcitabine, a nucleoside analog (Zheng et al., 2015). Consistent with these results, Ludwig et al. (Ludwig et al., 2018) found that inhibition of AXL reduced epithelial plasticity in models of PDAC, increased ENT1 expression and enhanced sensitivity to gemcitabine when compared to gemcitabine alone or control treated animals. To combat chemoresistance in cancer patients, intermittent dosing or "drug holidays" have been suggested, although recent studies have revealed that resistance driven by oncogenic KRAS is not reversible (Sale et al., 2019). However, in human cancer cell lines, therapy resistance driven by mutant *KRAS* was found to irreversibly drive ZEB1-dependent EMT and chemoresistance through the hyperactivation of ERK1/2 (Sale et al., 2019), arguing against the use of intermittent dosing in tumors driven by oncogenic KRAS. Fischer et al., (Fischer et al., 2015) showed in a spontaneous breast-to-lung metastasis model that EMT contributes to chemotherapy resistance, as mesenchymal-like tumor cells survived cyclophosphamide treatment, demonstrating reduced proliferation, apoptotic tolerance, and increased expression of chemoresistance-related genes. These observations highlight the potential increase in therapeutic efficacy that might result from combining standard therapy with strategies to combat epithelial plasticity.

The hypoxic state of pancreatic tumors increases tumor cell migration and chemoresistance (Yuen & Diaz, 2014). In fact, EMT can be driven by hypoxia often via the induction of TGFβ (Aguilera et al., 2014). Additionally, in human pancreatic cancer cell lines, hypoxia has been shown to drive EMT in an NFκB dependent manner through the stability of hypoxia-inducible factor 1α (HIF-1α) and subsequent activation of RelA (p65) (Cheng et al., 2011; Z. X. Cheng et al., 2014; X. Zhao et al., 2014; G. H. Zhu, Huang, Feng, Lv, & Qiu, 2013), a subunit of the NFκB family of transcription factors (Hoesel & Schmid, 2013; Ryseck, Weih, Carrasco, & Bravo, 1996). NFκB is considered a crucial component of drug resistance in mutant KRAS driven tumors such as pancreatic cancer and colorectal cancer, which typically expresses high levels of the protein (Karin, 2006). The activation of NFκB has been shown to upregulate anti-apoptosis proteins such as Bcl-XL and Bcl-2, promoting chemoresistance (Greten et al., 2002; Li et al., 2016). As such, NFκB inhibition might be an approach to combat chemoresistance in tumors with KRAS-driven EMT.

Resistance to targeted therapy has also been associated with a mesenchymal state. In non-small cell lung cancer (NSCLC), the expression of an EMT gene signature, which included AXL expression, was associated with resistance to treatment with epidermal growth factor receptor (EGFR) and phosphatidylinositol 3-kinase (PI3K) inhibitors (Byers et al., 2013; Farmer et al., 2009; Sequist et al., 2011; F. Wu, Li, Jang, Wang, & Xiong, 2014; Zhang et al., 2012). Similarly, in vitro studies suggested that epithelial NSCLC cell lines are more sensitive to EGFR inhibitors than mesenchymal cell lines (Collisson et al., 2011), and that when AXL is inhibited, sensitivity to EGFR inhibitors is increased (Brand et al., 2015; Choi

et al., 2015). In breast cancer patients, the EMT program also serves as a major driver of drug resistance, disease occurrence, and systemic dissemination (Q. Cheng et al., 2014; Creighton et al., 2009; Oliveras-Ferraros et al., 2012).

In addition to targeted and chemotherapy, EMT has been associated with resistance to immunotherapy (Terry et al., 2017). In murine melanoma cells, Snail, a canonical EMT-TF, was found to be necessary and sufficient for resistance to cytotoxic T-cell–mediated killing via the induction of regulatory T cells. The effect was driven by immunosuppressive $CD11c^{+}$ dendritic cells, which were generated in response to Snail-expressing melanoma cells (Kudo-Saito et al., 2009). Similarly, immune therapy-resistant melanomas display a mesenchymal gene signature, including the downregulation of E-cadherin and upregulation of factors involved in extracellular matrix (ECM) remodeling, angiogenesis, and wound healing (Hugo et al., 2016). Additionally, the immune system is a key component of chemotherapy responses, as many chemotherapeutic agents directly affect the immune landscape of tumors (Galluzzi, Buque, Kepp, Zitvogel, & Kroemer, 2015). Therefore, identification of key signaling pathways involved in epithelial plasticity could reveal overlap with tumor immune evasion and new therapeutic targets, inhibition of which increases the efficacy of chemo- and immunotherapy.

EMT and Tumor Metabolism

Metabolic alterations are associated with mutant KRAS-induced EMT. Cancer cells often increase glycolytic flux to meet the high energy demand to support rapid cell growth and

division (F. Wang et al., 2018). In contrast to normal cells that typically generate energy via the breakdown of pyruvate, cancer cells generate energy by the nonoxidative breakdown of glucose with tumor cells displaying glycolytic rates up to 200 times higher than normal cells in the body (Alfarouk, 2016). This preferential activation of glycolysis for energy supply is referred to as the "Warburg Effect" (Alfarouk, 2016). In pre-clinical models as well as human patient samples, oncogenic Kras signaling can transcriptionally upregulate the glucose transporter GLUT1, as well as multiple enzymes in the glycolytic pathway (e.g., Hexokinase1 (HK1), Hexokinase2 (HK2), Phosphofructokinase1 (PFK-1), and Lactate dehydrogenase A (LDHA)) (Biancur & Kimmelman, 2018; Halbrook & Lyssiotis, 2017; F. Wang et al., 2018). Hypoxia, a common environmental condition in solid tumors, triggers O-linked N-acetylglucosamine (O-GlcNAcylation) at S529 of PFK-1, inducing glycolysis and giving a selective growth advantage to the cancer cells (Gomez et al., 2013; Yi et al., 2012). Cancer induced HIF-1α and MUC1 have also been shown to upregulate the expression of key glucose transporters and glycolytic enzymes, including GLUT1 and aldolase A, which leads to increased glucose uptake and glycolysis (Halbrook & Lyssiotis, 2017; Vaziri-Gohar, Zarei, Brody, & Winter, 2018; F. Wang et al., 2018). In addition to glycolysis, recent evidence suggests oncogenic KRAS drives glucose into the hexosamine biosynthetic pathway (HBP), which is required for multiple glycosylation events (Bond & Hanover, 2015; Hanover, Krause, & Love, 2012). Taparra et al. (Taparra et al., 2018), recently showed in models of lung tumorigenesis, that KRAS and the EMT program coordinated elevated expression of key enzymes within the HBP pathway. Additionally, they showed that elevated O-GlcNAcylation of intracellular proteins such as the EMT-TF Snail

results in suppressed oncogenic-induced senescence and accelerated lung tumorigenesis (Taparra et al., 2018). Understanding the evident metabolic changes driven by oncogenic KRAS and reinforced by epithelial plasticity may reveal novel therapeutic targets for KRAS-driven tumorigenesis.

Drivers of EMT

A variety of stimuli can induce EMT, including soluble factors, ECM components, environmental conditions, and oncogenic transcriptional programs (Lamouille, Xu, & Derynck, 2014). These stimuli, which include signaling factors such as TGFβ, Wnt, Notch, and Sonic hedgehog (Shh), as well as growth factors such as EGF and platelet-derived growth factor (PDGF) and vascular endothelial growth factor (VEGF), serve as ligands for the signaling pathways they activate **(Figure 1)**. EMT programs can also be activated in response to several paracrine signals in parallel (Thiery et al., 2009). These networks activate signal cascades and intermediates that include mitogen-activated protein kinases (MAPKs), PI3K, AKT, Smads, RhoB, c-Fos, and RAS (Tse & Kalluri, 2007), which then regulate EMT-TFs. RTKs are common initiation sites for signaling that induces EMT-TF activity.

AXL

AXL is an archetypal receptor tyrosine kinase (RTK) associated with EMT (Gjerdrum et al., 2010; Kirane et al., 2015; Koorstra et al., 2009) and with worse outcomes in multiple tumor types (Koorstra et al., 2009; Leconet et al., 2014; Song et al., 2011; Zhang et al., 2012). Consistent with poor outcomes, AXL expression also is associated with metastasis and resistance to therapy (Kirane et al., 2015; Ludwig et al., 2018). AXL is a member of the

TAM (Tyro3, AXL, MerTK) family of RTKs (Du & Brekken, 2018). Its ligand, growth arrest-specific gene 6 (GAS6) induces AXL signaling by stimulating the auto-phosphorylation of several tyrosine residues of AXL, which function as docking sites for multiple substrates including PI3K, phospholipase C, and c-SRC (Braunger et al., 1997; Weinger et al., 2008). Additionally, AXL can be activated by forming heterodimers with non-TAM family proteins, such as EGFR, PDGFR, or another TAM family member (Zhang et al., 2012). Elevated AXL expression is found in multiple cancer types, including lung, breast, ovarian, gastric, colon, pancreatic, and prostate (Asiedu et al., 2014; Byers et al., 2013; Del Pozo Martin et al., 2015; Gjerdrum et al., 2010; Koorstra et al., 2009; Song et al., 2011; F. Wu et al., 2014; Zhang et al., 2012). AXL expression is induced by drivers of EMT, for example TGFβ, and is generally associated with markers of EMT including N-cadherin and vimentin (Cruz, Arner, Du, Bremauntz, & Brekken, 2019; H. J. Lee, Jeng, Chen, Chung, & Yuan, 2014).

Our lab and others have shown that AXL expression in RAS-driven cancers, such as PDAC, maintains epithelial plasticity (Kirane et al., 2015). GAS6-AXL signal transduction is required to maintain epithelial-mesenchymal plasticity traits of PDAC (Kirane et al., 2015). When AXL was inhibited in genetically engineered mouse models (GEMMs) of pancreatic cancer, Ludwig et al. (Ludwig et al., 2018) observed an increase of epithelial differentiated tumor cells. In addition to chemotherapy resistance, AXL has been strongly implicated in resistance to targeted therapy such as EGFR and PI3K/AKT inhibitors (Byers et al., 2013; F. Wu et al., 2014).

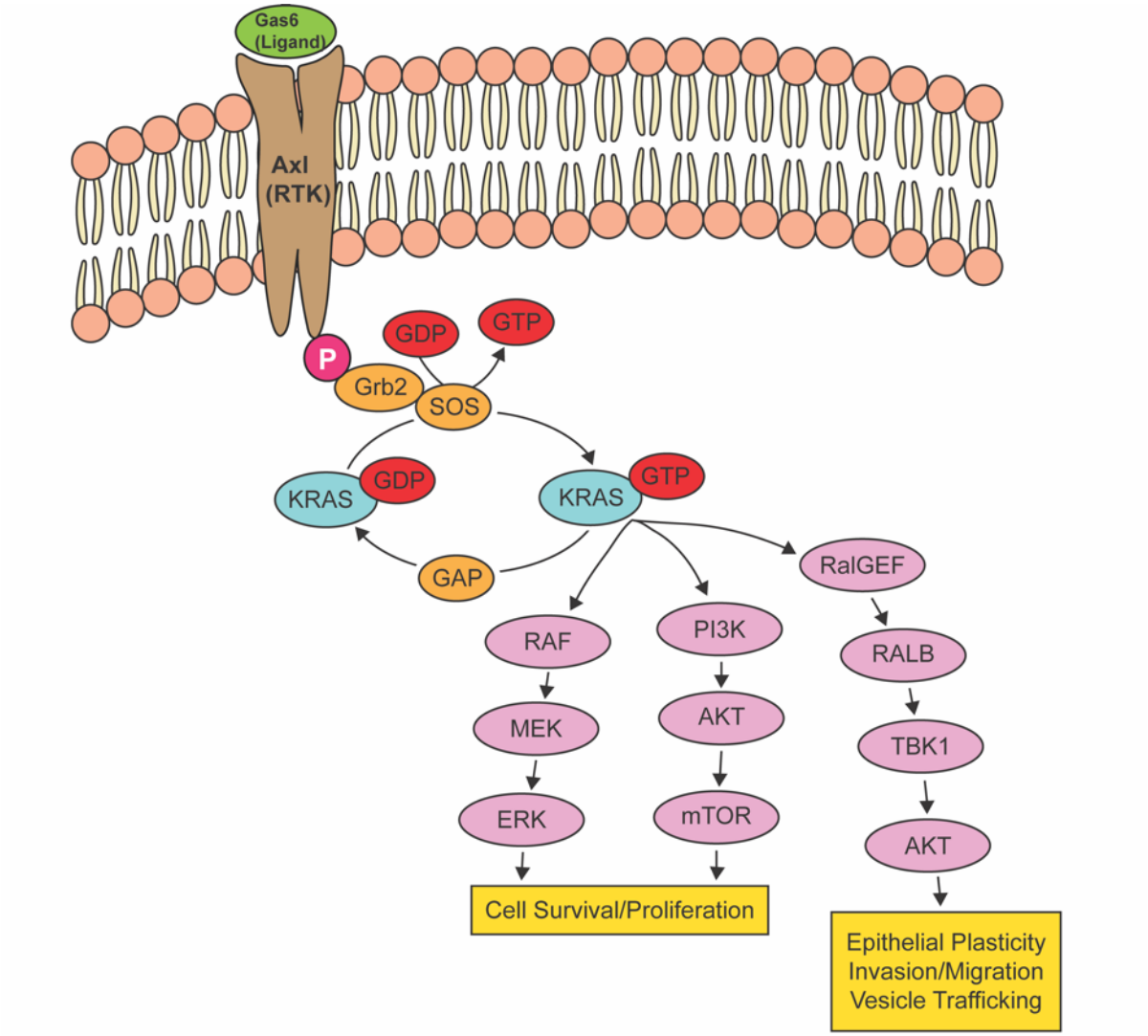

Figure 2. Oncogenic KRAS effector pathways. When a receptor tyrosine kinase (RTK) is activated by its ligand, KRAS binds to GTP, rendering it active until the GTP hydrolyzes to GDP, turning KRAS off. When KRAS is mutated, KRAS remains bound to GTP, leading to the overstimulation of KRAS signaling pathways, resulting in cell survival and proliferation, epithelial plasticity, and migration. The activation of RTK AXL by GAS6 is shown as a potential signaling pathway that can drive an epithelial-to-mesenchymal transition via the activation of KRAS.

RAS genes (HRAS, KRAS, and NRAS) are the most frequently mutated gene family in cancer (Prior, Lewis, & Mattos, 2012). Of these, KRAS is the most mutated (86% of all RAS-mutant cancers), followed by NRAS (12%), and HRAS (4%) (Cox, Fesik, Kimmelman, Luo, & Der, 2014). KRAS mutations are frequent in PDAC, lung, and colorectal cancers, and also occur in other cancers such as multiple myeloma (Cerami et al., 2012; Haigis, 2017).

KRAS, a small GTPase, functions as a molecular switch, cycling between an active guanosine triphosphate (GTP)-bound and inactive guanosine diphosphate (GDP)-bound states (Vigil, Cherfils, Rossman, & Der, 2010). In non-transformed cells, RAS is typically GDP-bound and inactive, but upon activation of RTKs, there is a rapid activation of RAS-GTP, leading to the activation of intracellular signaling networks that promote growth, proliferation, and migration (Cox & Der, 2010) **(Figure 2)**. Because KRAS-activating mutations cluster around the nucleotide-binding pocket (Haigis, 2017), these mutations cause RAS to be persistently GTP-bound and constitutively active, resulting in the hyperactivation of signaling networks to drive cancer growth and progression (Waters & Der, 2018).

Multiple RTKs, including AXL and EGFR, can activate KRAS (Krebs et al., 2017). Signaling networks downstream of RAS such as ERK/MAPK and PI3K/AKT can mediate mutant Ras-induced EMT, such that the inhibition of MEK1 or AKT (Janda et al., 2002) can reverse RAS-stimulated epithelial plasticity. Genovese et al. (Genovese et al., 2017) completed a gene set enrichment analysis of highly metastatic and poorly metastatic clonal cells lines isolated from a GEMM of PDAC, i.e., KPfC mice ($KRAS^{LSLG12D/+}$; $Trp53^{Lox/Lox}$;

Pdx1$^{Cre/+}$). Their analysis revealed that “metastasis-low” clones exhibited a downregulating of KRAS signature genes, whereas “metastasis-high” clones exhibited a higher expression of KRAS signature genes (Genovese et al., 2017). After validation through in vivo lineage tracing, their study demonstrated that in PDAC, cells reside in a spectrum of epithelial-mesenchymal states where mesenchymal cells activate KRAS signaling at a higher level.

Other genome-sequencing studies revealed genetic heterogeneity beyond a few frequently mutated drivers in human PDAC (Bailey et al., 2016; Biankin et al., 2012; Campbell et al., 2010; Jones et al., 2008; Makohon-Moore et al., 2017; Waddell et al., 2015; Witkiewicz et al., 2015). The heterogeneity in genomic changes makes it challenging to link definitive genomic alterations to biological, morphological, or clinical phenotypes (Campbell et al., 2010; Makohon-Moore et al., 2017). Despite these challenges, Mueller et al. (Mueller et al., 2018), found that the gene dosage of KRAS G12D in human and mouse PDAC correlated with a markedly increased metastatic potential and a mesenchymal phenotype. These results link the aggressive mesenchymal PDAC subtype with the highest dosage of mutant KRAS and Ras-related transcriptional programs. Additionally, oncogenic Ras is closely associated with resistance to drug therapy and pathways that drive PDAC initiation, progression, and metastasis.

TBK1

Although the majority of RAS effector-targeted therapies inhibit the RAF and PI3K signaling networks, the RALGEF pathway encompassing RALA and RALB GTPases are more consistently activated than RAF or PI3K in human PDAC (Lim et al., 2006; Neel et al.,

2011). Additionally, it has been demonstrated in human cell lines that RALGTPase activation is an essential component of RAS-induced transformation in a large spectrum of human epithelial cells and that RALGTPase activation alone is sufficient to induce a tumorigenic phenotype in some settings (Hamad et al., 2002; Rangarajan, Hong, Gifford, & Weinberg, 2004). Given that RAS signaling is a driver of epithelial plasticity and that the RALGEF pathway is a critical effector of RAS, investigating RALGEF signaling has the potential to reveal novel targets involved in epithelial plasticity, metastasis, and therapy resistance in *RAS*-mutant tumors.

The serine/threonine protein kinase TANK-binding kinase 1 (TBK1) is an atypical Ikk kinase, that together with its homologue, IKKε, contributes to innate immunity by activating interferon regulatory factor 3/7 (IRF3/7) thereby inducing type 1 interferon gene expression in response to pathogen exposure (Perry, Chow, Goodnough, Yeh, & Cheng, 2004; Sharma et al., 2003). Additionally, TBK1 kinase activity supports cell growth, self-renewal, pathogen clearance, and organelle function (Chien et al., 2006; Ou et al., 2011; Radtke, Delbridge, Balachandran, Barber, & O'Riordan, 2007; Wild et al., 2011). TBK1 is a major constituent of the RAL pathway and is crucial to the development of RAS-driven cancers (Barbie et al., 2009; Canadas et al., 2018; Cruz et al., 2019; Ou et al., 2011). Additionally, TBK1 has been linked to the survival of mutant KRAS-expressing cells (Chien et al., 2006) and can directly activate AKT (Ou et al., 2011). The critical contribution of RALB and TBK1 to RAS-induced lung cancer growth was confirmed in an RNA inhibitor screen of synthetic lethal partners of oncogenic KRAS, where RALB and TBK1 were identified as top targets (Barbie

et al., 2009). Further, Cooper et al. (Cooper et al., 2017) screened 100 NSCLC lines for sensitivity to TBK1 inhibitors Bx795 and compound II to tease out biological features of TBK1-dependent cell lines. Sensitivity profiles correlated strongly with the profiles of multiple AKT/mTOR pathway inhibitors, particularly in mutant *KRAS* NSCLC lines, suggesting a mechanistic interaction between TBK1 and the mTOR pathway (Cooper et al., 2017). Further analysis of TBK1 inhibitor (TBK1i)-sensitive cell lines revealed mutations in RAS family members and a greater mesenchymal gene expression compared to TBK1i-resistant lines that had a more differentiated gene expression profile.

In support of the contribution of TBK1 to RAS-induced EMT, we reported that TBK1 expression is associated with a poor prognosis in pancreatic cancer patients (Cruz & Brekken, 2018). Furthermore, we found that the loss of TBK1 function resulted in reduced invasion, migration, and tumor growth, and reduced metastatic events in preclinical models of mutant *KRAS* PDAC, indicating that TBK1 actively contributes to the highly aggressive behavior of pancreatic cancer (Cruz et al., 2019). In fact, one of the most significant and top dysregulated gene networks between *TBK1* Wildtype (Roberts et al., 1980) and *TBK1*-mutant (MUT) tumors identified by Ingenuity pathway analysis was the cancer/cellular movement networks, including many genes involved in EMT. In comparison with *TBK1* WT tumors, tumors with mutant *TBK1* showed a trend toward higher expression of epithelial markers and lower expression of mesenchymal markers; this trend was confirmed at the protein level (Cruz et al., 2019). Mechanistic studies established that TBK1 promotes EMT downstream of AXL in PDAC, in a RAS-RALB dependent manner (Cruz et al., 2019). Although the precise

mechanism of how TBK1 promotes EMT is unclear, evidence suggests that TBK1 can directly activate AKT (Ou et al., 2011), which has been shown to drive EMT via the induction of Snail and Slug that transcriptionally repress E-cadherin and induce vimentin, Twist1, and matrix metallopeptidases MMP-2 and MMP-9 to promote tumor cell invasion (Grille et al., 2003; Larue & Bellacosa, 2005; Xu, Yang, & Lu, 2015). Further evidence is needed in understanding the interaction between TBK1 and AKT to drive the mesenchymal phenotype in PDAC as well as the identification of additional TBK1 substrates that promote EMT programs.

In contrast, the knockdown of TBK1 in estrogen receptor α-positive (ERα) breast cancer cells reportedly induced EMT and enhanced tumorigenesis and lung metastasis by suppressing ERα expression (K. M. Yang et al., 2013). Further studies are required to investigate if this pathway is dependent on oncogenic RAS. Another group observed that TBK1 is active in mutant *NRAS* melanoma and promoted migration and invasion of these cells (Vu & Aplin, 2014), suggesting that RAS-driven epithelial plasticity may be active in the presence of other RAS isoform-driven cancers. Regardless, these studies suggest that therapies targeting TBK1 could be used to reduce EMT in *Ras*-mutant tumors.

cGAS-STING and innate immunity in EMT

In agreement with the thought that TBK1 loss produces antitumor immunity, studies by the Cantley (Bakhoum et al., 2018) and Barbie (Canadas et al., 2018) groups have reported that immune evasion and metastatic behavior are associated with the cGAS/STING/TBK1 innate

immune pathway in cancer cells (Bakhoum & Cantley, 2018; Bakhoum et al., 2018; Canadas et al., 2018). Canadas et al. (Canadas et al., 2018) revealed that mesenchymal tumor subpopulations with high AXL expression and low histone-lysine N-methyltransferase levels trigger the expression of a specific set of interferon-stimulated antisense endogenous retroviruses (ERVs). These ERVs were present in human cancer cells that produced tumors with hyperactive innate immune signaling, myeloid cell infiltration, and immune checkpoint activation. Therapeutically, this may have important implications for drug combinations with immune checkpoint blockade. In the second study, Bakhoum et al., (Bakhoum et al., 2018) found that chromosomal instability (CIN) of cancer cells, caused by errors in chromosomal segregation during mitosis, promoted cellular invasion and metastasis through the presence of double-stranded DNA in the cytosol. Clustering of single cells via EMT genes accurately classified most cells according to their CIN status and revealed that the CIN-high cells were highly enriched in mesenchymal markers. This CIN-high population also exhibited increased migratory and invasive behavior in vitro, underwent actin cytoskeletal reorganization, and stained positive for mesenchymal markers such as vimentin and β-catenin. Additionally, cells derived from metastases exhibited a higher population of cytoplasmic micronuclei than CIN-low or primary tumor-derived cells, respectively. These studies showed that cytosolic DNA activates the cGAS/STING pathway to mediate EMT, invasion, and metastasis (Bakhoum et al., 2018). Under normal conditions, the cGAS-STING pathway acts as an innate cellular defense mechanism against viral infections. Once STING activates TBK1, TFs such as IRF3 and NF-κB are phosphorylated and translocate to the nucleus (Abe & Barber, 2014), where they mediate the transcription of a myriad of inflammatory genes (Dou et al., 2017; Galluzzi,

Vanpouille-Box, Bakhoum, & Demaria, 2018; Gluck et al., 2017; Takahashi et al., 2018). In human breast and lung cancer-derived cell lines, chronic cGAS-STING activity resulting from chromosome instability has been shown to drive migration, invasion, and metastasis (Bakhoum et al., 2018). Additionally, chromosome instability can lead to increased mutant *KRAS* gene dosage in pancreatic cancer, resulting in a higher expression of EMT gene signatures and increased metastasis (Mueller et al., 2018).

Similar to epithelial plasticity, CIN has been implicated in treatment resistance by generating heterogeneity within the tumor that enhances natural selection, thereby promoting tumor cell survival, immune evasion, drug resistance, and metastasis (G. Chen, Bradford, Seidel, & Li, 2012; Davoli, Uno, Wooten, & Elledge, 2017; Laughney, Elizalde, Genovese, & Bakhoum, 2015; Mueller et al., 2018; Notta et al., 2016; Pavelka et al., 2010; Potapova, Zhu, & Li, 2013). Given the widespread nature of CIN in human cancer, therapies targeting CIN and cGAS/STING have the potential to have an effect on metastatic disease and on minimizing therapy resistance and positively impacting clinical prognosis.

Downstream transcriptional networks of epithelial plasticity

EMT is thought to be regulated largely through changes in the expression of genes necessary for the epithelial state, such as adherens junctions and tight junction components, which are transcriptionally repressed through the activation of EMT TFs including Snail, Twist, and Zeb (Nieto, Huang, Jackson, & Thiery, 2016). These markers of EMT are often associated with poor patient outcomes. As previously mentioned, EMT can be induced by many

signaling factors, such as TGFβ, EGF, FGF, HGF, NOTCH, and Wnt ligands. These factors initiate signaling cascades, leading to the expression of one or more EMT-TFs, which inhibit E-cadherin transcription by binding to E-boxes within the E-cadherin promoter region (Gheldof & Berx, 2013; Wong, Gao, & Chan, 2014).

EMT-TFs are often associated with poor patient outcomes. In resected PDAC, nearly 80% of tumors expressed moderate to strong levels of SNAI1, while only 50% showed SNAI2 expression, and very few expressed TWIST (Hotz et al., 2007). Additionally, ZEB1 expression in pathologic specimens correlated with advanced tumor grade and worse outcomes (Arumugam et al., 2009; Buck et al., 2007). Functions for different EMT-TFs in different cancers have been described: for ZEB1 and ZEB2 in melanoma (Caramel et al., 2013; Denecker et al., 2014), Snail and Slug in breast cancer (Ye et al., 2015), and for Sox4 (Tiwari et al., 2013), and Prrx (Ocana et al., 2012) in PDAC. These functions can be tissue-specific, as demonstrated by the different functions of Snail in the metastasis of breast cancer (H. D. Tran et al., 2014) and PDAC (Zheng et al., 2015). Such functional diversity of EMT-TFs suggests that different versions of the EMT programs operate in different tissues during tumor progression. With this in mind, therapeutic strategies targeting EMT-TFs should consider tissue context and target multiple factors simultaneously (Krebs et al., 2017).

ZEB1 is a zinc finger/ homeodomain protein that is associated with EMT and tumor progression. ZEB1 functions as a transcriptional activator by binding to CtBP co-repressors, histone acetyl-transferase TIP60, chromatin remodeling ATPase BRG1, and SIRT1, a histone

deacetylase (Thiery et al., 2009). Larsen et al., (Larsen et al., 2016) found that ZEB1-induced EMT was crucial for the development of NSCLC but required premalignant oncogenic mutations such those for *KRAS*. Moreover, they found that ZEB1-driven EMT was a crucial early event in the progression of human bronchial epithelial cells to malignancy (Larsen et al., 2016). These results supported previous in vitro (Takeyama et al., 2010) and in vivo (Ahn et al., 2012; Gibbons et al., 2009; Liu et al., 2012; Y. Yang et al., 2014) studies that established ZEB1 as a driver of EMT in lung cancer tumorigenesis. In PDAC, Krebs et al. (Krebs et al., 2017) demonstrated that ZEB1 is a key driver of PDAC progression from early tumorigenesis to late-stage metastasis, highlighting the important contribution of EMT activation in these processes (Krebs et al., 2017).

Beyond the levels of mRNAs, EMT-TFs have been shown to alter chromatin configurations to achieve the stable, long-term silencing of epithelial genes required for complete EMT (Tam & Weinberg, 2013). Snail, an EMT-TF, can recruit a series of chromatin-modifying enzymes to the E-cadherin promotor to erase a mark of active transport and replace it with a trimethylated H3K9 mark that promotes the recruitment of DNA methyltransferases, causing CpG methylation of the promoter and formation of a constitutive heterochromatin resistant to transcription activation (Y. Lin, Dong, & Zhou, 2014). Additionally, TFs of the Zeb family form a double-negative feedback loop with the miR-200 family of microRNAs (miRNA), causing this regulatory loop to operate as a switch between epithelial and mesenchymal states in a variety of tumor types (S. Brabletz & Brabletz, 2010; Burk et al., 2008; L. Hill, Browne, & Tulchinsky, 2013). Similarly, Snail represses the expression of miR-34, a miRNA that

binds to the 3' UTR of Snail mRNA to mark it for degradation (T. Brabletz, 2012; H. N. Kim, Narayanan, Lasano, & Narayanan, 2011).

Targeting AXL and TBK1 as a therapeutic strategy for metastatic cancer

Due to its implication in metastasis, EMT, and drug therapy resistance, large efforts are focused on pharmacologically inhibiting AXL. In fact, multiple strategies are being tested clinically, including blocking GAS6 or AXL with monoclonal antibodies and small molecules (Du & Brekken, 2018; Du, Huang, Sorrelle, & Brekken, 2018). One of the most advanced selective AXL inhibitors to date is bemcentinib (BGB324), developed by BerGenBio ASA. BGB324 has been investigated by our group in preclinical models of late-stage PDAC and shown promising therapeutic effects in enhancing gemcitabine efficacy and reducing metastasis (Ludwig et al., 2018). Other groups have also investigated BGB324, where it has been found to have antitumor, antimetastatic, and therapy-sensitizing effects in preclinical models of pancreatic cancer, breast cancer, glioblastoma, prostate cancer, chronic myeloid leukemia, ovarian cancer, and uterine serous cancer (Antony et al., 2016; Ben-Batalla et al., 2017; Holland et al., 2010; J. Z. Lin et al., 2017; Palisoul et al., 2017; Sadahiro et al., 2018; Vouri, An, Birt, Pilkington, & Hafizi, 2015). Recently phase II clinical trials have begun to enroll patients using bemcentinib in multiple cancer types as a single agent or in combination with targeted or chemo- and immunotherapies (Table 1). Another selective AXL inhibitor is TP-0903, developed by Tolero Pharmaceuticals. In preclinical models, TP-0903 has been shown to have antitumor and therapy-sensitizing effects on multiple cancers, including neuroblastoma, leukemia, and lung cancer (Aveic et al., 2018; Myers, Brunton, &

Unciti-Broceta, 2016; Park et al., 2015; Sinha et al., 2018). TP-0903 is currently being evaluated clinically in multiple indications (**Table 1**).

Target	Drug	Disease	Trial Phase	Results	Identifier
KRAS G12C	AMG 510	NSCLC	1/2	Ongoing	NCT03600883
KRAS G12C	MRTX849	Advanced solid tumors	1/2	Ongoing	NCT03785249
AXL	Bemcentinib (BGB324)	Glioblastoma	1	Ongoing	NCT03965494
AXL	Bemcentinib (BGB324)	Pancreas	1/2	Ongoing	NCT03649321
AXL	Bemcentinib (BGB324)	NSCLC	2	Ongoing	NCT03184571
AXL	Bemcentinib (BGB324)	NSCLC	1/2	Status unknown	NCT02424617
AXL	Bemcentinib (BGB324)	Malignant mesothelioma	2	Ongoing	NCT03654833
AXL	Bemcentinib (BGB324)	NSCLC	1	Ongoing	NCT02922777
AXL	Bemcentinib (BGB324)	TNBC	2	Completed	NCT03184558
AXL	Bemcentinib (BGB324)	Melanoma	1/2	Ongoing	NCT02872259
AXL	Bemcentinib (BGB324)	Acute myeloid leukemia	2	Ongoing	NCT03824080
AXL	TP-0903	NSCLC, colorectal, ovarian, melanoma	1	Ongoing	NCT02729298
AXL	TP-0903	Leukemia, lymphoma	1/2	Ongoing	NCT03572634
TBK1	Amlexanox	Type 2 diabetes	2	Finished recruitment	NCT01842282
TBK1	Amlexanox	Type 2 diabetes	2	Optimal drug dose wasn't reached.	NCT01975935

Table 1. Clinical trials targeting KRAS, AXL, and TBK1.

For TBK1 to be a relevant target in the clinic, it will be necessary to evaluate the therapeutic efficacy of TBK1 inhibition in preclinical cancer models. Currently there are at least six distinct small molecules that inhibit TBK1, including BX795, compound II, CYT387, MRT67307, GSK2292978A, and Amlexanox, although none are highly selective. Currently, Amlexanox is the only TBK1i known to enter clinical testing, which is in a phase 2 study for the treatment of type 2 diabetes, nonalcoholic fatty liver disease, or obesity (Table 1). Further investigations and better inhibitors will be needed before TBK1 can be directly targeted in RAS-driven cancer in preclinical and clinical settings. Moving forward, it will be vital to understand the distinct function of TBK1 in each relevant cell type within tumors. As mesenchymal tumor cells express high levels of active TBK1 (Cruz et al., 2019) and are associated with aggressive disease, metastasis, and poor patient outcomes (Ye & Weinberg, 2015), targeting TBK1 in RAS-driven cancers is a promising alternative strategy to reduce the tumor-promoting effects of KRAS-driven EMT.

CHAPTER TWO
Methodology

Reagents

The following antibodies were used for immunoblotting (IB) at 1:1,000 unless otherwise stated: Anti-AXL (8661S, Cell Signaling, IHC 1:500), anti-phospho AXL y702 (5724, Cell Signaling), anti-phosphoserine (AB1603, Millipore), anti-TBK1 (3013S, Cell signaling), anti-TBK1 (ab40676, Abcam, IF 1:250), anti-TBK1 (NB100-56705AF647, Novus, FC 1:100), anti-pTBK1 s172 (5483S, Cell Signaling), anti-SNAIL (3879, Cell Signaling), anti-SLUG (9585, Cell Signaling), anti-SLUG-AF488 (NBP2-74235AF488, Novus, FC 1:100), anti-E-cadherin (clone 24E10, 3195S, Cell Signaling), anti-N-cadherin (14215S, Cell Signaling), anti-B-Catenin (8480, Cell Signaling), anti-Claudin1 (13255, Cell Signaling), anti-IRF3 (sc-9082, Santa Cruz), anti-pP65 (3033, Cell Signaling), anti-Ras (ab108602, Abcam), anti-ZO-1 (8193, Cell Signaling), mouse anti-human Twist (Twist2C1a, Abcam, IHC), α-actin (A2066, Sigma, 1:2000), anti-α-tubulin (T6199, Sigma), anti-Vimentin (5741, Cell Signaling), anti-AKT1 (2967, Cell Signaling), anti-AKT2 (3063, Cell Signaling), anti-AKT3 (1586912, Millipore, IHC), anti-AKT3 (14982, Cell Signaling, IP, IB, and IF 1:250), anti-AKT3 (HPA026441, Sigma, IHC 1:200), anti-AKT3-PE (NBP2-71528PE, Novus, IF 1:250, FC 1:100), anti-pAKT (Ser473) (2971, Cell Signaling), anti-Lamin A/C IgG2b (Santa Cruz, sc-7292), anti-AKT (Cell signaling Technology, 9272), anti-Importin α (I1784, Sigma), anti-GAPDH (2118, Cell Signaling), anti-Phalloidin-AF546 (A22283, Invitrogen, IF 1:500), Hoechst 33342 (IF, 1:2000) and anti-FBXW7-PECY7 (NBP2-50403PECY7, Novus, FC 1:100). The following reagents were purchased from Sigma: Cycloheximide (01810-1g),

BafA1 (B1793-2UG), MG-132 (474787-10MG). The mammalian expression plasmid pCDH-CMV-MCS-TBK1-EF1-NEO was generously provided by Drs. Peiqing Shi and James Chen (UT Southwestern Medical Center, Dallas, TX). The CRU5-IRES-GFP retroviral vectors for expression of hSNAIL, hSLUG, myrAKT1, myrAKT3, AKT3, shLuc, and shAXL (RFP) were prepared as described (Gjerdrum et al., 2010). CRU5-IRES-GFP retroviral vectors for expression of AKT3-NLS and AKT3-NLS were generated by site-directed mutagenesis (Quik change #2200519). CRU5-IRES-GFP Luciferase AKT3-Luciferase and AKT3-NLS1-Luciferase were generated by cloning. All vectors were confirmed by DNA sequencing. Lentiviral shRNA constructs against human AKT1, AKT2, AKT3, and TBK1 were purchased from Dharmacon (TBK1, RHS3979-201735457, clone ID: TRCN0000003184)(AKT1, RHS3979-201768650, clone ID: TRCN0000039797)(AKT2, RHS3979-201732837, TRC00000005630)(AKT3, RHS3979-201733886, TRCN0000001612). Retroviral production and infections were conducted using Phoenix A retroviral packaging cells as described (Swift, Lorens, Achacoso, & Nolan, 2001). Lentiviral-based expression constructs were packaged by co-transfection of HEK293T cells with psPAX2 and pMD2.G packaging system (4:2:1). Polyethylenimine (PEI) was used for transfection at a 3:1 ratio of total DNA. Transfection media was replaced with 10% complete DMEM 24 hours post transfection, and incubated a further 24 hours prior to viral particle collection. *Tbk1*$^{+/+}$ and *Tbk1*$^{\Delta/\Delta}$*: KIC* cells were seeded at a density of 1 x 10^6 cells per 10 cm dish. Twenty-four hours later, the cells were infected with lentiviral particles and polybrene (10 μg/ml). At 24 hours post infection, cells were given fresh medium containing G418 (400 μg/mL, InvivoGen) or puromycin (1ug/mL, Sigma) for selection and maintained in culture

under selection for 3 weeks following initial infection. Human Gas6 from conditioned media was prepared as previously described (Kirane et al., 2015). AKTVIII (Sigma), Imatinib (LC laboratories I-5508) and BGB324/R428, BGB214, were prepared in DMSO. AF854 (R&D Systems, Minneapolis, MN) was previously shown to activate mouse AXL and was used at indicated concentrations to stimulate mouse AXL (Zagorska, Traves, Lew, Dransfield, & Lemke, 2014).

Cell lines

Cell culture, retroviral transductions, siRNA transfection HMEC strains (4th passage) were established and maintained as described (Labarge, Garbe, & Stampfer, 2013) in M87A medium with oxytocin and cholera toxin (Garbe et al., 2012). siRNA transfections were conducted as previously described (Vuoriluoto et al., 2011). Human and mouse cancer cell lines (AsPC-1, Capan-1, Hs766T, MCF7, MIA PaCa-2, PANC1, PL-45, MDA-MB-231, 4T1, and MCF10A)) were obtained from ATCC (Manassas, VA). HPNE (human pancreatic nestin-expressing) cells were generated as previously described (K. M. Lee, Yasuda, Hollingsworth, & Ouellette, 2005) and obtained from the UT MD Anderson Cancer Center (Houston, TX). HMLE and HMLER cells (a gift from Dr. R. Weinberg) were maintained as per Mani et al (Mani et al., 2008). The *KPC*-M09 and *KPfC*-8 cell lines were isolated from spontaneous tumors originating in a *KPC* and *KPfC* (*Kras*$^{LSL\text{-}G12D/+}$; *Trp53*$^{lox/lox}$; *Ptf1a*$^{Cre/+}$) mouse, respectively, as previously described (Ludwig et al., 2018). All cell lines were cultured in DMEM or RPMI (Invitrogen, Carlsbad, CA) containing 10% FBS and 1X pen/strep and maintained in a humidified incubator with 5% CO_2 at 37°C. The human cell

lines were DNA fingerprinted for provenance using the Power-Plex 1.2 kit (Promega) and confirmed to be the same as the DNA fingerprint library maintained by ATCC. All cell lines were confirmed to be free of *mycoplasma* (e-Myco kit, Boca Scientific) before use.

Isogenic cell lines were derived from individual tumors of 8-week-old *Tbk1*$^{+/+}$: *KIC* and *Tbk1*$^{\Delta/\Delta}$: *KIC* mice and three to five-month-old *Tbk1*$^{+/+}$: *KPC* and *Tbk1*$^{\Delta/\Delta}$: *KPC* mice. Each tumor was minced and digested with 1% collagenase type I, DMEM, 10 mM HEPES, and 1% FBS at 37°C to obtain a single-cell suspension. Cell suspensions were centrifuged at low speed to pellet large debris, resuspended in wash buffer, and passed through a 70 μm cell strainer. The resulting cell suspension was plated at low density to isolate tumor cell populations using cloning rings. Cells were confirmed to be tumor cells by immunocytochemistry and PCR. These cell lines were expanded and stained for tumor cell markers. Cell lines were confirmed to be pathogen-free before use. Clones *Tbk1*$^{+/+}$: *KIC*-A, *Tbk1*$^{+/+}$: *KIC*-B, *Tbk1*$^{+/+}$: *KIC*-D, *Tbk1*$^{\Delta/\Delta}$: *KIC*-A, *Tbk1*$^{\Delta/\Delta}$: *KIC*-B, and *Tbk1*$^{\Delta/\Delta}$: *KIC*-C were used in subsequent experiments, as well as *Tbk1*$^{+/+}$: *KPC* and *Tbk1*$^{\Delta/\Delta}$: *KPC* cell lines. Cells were cultured in DMEM containing 10% FBS and maintained at 37°C in a humidified incubator with 5% CO_2 and 95% air.

Immunoblotting and Flow Cytometry

Western blot analysis and flow cytometry analysis of cell lines were conducted as previously described (Gjerdrum et al., 2010). Tissues and cells were lysed in ice-cold RIPA buffer (50 mM Tris-Cl, 150 mM NaCl, 1% Nonidet P-40, 0.5% sodium deoxycholate, and 0.1% SDS)

containing cocktails of protease (Thermo Fisher) and phosphatase inhibitors (Sigma-Aldrich, St. Louis, MO) and centrifuged for 20 min at 13,000 × *g* at 4°C. Total protein concentration was calculated using a bicinchoninic acid assay kit (Thermo Fisher). Proteins were resolved by SDS-PAGE and transferred to a methanol-activated polyvinylidene difluoride membrane. All primary and secondary antibodies were diluted in 5% milk in TBS with 0.05% tween. Horseradish peroxidase-conjugated donkey anti-rabbit, donkey anti-mouse, and donkey anti-goat IgG (1:10,000; Jackson ImmunoResearch) were used as a secondary antibodies. Membranes were exposed with Clarity Western ECL Blotting Substrate (Bio-Rad) and visualized with the Odyssey Fc imager (LI-COR Biotechnology, Lincoln, NE). Each western blot was repeated at least 3 times; representative experiments are displayed. MCF10A cells were treated with TGFβ (10 ng/ml) for 4 days and then lysed using NP40 Cell Lysis Buffer (40 mM HepesNAOH, 75 mM NaCl, 2 mM EDTA, 1% NP40, phosphatase inhibitor cocktail tablet, protease inhibitor cocktail tablet (Roche)). For immunoprecipitation, antibodies against separate AKT isoforms (1, 2 and 3) and control IgG antibodies (1µg/lysate) were added to lysates and incubated overnight at 4°C. Next day the pre-blocked protein-A/G beads (GE Healthcare) in lysis buffer were added and allowed to bind at 4°C for 1 hr. Beads were then washed 3 times (20 mM Tris-HCl (pH 7,5), 150 mM NaCl, 1% NP40) and protein eluted by boiling in SDS-PAGE loading buffer. Running of SDS/PAGE gel and immunoblotting were carried out according to standard procedures. Membranes were probed using anti-pAKT (Ser473) and Pan-AKT antibodies. Nuclear extraction of MDA-MB-231 cells was done according to manufacturer´s instructions (Universal Magnetic Co-IP Kit, Active Motif, 54002). Imaging flow cytometry analysis was conducted on an Amnis

Imagestream Mk (>100,000 events) using the Imagestream software (Tree Star, Inc., Ashland, OR, USA) in the Flow Cytometry Core at UT Southwestern. All Western and flow cytometry results shown were performed in at least three independent experiments.

Active GTPase assays

Active RAS in cell lysates was measured via precipitation with GST-tagged RAF-RBD beads (Ras Pull-down Activation Assay Biochem Kit; Cytoskeleton, Denver, CO). Active RalB in cell lysates was measured via precipitation with RalBP1 PBD Agarose beads (Cell BioLabs, San Diego, CA). Lysates were prepared and precipitation was performed per manufacturer instructions. Subsequently, pull-down samples and respective whole cell lysates were immunoblotted with anti-RAS (pan) or anti-RALB (pan) and indicated loading controls.

Biochemical assays for AKT activity

An AKT activation assay was used in which PDK1 was used to phosphorylate inactive AKT enzymes, which then phosphorylated a GSK3α-derived LANCE *Ultra* U*light*-labelled crosstide substrate (Perken Elmer, TRF0106-M). Addition of a Europium-labelled antibody specific to the phosphopeptide (LANCE *Ultra* Europium-anti-phospho-Crosstide (anti-GSK-3α Ser21, Perkin Elmer, TRF0202-M) allows proximity-dependent energy transfer from the Europium donor to the *Ultra* U*light*™ acceptor. Briefly, 5 µL enzyme in 1X AB (50 mM HEPES pH 7.5, 1 mM EGTA, 10 mM $MgCl_2$, 0.01% Tween, 2 mM DTT) was incubated with 2.5 µL test compound. To start the reaction 2.5 µL reaction mix was added which consisted of PDK1, lipid preparations, crosstide and ATP in 1X AB. Final assay

concentrations were: 1% DMSO, 5 nM AKT1/5-15 nM AKT2/3-5 nM AKT3 as appropriate, 5 nM PDK1, 5.5 μM DOPS, 5.5 μM DOPC, 0.55 μM PtdIns(3,4,5)P_3, 100 μM ATP, 100 nM crosstide. After 30 min, the reaction was stopped using 5 μL 40 μM EDTA in 1X LANCE Detection buffer (Perkin Elmer, CR97-100) for 5 min. For detection, 5 μL 8 nM Europium-anti-phospho-Crosstide antibody in 1X Detection buffer was added to each well and incubated for 1 h. Plates were read with an EnVision® Multilabel Plate Reader, excitation at 320 nm and emission at 665 nm and 615 nm. Results were converted to percent inhibition of phosphorylation by normalizing to positive and negative controls, and compound IC_{50} was determined using a 3-parameter equation (Prism, GraphPad).

Wound healing and invasion assays

Wound healing assays were conducted in 6-well plates. Monolayers of cells were grown in low-serum media until 90% confluency was reached. Each well was scratched with a P200 pipette tip to create an artificial wound, washed with PBS to remove residual cells and replaced with fresh media containing 10% FBS. Cells were photographed at indicated time points after wounding. Wound closure was measured as a percentage of original wound width with MRI Wound Healing Tool macro (ImageJ).

Invasion assays were carried out with QCM ECMatrix Cell Invasion Assays (EMD Millipore, Burlington, MA). In brief, cells were serum-starved overnight and then seeded the next day on transwell inserts (8 μm pore size) that were lined with a reconstituted basement membrane matrix of proteins derived from the Engelbreth Holm-Swarm mouse tumor. The

inner chambers were filled with serum-free medium while the outer chambers were filled with medium containing 10% FBS as the chemoattractant. After the indicated time points, invaded cells on the bottom of the insert membrane were dissociated from the membrane when incubated with cell detachment buffer and subsequently lysed and detected by CyQuant GR dye. Each experiment was repeated at least 3 times; representative experiments are displayed.

3D embedded laminin-rich ECM assay

MCF10A or c-KIT-enriched HMEC were resuspended in media (50000 cells/μL) and 200 μL of matrigel (BD Sciences 356234) were added to the cells and transferred to a 24-well plate pre-coated with 50 μL of Matrigel, then cultured 10-12 days prior to microscopy analysis.

Organotypic culture and immunocytochemistry

For each cell line, 2000 cells were plated in 8-well chamber slides (for 3D assays) or 96-well plate (for vertical invasion assays) onto a base layer of growth factor-reduced Matrigel (5 mg/ml; BD Biosciences, Lot A6532) and collagen I (1.5–2.1 mg/ml; BD Biosciences) and cultured for 3 to 4 days in a humidified 37°C incubator as previously described (Westcott et al., 2015). For immunocytochemistry, cultures were fixed in 2% formalin (Sigma-Aldrich) in PBS for 20 min, permeabilized with 0.5% Triton X-100 in PBS for 10 min at room temperature, incubated with Alexa Fluor 488 Phalloidin (A12379, Invitrogen) or Alexa Fluor 546 Phalloidin (A22283, Invitrogen) in immunofluorescence buffer as described (Pearson & Hunter, 2007) for 1 hour at room temperature and mounted using ProLong Gold antifade

reagent with DAPI (Invitrogen). Images were acquired using a confocal laser-scanning microscope (LSM880, Zeiss) through UT Southwestern Live Cell Imaging Core (Dallas, TX) and a Nikon Eclipse E600 microscope with a Nikon Digital Dx1200me camera. A 120-µm span on the *z*-axis is shown for the vertical invasion assays.

Mammosphere and tumorsphere formation assay

Mammosphere cultures were performed as previously described (Dontu et al., 2003). Single cells were plated in ultra-low attachment plates (Corning, Acton, MA, USA) at a density of 20,000 viable cells/ml. Total mammospheres per well were quantified using ImageJ.

Miniaturized 3D cultures

Bottom wells of angiogenesis µ-slide (Ibidi) were filled with 10 µl of Matrigel/culture medium (1:1) (2% FBS). To allow the gels to polymerize the slides were incubated at 37˚C for 30 minutes. Cells were seeded at 20000 cell/ml density (50 µl=1000 cells/well) and then incubated for 2 hrs in the CO2 incubator for the cells to attach. After attachment, cells were covered with 20 µl of Matrigel/culture medium (1:4) for polymerization O/N in the CO2 incubator. Next day the wells were topped up with 30 µl culture medium and after that the culture medium was changed every second day. At day 9 3D cultures were stained with Calcein AM live cell dye (ThermoFisher Scientific) in PBS for 30 minutes in the CO_2 incubator. Imaging of the 3D cultures was carried out using a Nikon TE2000 fluorescence microscope with an 5X objective and the images were analyzed with the automated image

analysis program AMIDA, developed for dynamic morphometric measurements in multicellular spheroids (Harma et al., 2014).

RNA isolation and microarray analysis

Tumor tissues were excised from 8-week-old *Tbk1*$^{\Delta/\Delta}$ and *Tbk1*$^{+/+}$: *KIC* mice and snap-frozen with liquid nitrogen (n = 3 tumors per genotype). Total RNA was isolated after tissue homogenization in TRIzol (Thermo Fisher, Waltham, MA) and RNA was extracted using an RNeasy RNA extraction kit (Qiagen, Germantown, MD). RNA was quantified using a NanoDrop instrument (Thermo Fisher) and checked for quality with a Bioanalyzer Instrument (Agilent). Gene expression was analyzed on a MouseWG-6 v2.0 Expression BeadChip (Illumina, San Diego, CA) through the UT Southwestern microarray core (Dallas, TX). Gene expression data analysis was performed through IPA software (Ingenuity Pathway Analysis, Qiagen). Java TreeView (Alok Saldanha) and Cluster 3.0 software (Michael Eisen, Berkeley Lab) were employed for hierarchical clustering gene expression analysis (Keil).

Gene Expression Analysis and RNA sequencing

The expression analysis of the breast cancer cell lines and human samples (cancer, normal) was performed from published and GEO-submitted Affymetrix data as described (Kilpinen et al., 2008). Global gene expression analysis of HMEC lineage was performed on FACS sorted (FACSVantageSE) pre-stasis HMEC strains 240L and 122L (4th passage) cells. Total RNA from FACS-enriched primary culture cells were isolated with TRIzol (Invitrogen) and RNeasy Mini column (Qiagen) and evaluated using Bioanalyzer (Agilent Technologies).

Gene expression levels were measured using the Illumina HumanHT-12 v4 Expression BeadChip whole-genome expression array. The Illumina Bead Array data were quality controlled in Genome Studio and both probe level and gene level data were imported into JExpress Pro (http://jexpress.bioinfo.no) for analysis. After quantile normalization both datasets were log2 transformed. Correspondence Analysis (Fellenberg et al., 2001) was performed on the datasets, together with Hierarchical Clustering of the samples using a Pearson correlation measure on a per gene mean centered version of the data. Differentially expressed genes between AXL^+ and AXL^- groups were identified using the Rank Product method on both datasets (Breitling et al., 2004). The resulting lists of differentially expressed genes with a false discovery rate value q=10% from these two analysis was considered differentially expressed between the two groups. Cells were plated on 10 cm dishes until cell densities of 70% were achieved. Total RNA was extracted from cells using QIAGEN RNeasy Mini kit and stored at -80ºC. 1 µg total RNA per sample were subjected to library generation using the TruSeq stranded total RNA sample preparation kit, according to the manufacturer's protocol (Illumina). The libraries were pooled and sequenced on a NextSeq 500 instrument (high output flowcell) at 1x75 bp single end reads (Illumina). Raw RNAseq reads were aligned against to the human genome release GRCh38/hg38 using HISAT2 (D. Kim, Paggi, Park, Bennett, & Salzberg, 2019) and exons were counted using RSubread.featureCounts (Liao, Smyth, & Shi, 2014). Libraries were filtered to remove gene counts of less than 1 CPM across all libraries and normalized. Differentially expressed genes between GFP control group and AKT3 overexpressing MCF10A cells were calculated using

edgR (McCarthy, Chen, & Smyth, 2012; Robinson, McCarthy, & Smyth, 2010). Genes were considered differentially expressed with a fold change >2 and $p<0.05$.

AKT3 score and Metabric dataset

To assess the influence of AKT3 signaling and its downstream targets on survival of breast cancer patients, we derived a score capturing the expression of these genes. Genes that were found to be differentially expressed after AKT3 overexpression in MCF10A cells were used to generate an AKT3 score. The score essentially represented the sum of expression of 42 differentially expressed genes, adjusted for expected directionality. Initially, we examined 46 different genes, but only 42 of them where represented with probes on the expression array. For genes represented by multiple probes (the 42 genes mapped to 71 different probes), mean signal intensity was used. The influence on breast cancer specific survival and the putative difference between molecular subtypes was investigated in the Metabric cohort, composed of 1980 breast cancer patients enrolled at five different hospitals in the UK and Canada (Curtis et al., 2012). Gene expression was assessed using the Illumina HT-12 v3 microarray and normalized data was downloaded from the European Genome-phenome Archive (EGA) data portal. Missing values were imputed using the impute.knn function as implemented in the R library 'impute' with default settings (Hastie T, c R, Narasimhan B and Chu G (2016). Impute: Imputation for microarray data. R package). The data was batch adjusted for hospital effect using the pamr.batchadjust function in the 'pamr' library with default settings (T. Hastie, R. Tibshirani, Balasubramanian Narasimhan and Gil Chu (2014). Pam: prediction analysis for microarrays). Association between the score and molecular subtypes (Curtis et

al., 2012; Parker et al., 2009) was tested using Kruskal-Wallis rank test, and correlations were estimated with Spearman's rank correlation. Survival analyses were performed using Cox proportional hazards regression model as implemented in the R library ‘rms’ (Frank E Harrell Jr (2016). rms: Regression Modeling Strategies). Survival plots were generated using the survplot function, as implemented in the rms library. All analyses were performed using R version 3.3.1.

Confocal Microscopy

Cells were plated on coverslips (Bae, Cho, Mu, & Birnbaum, 2003.5, Marienfeld-Superior) overnight under low serum (1%) conditions. Cells were fixed with 4% formaldehyde diluted in warm PBS for 15 min, washed 3 times, blocked, and permeabilized with 5% goat serum, 0.3% Triton X100 in PBS for 1h. Cells were incubated with the appropriate primary antibody overnight followed by 3 wash steps with PBS and secondary antibody incubation for 2h in 5% BSA in PBS. After 3 wash steps with PBS, coverslips were mounted on slides with Prolong Diamond Antifade Reagent (Thermo Fisher). The images were acquired using Leica SP5, Leica SP8, Zeiss LSM780, or Zeiss LSM880 inverted microscopes.

Immunohistochemistry

For mouse tissues, pancreas/tumors, livers, lungs, spleens, and kidneys were excised and fixed with 10% neutral buffered formalin solution for 48hrs on shaker at room temperature. Tissues were then washed and store in PBS at 4˚C and embedded in paraffin for sectioning by the UT Southwestern Molecular Pathology Core (Dallas, TX). All tissues were sectioned

at 5 μm. After sectioning, slides were deparaffinized with xylene and rehydrated in decreasing ethanol dilution series and then stained with H&E, Masson's Trichrome, Alcian Blue, or fixed in 10% neural buffered formalin for 30min prior to antigen retrieval. Sections for immunohistochemical fluorescence analysis were blocked with 5% BSA and incubated with rabbit anti-Vimentin (Cell Signaling, #5741) in blocking solution (5% BSA in TBS with 0.05% tween) at 4°C overnight. TRITC-conjugated donkey anti-rabbit IgG (Jackson ImmunoResearch) was used as a secondary antibody. Sections for immunohistochemical DAB analysis were stained as previously described (Sorrelle et al., 2019). Briefly, antigen retrieval was performed using Ag retrieval buffer (10mM Tris-Hcl and 1mM EDTA with 10 glycerol [pH 9]) heated at 110˚C for 18 minutes. Sections were blocked with 2.5% goat serum (Vector Laboratories) for 30 min and incubated with rabbit anti-CK19 (Abcam, ab15463), rabbit anti-E-Cadherin (Cell Signaling, #3195), rabbit anti-Claudin-1 (Cell Signaling, #13255), anti-rabbit Ki-67 (Abcam, #15580), anti-rabbit Slug (Cell Signaling, #9585), anti-rabbit Zeb-1 (Cell Signaling, #3396), or rabbit anti-Vimentin (Cell Signaling, #5741) in blocking solution (2.5% Goat serum) at 4°C overnight. HRP-conjugated secondary anti-Rabbit (ImmPRESS, Vector Laboratories), was used as secondary antibody. For chromogenic detection, sections were developed using Betazoid DAB (Biocare Medical, BDB2004L). After development, slides were counter stained with hematoxylin. Slides were mounted and coverslipped using VectaMount (Vector Laboratories, H-5501). Negative controls included omission of primary antibody. All slides were visualized at 20X using Hamamatsu Nanozoomer 2.0-HT. Image analysis was conducted using Fiji software as previously described (Sorrelle et al., 2019).

For patient samples, paraffin-embedded Human PDAC samples were provided by the Tissue Management Shared Resource within the Simmons Comprehensive Cancer Center at UT Southwestern. Both AXL and AKT3 antibodies were optimized and stained using a Leica Autostainer. Paraffin-embedded normal human breast tissue sections (n=20; generously provided by Dr. A.Borowsky) were prepared for immunofluorescence and stained with as previously described (Garbe et al., 2012). For N-cadherin analysis, antigen retrieval was performed by boiling for 20 min at in Tris EDTA buffer, ph 9 in a microwave oven. A Dako Autostainer was used for staining. The slides were incubated 60 minutes at room temperature with a monoclonal antibody against N-cadherin (M3613), dilution 1:25 (Dako). Immunoperoxidase staining was carried out using the Dako Envision Kit with diaminobenzidin tetrachloride peroxidase. For analysis of Twist-2, antigen retrieval was performed by boiling in TRS buffer (pH 6.0) (Dako) for 25 minutes, and incubated for 1 hr in room temperature with the rabbit polyclonal antibody Twist-2 diluted 1:500, and stained with HRP EnVision rabbit (Dako) for 30 minutes in RT. The peroxidase was localized by the diaminobenzidine tetrachloride peroxidase reaction and counterstained with Mayer`s hematoxylin. For AXL analysis, the sections were boiled in TRS buffer (pH 6.0) (Dako) in 20 minutes, followed by incubation overnight at room temperature with goat IgG antibody AXL, dilution 1:50 (R&D AF154) and stained with EV rabbit for 30 minutes. The peroxidase was localized by the diaminobenzidine tetrachloride peroxidase reaction and counterstained with Mayer’s hematoxylin. The human breast cancer tumor sections were obtained from the IRO database and assayed for quality control by a pathologist. IHC staining was carried out

using DAKO, EnVision™ FLEX kit with DAB before counterstaining with hematoxylin (DAKO, EnVision™ FLEX Hematoxylin K8008). Stained samples were acquired using with Zeiss Axio Observer Z1 microscope and analyzed with TissueGnostics software for acquisition and analysis. Representative regions were analyzed from each sample slide and mean intensity of DAB-AKT3 staining from nuclei and cytoplasm was used to separate nuclear AKT3 cases from cytoplasmic AKT3 cases.

Recombined Cdkn2a allele detection

Liver micrometastasis was assessed by quantitative RT-PCR (qPCR) for the recombined *Cdkn2a*(*Ink4a*/*Arf*) allele. Briefly, frozen livers were homogenized in SDS lysis buffer (100 mM Tris pH 8.8, 5 mM EDTA, 0.2% SDS, 100 mM NaCl) and digested at 56˚C overnight. DNA was extracted using phenol-chloroform-isoamyl-alcohol (25:24:1) and quantitative RT-PCR was performed using iQ SYBR Green Supermix (Bio-Rad, California, USA). The following validated primers were used for analysis of CDKN2A: gccgacatctctctgacctc (forward) and ctcgaaccaggtttccattg (reverse). Each sample was analyzed in triplicate.

Animals

NOD SCID mice were purchased from the UT Southwestern mouse breeding core (Dallas, TX). $Tbk1^{\Delta/\Delta}$, $Tbk1^{+/+}$, $Kras^{LSL\text{-}G12D/+}$; $Cdkn2a^{Lox/Lox\text{-}}$ (KI) and $Cdkn2a^{Lox/Lox}$; $Ptf1a^{Cre/+}$ (IC) mice were generated as previously described (Aguirre et al., 2003; Bardeesy & DePinho, 2002; Marchlik et al., 2010). $Tbk1^{\Delta/\Delta}$ and $Tbk1^{+/+}$ mice were used to breed with KI and IC

mice to generate *Tbk1*$^{+/+}$; *Kras*$^{LSL\text{-}G12D/+}$; *Cdkn2a*$^{Lox/Lox}$; *Ptf1a*$^{Cre/+}$ (*Tbk1*$^{+/+}$: *KIC*) mice and *Tbk1*$^{\Delta/\Delta}$: *KIC* mice. *LSL-Trp53*$^{R172H/+}$ mice were obtained from the National Cancer Institute Mouse Repository (Hingorani et al., 2005). *Tbk1*$^{\Delta/\Delta}$ and *Tbk1*$^{+/+}$ mice were also used to breed with *Kras*$^{LSL\text{-}G12D/+}$; *LSL-Trp53*$^{LSL\text{-}R172H/+}$ (KP) and *Ptf1a*$^{Cre/+}$ mice to generate *Kras*$^{LSL\text{-}G12D/+}$; *LSL-Trp53*$^{LSL\text{-}R172H/+}$; *Ptf1a*$^{Cre/+}$ (*KPC*) mice and *Tbk1*$^{\Delta/\Delta}$: *KPC* mice. All mice were bred and maintained in a pathogen-free barrier facility with access to food and water *ad libitum*. All protocols for mouse use and euthanasia were reviewed and approved by the institutional animal care and use committee of the University of Texas Southwestern Medical Center (Dallas, TX) or by The Norwegian Animal Research Authority and performed in accordance with The European Convention for the Protection of Vertebrates Used for Scientific Purposes.

Animal studies

All experiments were conducted using littermate-controlled mice. All mice were fed a normal chow diet (16% protein diet, irradiated; Teklad Global Diets; Envigo, East Millstone, NJ). For endpoint studies, *Tbk1*$^{+/+}$: *KIC* and *Tbk1*$^{\Delta/\Delta}$: *KIC* mice were sacrificed and entire tissues, including pancreas/tumor, liver, lungs, and spleen, were harvested and weighed at 6, 8 and 10 weeks old, with n = 5-11 mice per time point per group. *Tbk1*$^{+/+}$: *KPC* and *Tbk1*$^{\Delta/\Delta}$: *KPC* mice were sacrificed between 4 and 5 months, with n ≥ 8 mice per time point per group. For all survival studies, mice were carefully monitored and sacrificed when they appeared moribund.

Lung colonization studies:

Tbk1$^{+/+}$: *KIC* and *Tbk1*$^{\Delta/\Delta}$: *KIC* cells (1 x 10^5) were resuspended in 200 µl PBS and injected intravenously into the tail vein of 8-week-old female NOD SCID mice. Lungs were harvested at 7 or 12 days post injection and fixed in Bouin's fixative for gross analysis of tumor nodules. Tumor colonization was analyzed by H&E. Female NOD/SCID mice (6–8 weeks old; Gades Institute, University of Bergen) were used for breast tumor studies. HMLER (GFP, AKT3, AKT-NLS1)-luciferase cells suspended in PBS with 5*10^5 cells per 50 µL were injected intravenous in 4-6 weeks old NOD/SCID mice. Tumor growth was measured every 48h via IVIS Spectrum in vivo bioluminescence imaging for luciferase activity. Before imaging mice were intraperitoneally injected with 150 mg/kg of D-luciferin solution in PBS for 10 min in awake animals. For quantification, the total flux was determined in the thorax area of all animals.

Tumor cell titration studies:

Xenograft tumor-initiation studies were conducted as described by (Gupta et al., 2009). HMLER cells (GFP, myrAKT1, myrAKT3 or AKT3) were suspended in DMEM/Matrigel (1:1) in 50 µL) and injected subcutaneously into 3-6 weeks old NOD-SCID mice. Tumor incidence was monitored with hand held caliper for up to 60 days after injection; tumor threshold was set at 20 mm3 (AKT3) or 25 mm3 (myrAKT3). Animals were treated with BGB214 dissolved in 0.5% HPMC/0.1% Tween 80 (Vehicle) as indicated in figure legends starting at the day of cell injection. For some studies, cells were treated for 24 hrs with 0.54 µM BGB214 prior to implantation.

In vitro kinase assay

1.5 µg of recombinant GST-AKT3 (BML-SE369-0005, Enzo Life Sciences), 0.1 µg of Recombinant Active TBK1 (T02-10G-05, SignalChem), and 1 µL 10 mM ATP were combined in kinase reaction buffer (20 mmol/L Tris-HCl pH 7.4, 500 mmol/L β-glycerol phosphate, 12 mmol/L magnesium acetate) up to a total of 30 µL. Kinase reaction was carried out at 30˚c, 500 rpm for 1hr. After reaction, AKT3 protein was resolved by SDS-PAGE and stained by Coomassie Brilliant Blue. Bands were cut out for MS analysis to identify phosphorylation site by the UT Southwestern Proteomics core.

Statistical analysis

GraphPad Prism 5.0 for PC, and MatLAB were used for statistical analysis using tests stated in the Figure Legends. Comparisons of histological SI groups were performed by Pearson χ^2 test using cut-off values for staining index (SI) categories based on median values. Grouped analyses were performed with Bonferroni's test for multiple comparisons. Significance was established when $p<0.05$.

CHAPTER THREE

AXL-MEDIATED ACTIVATION OF TBK1 DRIVES EPITHELIAL PLASTICITY IN PANCREATIC CANCER

TBK1 expression in pancreatic cancer

TBK1 is expressed in numerous epithelial tumors, including breast, lung, and colon (Barbie et al., 2009; Korherr et al., 2006; Shen & Hahn, 2011; K. M. Yang et al., 2013). However, the function and activity of TBK1 in human pancreatic cancer has not been characterized extensively. We found that TBK1 was expressed and was active (pTBK1) under basal conditions in a panel of human *KRAS*-mutant PDA cell lines. In contrast, TBK1 was expressed but with reduced activity in normal pancreatic ductal epithelial cells (HPNE) (K. M. Lee et al., 2005) or *KRAS wild-type* PDA cells. Mouse embryonic fibroblasts isolated from *Tbk1*-mutant mice (*Tbk1*$^{\Delta/\Delta}$) (Marchlik et al., 2010) served as a negative control with no detectable expression of TBK1 or pTBK1 **(Figure 3A)**. Additionally, we observed higher

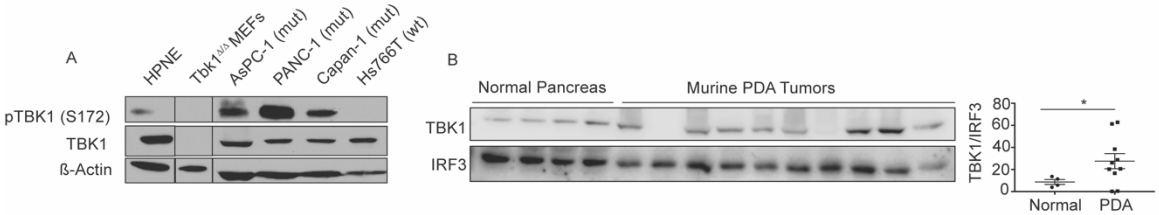

Figure 3. TBK1 is expressed highly in pancreatic cancer. A) Total and pTBK1 (S172) expression in wild-type KRAS (wt) or mutant active KRAS (mut) human normal (HPNE) or pancreatic ductal adenocarcinoma (PDA) cell lines. Tbk1Δ/Δ mouse embryonic fibroblasts (MEFs) served as a negative control. β-actin was used as a loading control. Solid line indicates where blot was cropped; however, all samples were run on the same gel and exposed simultaneously. Western blots displayed are representative of n > 3 repeats. **B)** Total TBK1 expression in murine PDA tumors relative to normal pancreas from nontumor-bearing littermate controls. Total IRF3 was used as a loading control. Intensity quantification is representative of mean +/- SEM. Unpaired two-tailed t test, *p < 0.05.

TBK1 protein levels in spontaneous pancreatic tumors from genetically engineered mouse models (GEMMs) compared to normal pancreas from littermate controls **(Figure 3B)**. Though not causative, this data suggests that TBK1 expression and activity is important in human pancreatic cancer.

KRAS-driven pancreatic cancer growth is disrupted by restricting TBK1 kinase activity

To assess the contribution of TBK1 to PDA progression in vivo, we crossed *Tbk1* mutant mice ($Tbk1^{\Delta/\Delta}$) that harbor two copies of a null *Tbk1* allele into a GEMM of PDA. The "null" *Tbk1* allele encodes a truncated TBK1 protein that is kinase-inactive and expressed at low levels, thereby allowing analysis of global TBK1 kinase loss in vivo (Marchlik et al., 2010). $Tbk1^{\Delta/\Delta}$ animals were crossed with *KIC* ($Kras^{LSL\text{-}G12D/+}$; $Cdkn2a^{Lox/Lox}$; $Ptf1a^{Cre/+}$) mice. *KIC* mice present with low-grade ductal lesions by 3 weeks of age (Aguilera et al., 2014; Aguirre et al., 2003; Bardeesy & DePinho, 2002) that progress to pancreatic adenocarcinomas such that all mice are moribund between 7 and 11 weeks of age. We hypothesized that TBK1 was critical for RAS-mediated oncogenesis in pancreatic cancer, thus the expectation was that $Tbk1^{\Delta/\Delta}$: *KIC* mice would have smaller tumors and outlive $Tbk1^{+/+}$: *KIC* mice. In comparing tumor sizes, we observed that tumors from $Tbk1^{\Delta/\Delta}$: *KIC* mice were between 20%-40% smaller than $Tbk1^{+/+}$: *KIC* tumors at multiple time points, yet there was no difference in overall survival between the two groups **(Figure 4A-B)**. Although malnutrition resulting

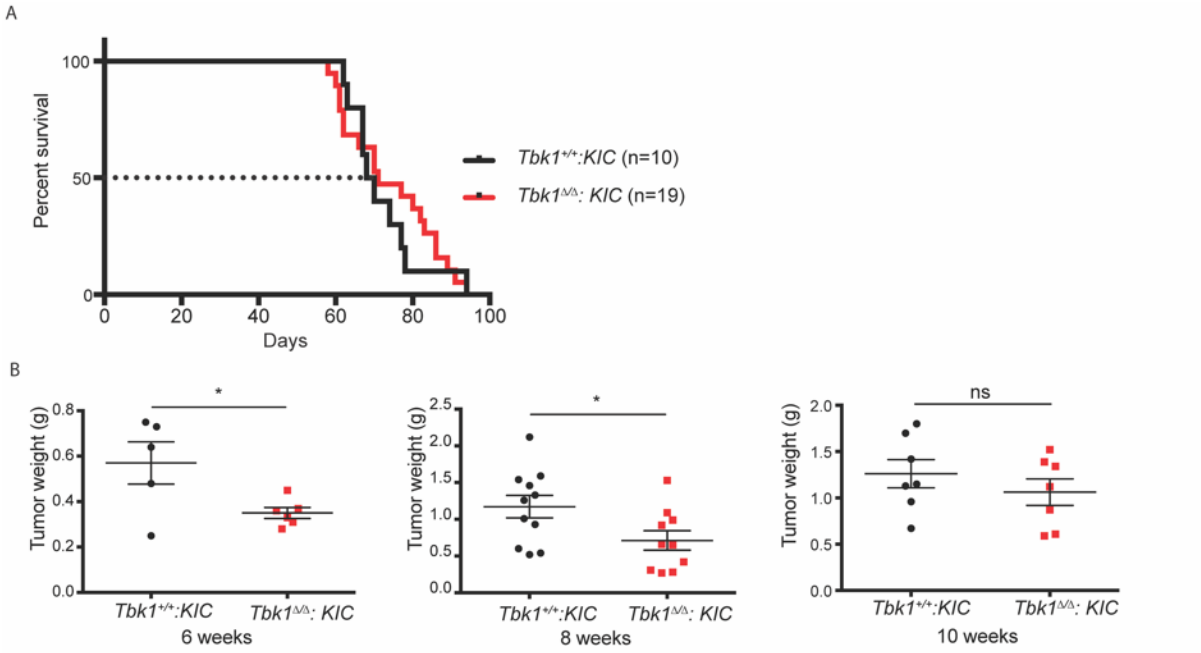

Figure 4. TBK1 promotes pancreatic ductal adenocarcinoma. A) Kaplan-Meier survival curve of Tbk1Δ/Δ: KIC and Tbk1+/+: KIC mice. A log-rank Mantel-Cox test was used for survival comparison. **B)** Endpoint tumor weights at 6, 8, and 10 weeks in Tbk1Δ/Δ: KIC and Tbk1+/+: KIC mice. Results are representative of mean +/- SEM. Unpaired two-tailed t test, *p < 0.05; ns, not significant.

from loss of normal exocrine pancreas function and pancreatic enzyme insufficiency can contribute to early death in the *KIC* model (Zolghadri et al., 2018). Thus, we cannot exclude the possibility that the antitumor effects of *Tbk1* loss are surpassed by malnutrition induced the *KIC* model.

Tbk1$^{\Delta/\Delta}$: *KIC* tumors are differentiated

To better understand TBK1-dependent mechanisms of tumor cell growth contributing to larger tumors in *KIC* mice, we performed gene expression analysis using RNA isolated from

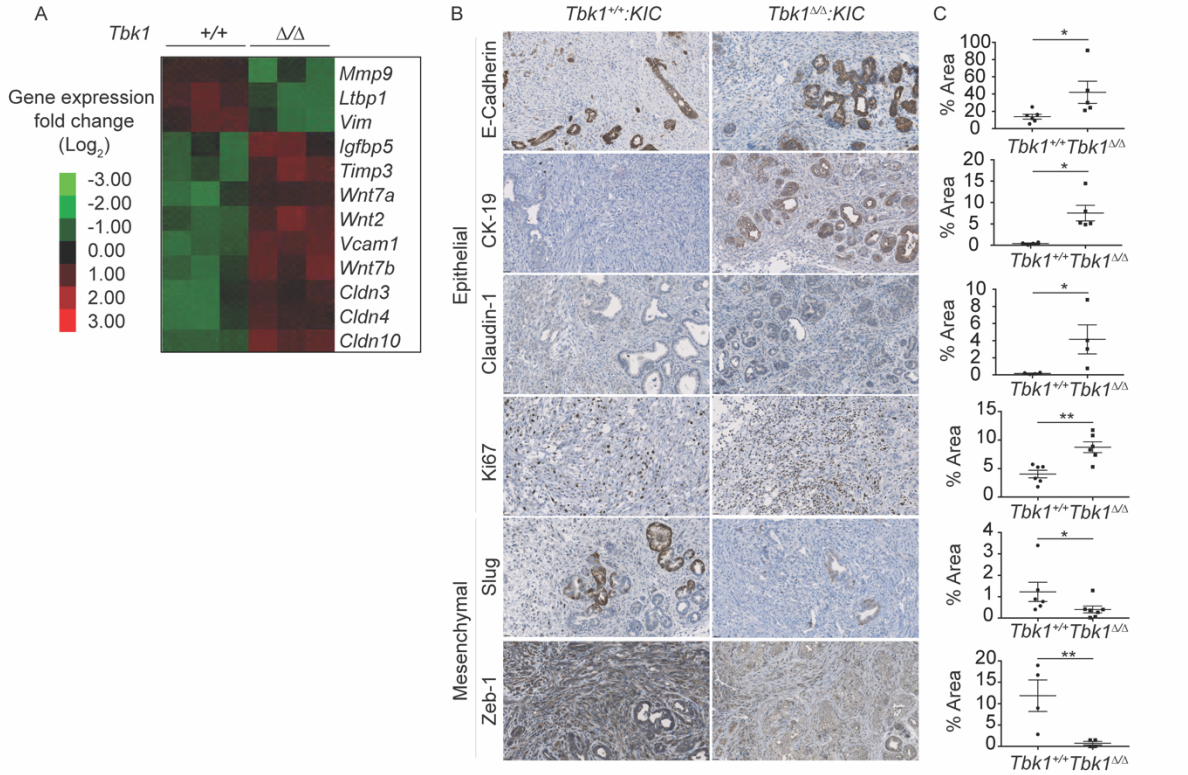

Figure 5. Loss of Tbk1 results in tumor cell epithelial differentiation. A) Heatmap representing gene expression fold change (log2) of epithelial-to-mesenchymal transition (EMT)-related genes from Tbk1+/+: KIC and Tbk1Δ/Δ: KIC tumors. Color key indicates gene expression fold change; n = 3 tumors/genotype, $p < 0.05$ for all genes between Tbk1+/+: KIC and Tbk1Δ/Δ: KIC tumors.
B) Representative images of E-Cadherin, CK-19, Claudin-1, Ki67, Slug, and Zeb-1 stained tumors f rom Tbk1+/+: KIC and Tbk1Δ/Δ: KIC mice. Images were taken at 20X and quantified by normalizing the percent DAB to percent area of tumor; $n \geq 4$ mice/group. Results are representative of mean +/- SEM. Unpaired two-tailed t test, *$p < 0.05$, **$p < 0.01$.

8-week-old *Tbk1*$^{\Delta/\Delta}$: *KIC* and *Tbk1*$^{+/+}$: *KIC* tumors. One of the most significant and top dysregulated gene networks between *Tbk1*$^{\Delta/\Delta}$: *KIC* and *Tbk1*$^{+/+}$: *KIC* tumors identified by Ingenuity Pathway Analysis (Qiagen) was the "cancer/cellular movement" network. This network included a large number of genes involved in epithelial-to-mesenchymal transition (EMT). In comparison to *Tbk1*$^{+/+}$: *KIC* tumors, all three *Tbk1*$^{\Delta/\Delta}$: *KIC* tumors showed a trend of lower expression of mesenchymal genes, such as vimentin and matrix metallopeptidase 9

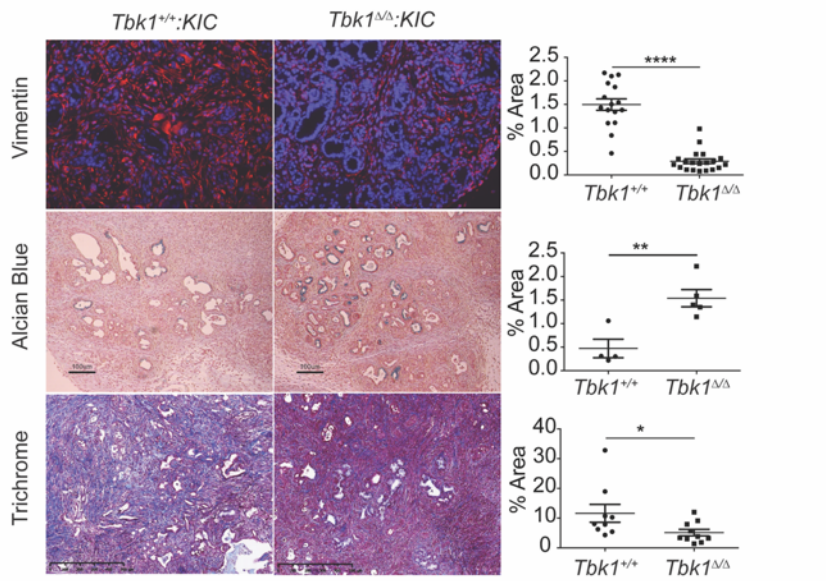

Figure 6. Tumors in Tbk1Δ/Δ: KIC mice display enhanced epithelial differentiation. Representative images of vimentin, alcian blue, and trichrome stained tumors from 8-week old Tbk1+/+: KIC and Tbk1Δ/Δ: KIC mice. Scale bars indicate 100μm for alcian blue images and 500μm for trichrome images; n ≥ 4 mice/group, 4 images/mouse.

(MMP9), and higher expression of epithelial genes including claudin 3, 4, and 10 and tissue inhibitor of metalloproteinase 3 (TIMP3) **(Figure 5A)**. *Tbk1*$^{+/+}$ and *Tbk1*$^{\Delta/\Delta}$: *KIC* tumors were characterized by IHC for epithelial and mesenchymal markers. *Tbk1*$^{\Delta/\Delta}$: *KIC* tumors expressed significantly higher levels of epithelial markers such as E-Cadherin, Cytokeratin-19 (CK-19) and Claudin-1; whereas *Tbk1*$^{+/+}$: *KIC* tumors showed significantly higher levels of mesenchymal markers such as Slug and Zeb-1 (**Figure 5B**). Additionally, *Tbk1*$^{\Delta/\Delta}$: *KIC* tumors also expressed a higher level of the mitotic marker Ki-67, indicative of increased cell proliferation, a phenotype consistent with epithelial/differentiated tumors (**Figure 5B**). Low

vimentin expression was also confirmed at the protein level by immunofluorescent staining in tumors from 8-week-old animals **(Figure 6)**. Further, this EMT gene expression signature was consistent with alcian blue staining of *Tbk1*$^{\Delta/\Delta}$: *KIC* and *Tbk1*$^{+/+}$: *KIC* tumors. Alcian blue stain mucins that are expressed by ductal epithelial cells in pancreatic intraepithelial neoplasia (PanIN) lesions (Aguilera et al., 2014). Representative images show that *Tbk1*$^{\Delta/\Delta}$: *KIC* tumors contain more alcian blue positive epithelial cells compared to less differentiated *Tbk1*$^{+/+}$: *KIC* tumors **(Figure 6)**. Furthermore, we evaluated collagen deposition, a hallmark of pancreatic cancer that promotes EMT in PDA and is upregulated in response to epithelial plasticity (Aguilera et al., 2014; Shintani et al., 2008). *Tbk1*$^{+/+}$: *KIC* tumors showed higher levels of fibrillar collagen than *Tbk1*$^{\Delta/\Delta}$: *KIC* tumors by trichrome histology **(Figure 6)**.

To confirm the tumor cell epithelial phenotype observed in *Tbk1*$^{\Delta/\Delta}$: *KIC* tumors, we isolated single cell clones from *Tbk1*$^{+/+}$: *KIC* and *Tbk1*$^{\Delta/\Delta}$: *KIC* tumors. In total, 3 cell lines per genotype were generated, each from individual tumors. In accordance with gene expression data from *Tbk1*$^{+/+}$: *KIC* tumors, each cell line isolated showed evidence of EMT with an elongated spindle-like cell shape, a characteristic often associated with mesenchymal cells. Moreover, cell lines from *Tbk1*$^{\Delta/\Delta}$: *KIC* tumors exhibited a “cobblestone” morphology, a feature consistent with epithelial cells. These differences in morphology were observed in organotypic culture after the cells were plated on a mixed layer of collagen and Matrigel and fixed and stained to highlight the F-actin **(Figure 7A)**. Evaluation of EMT-related markers revealed higher expression of epithelial proteins, ZO-1 and E-cadherin and lower expression of the mesenchymal proteins Vimentin, Slug and Snail in *Tbk1*$^{\Delta/\Delta}$: *KIC* cell lines

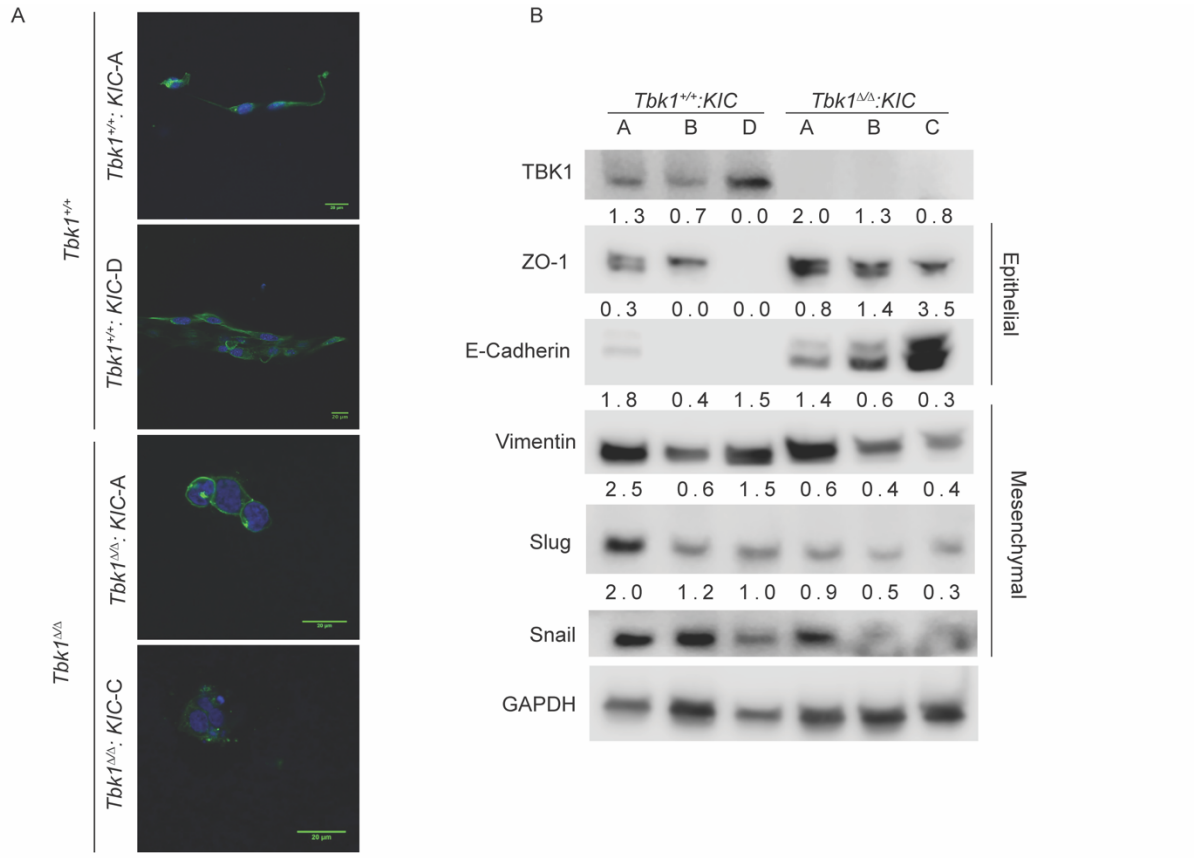

Figure 7. Tbk1 promotes pancreatic cancer epithelial plasticity. A) Representative confocal images of single-cell clones isolated from Tbk1+/+: KIC and Tbk1Δ/Δ: KIC tumors plated on a mixed layer of collagen and Matrigel. Cells were fixed and Nuclei were labeled with DAPI (blue); F-actin was labeled with phalloidin (green). Scale bars indicate 20 μm. **B)** Protein lysates isolated from Tbk1+/+: KIC and Tbk1Δ/Δ: KIC cell lines were immunoblotted for indicated epithelial and mesenchymal markers. GAPDH was used as a loading control. Signal intensity of each sample was quantified and normalized to the mean Tbk1+/+: KIC signal. Western blot is representative of n > 3 repeats.

(Figure 7B). Because these generated cell lines are made from single clones from individual animals, some heterogeneity was observed. This is to be expected, as pancreatic cancer is known to be a heterogeneous disease. These results illustrate a unique epithelial signature in

Tbk1$^{\Delta/\Delta}$: *KIC* tumor cells and have implications for functional differences in tumor cell motility.

Tbk1$^{\Delta/\Delta}$*: KIC* tumor cells are less migratory and less invasive

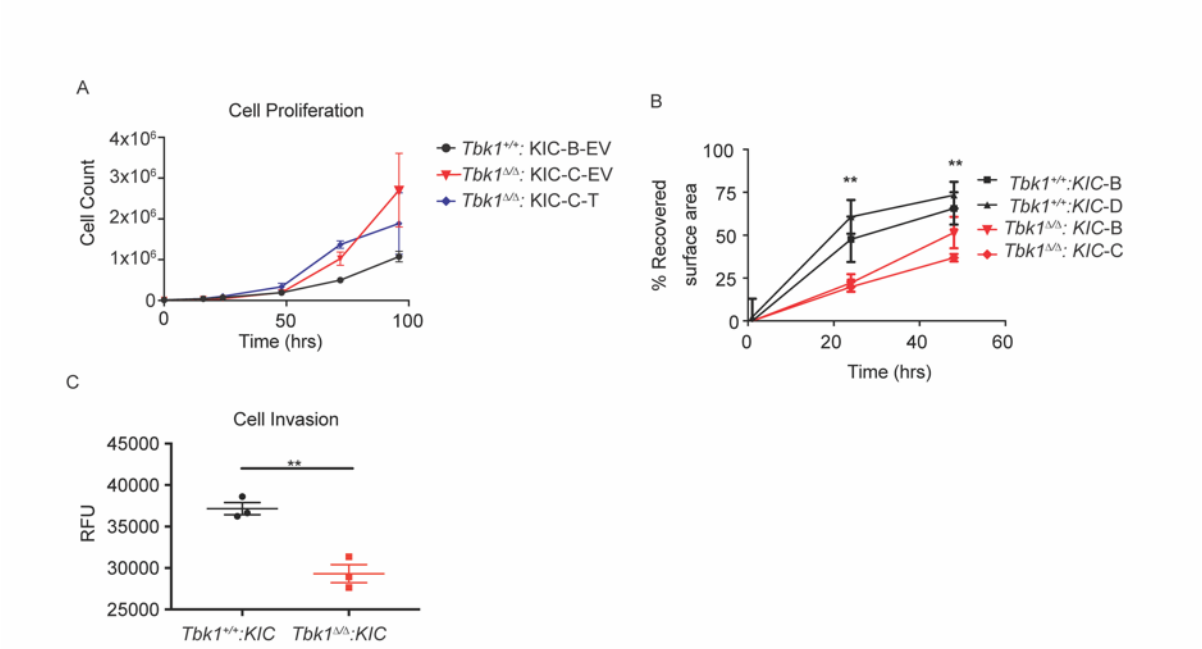

Figure 8. Tbk1Δ/Δ: KIC tumor cells are less migratory and invasive than Tbk1+/+: KIC cells. A) Cell proliferation of Tbk1: KIC cell lines infected with EV or T. Cells were counted over 96 hours, n = 3 plates/cell line. The migratory capacity of cell lines derived from Tbk1: KIC tumors was investigated using scratch **(B)** and transwell migration **(C)** assays. **B)** Recovered surface area of Tbk1: KIC cell lines at 0, 24, and 48 hours post. **C)** Quantification (expressed as relative fluorescent units) of Tbk1: KIC cells after migration through ECM-coated transwell membranes 24 hours after plating in serum-free media. The lower chamber of the transwell were filled with 10% FBS containing media as the chemoattractant. Assays are representative of n> 3 repeats. Results are representative of mean +/- SEM. Results are representative of mean +/- SEM. Unpaired two-tailed t test,
*p < 0.05, **p < 0.01.

Epithelial plasticity changes commonly correspond with alterations in tumor cell motility and invasiveness (Krebs et al., 2017). Given that *Tbk1*$^{\Delta/\Delta}$: *KIC* tumors and cell lines are less mesenchymal in gene expression and morphology, we hypothesized that functional TBK1 is important for tumor cell migration. To compare motility and invasiveness between *Tbk1*$^{+/+}$: *KIC* and *Tbk1*$^{\Delta/\Delta}$: *KIC* tumor cell lines, we performed a series of wound healing and transwell invasion assays. Despite the fact that *Tbk1*$^{\Delta/\Delta}$: *KIC* cell lines proliferate more quickly in culture **(Figure 8A)**, they did not migrate as well as *Tbk1*$^{+/+}$: *KIC* cells **(Figure 8B)**. ECM-coated transwell migration assays also revealed a 20%-50% decrease in invasive capacity in *Tbk1*$^{\Delta/\Delta}$: *KIC* cell lines when compared to *Tbk1*$^{+/+}$: *KIC* cells at 24 hours (**Figure 8C**). These results further highlight the reduced migratory ability of *Tbk1*$^{\Delta/\Delta}$: *KIC* cells.

Evaluation of *Tbk1* loss on pancreatic cancer metastases

Next, we asked whether the reduction in tumor cell motility with kinase-dead *Tbk1* translated to fewer metastases in vivo. The *KIC* mouse model of PDA is an aggressive model with an average life span of ~10 weeks (Aguilera et al., 2014; Aguirre et al., 2003; Bardeesy & DePinho, 2002). As such, these mice rarely develop gross metastases, making this model less than ideal for comparing metastatic burden. However, it's worth mentioning that livers from *Tbk1*$^{+/+}$ (n = 14) and *Tbk1*$^{\Delta/\Delta}$ (n = 12) *KIC* mice were examined for micro-metastases using histology and qPCR **(Figure 9A-B)**. Lesions were identified in 6 livers from *Tbk1*$^{+/+}$

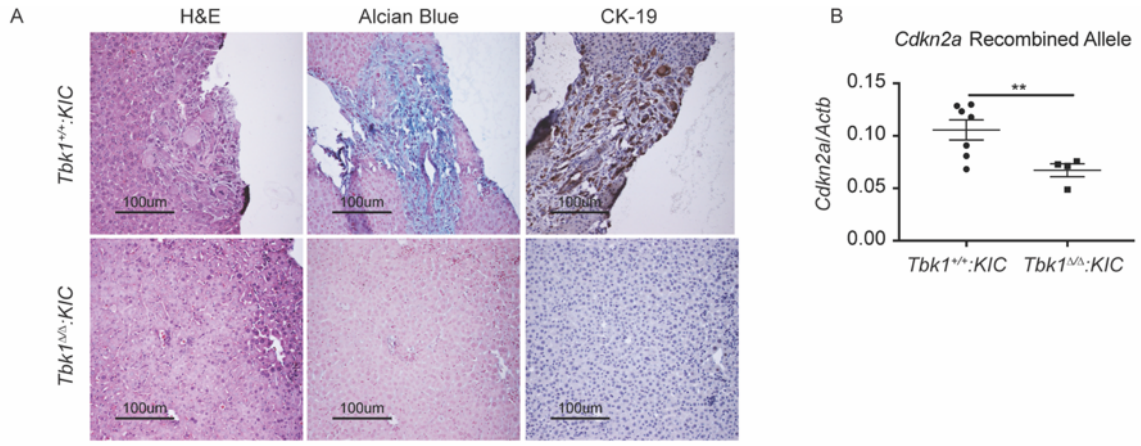

Figure 9. Tbk1Δ/Δ: KIC tumors are less metastatic than Tbk1+/+: KIC tumors. A) Representative liver histology in mice from 8-week-old Tbk1+/+: KIC and Tbk1Δ/Δ: KIC mice, including H&E, alcian blue, and CK19 immunohistochemical staining. Scale bars indicate 100 µm. **B)** Metastasis to the liver was quantified by qPCR for recombined Cdkn2a allele (n = 4-7 mice/group). Results are representative of mean +/- SEM. Unpaired two-tailed t test, *p < 0.05, **p < 0.01, ****p < 0.0001.

animals, but no lesions were found in livers from *Tbk1*-mutant mice. To more robustly study the effect of *Tbk1* loss on metastatic potential, we employed two different animal models. First, we exploited an experimental metastasis model where $Tbk1^{+/+}$ or $Tbk1^{\Delta/\Delta}$: *KIC* cell lines were injected intravenously (i.v.) into NOD SCID mice and lung colonization was determined after 12 days. *Tbk1*-mutant cells were less efficient at forming lung lesions as evidenced by gross lesion formation, by H&E and by lung weight **(Figure 10A-D)**.

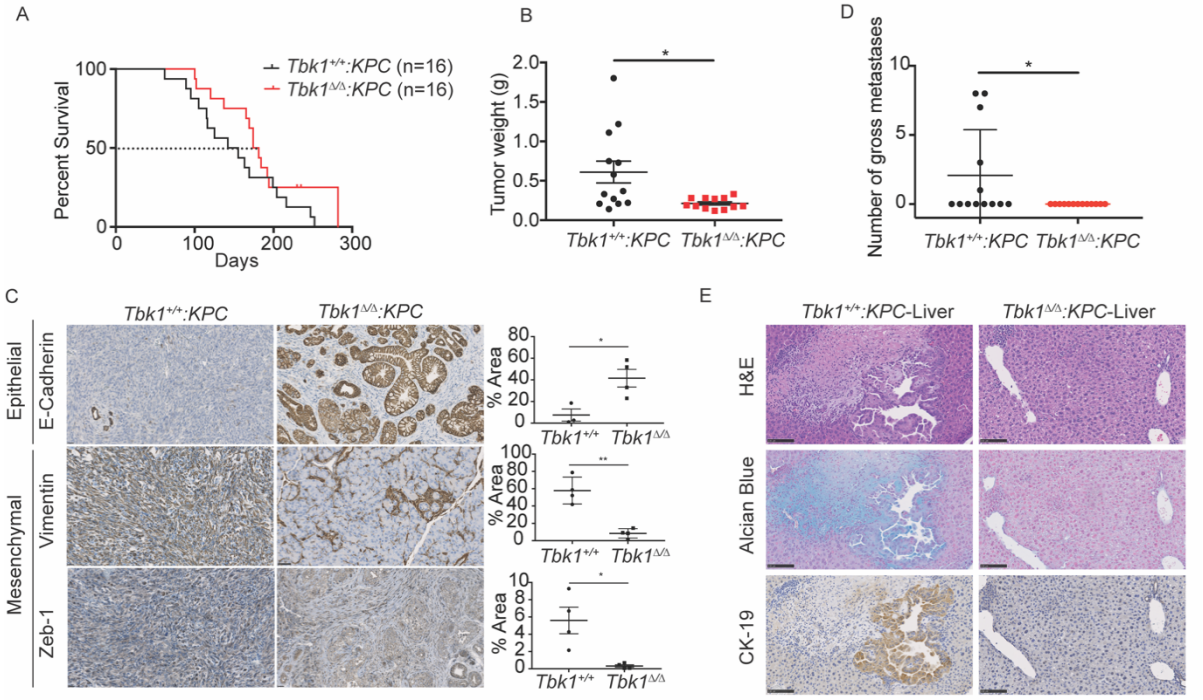

Figure 10. Loss of functional Tbk1 reduces metastasis. A) Kaplan-Meier survival curve of Tbk1Δ/Δ: KPC and Tbk1+/+: KPC mice (n = 16 mice/group). A log-rank Mantel-Cox test was used for survival comparison, p = 0.15. **B)** Tumor weights of Tbk1Δ/Δ: KPC and Tbk1+/+: KPC mice. **C)** Representative 20X images from E-Cadherin, Vimentin, and Zeb-1 stained tumors from Tbk1Δ/Δ: KPC and Tbk1+/+: KPC mice. Images were quantified by percent DAB divided by percent hematoxylin area; n ≥ 4 mice/group. **D)** Number of gross metastases in Tbk1Δ/Δ: KPC and Tbk1+/+: KPC mice (n=13 mice/group). **(E)** Representative liver histology in Tbk1Δ/Δ: KPC and Tbk1+/+: KPC mice including H&E, alcian blue, and CK19 immunohistochemical staining. Scale bar indicates 100 μm, images were taken at 20X magnification. Unpaired two-tailed t test, *p < 0.05, ***p < 0.001, ****p < 0.0001.

While the experimental metastasis assay results were striking, the effect of *Tbk1* loss on spontaneous metastatic development was also of interest. Therefore, we crossed $Tbk1^{\Delta/\Delta}$ mice to *KPC* ($Kras^{LSL\text{-}G12D/+}$; $LSL\text{-}Trp53^{LSL\text{-}R172H/+}$; $Ptf1a^{Cre/+}$) animals. The *KPC* model differs from the *KIC* model in that it contains a dominant negative p53 point mutation instead of loss of the tumor suppressor, *Cdkn2a* (Hingorani et al., 2005). *KPC* mice have a longer median

survival (5 months) allowing more time for tumor cells to metastasize (Hingorani et al., 2005; M. Wang et al., 2015). Although not statistically significant, *Tbk1*$^{\Delta/\Delta}$: *KPC* mice live 1 month longer than *Tbk1*$^{+/+}$: *KPC* mice, shifting the median survival from 5 months to 6 months (p = 0.15) **(Figure 11A)**. Primary tumor burden was significantly reduced in *Tbk1*$^{\Delta/\Delta}$:

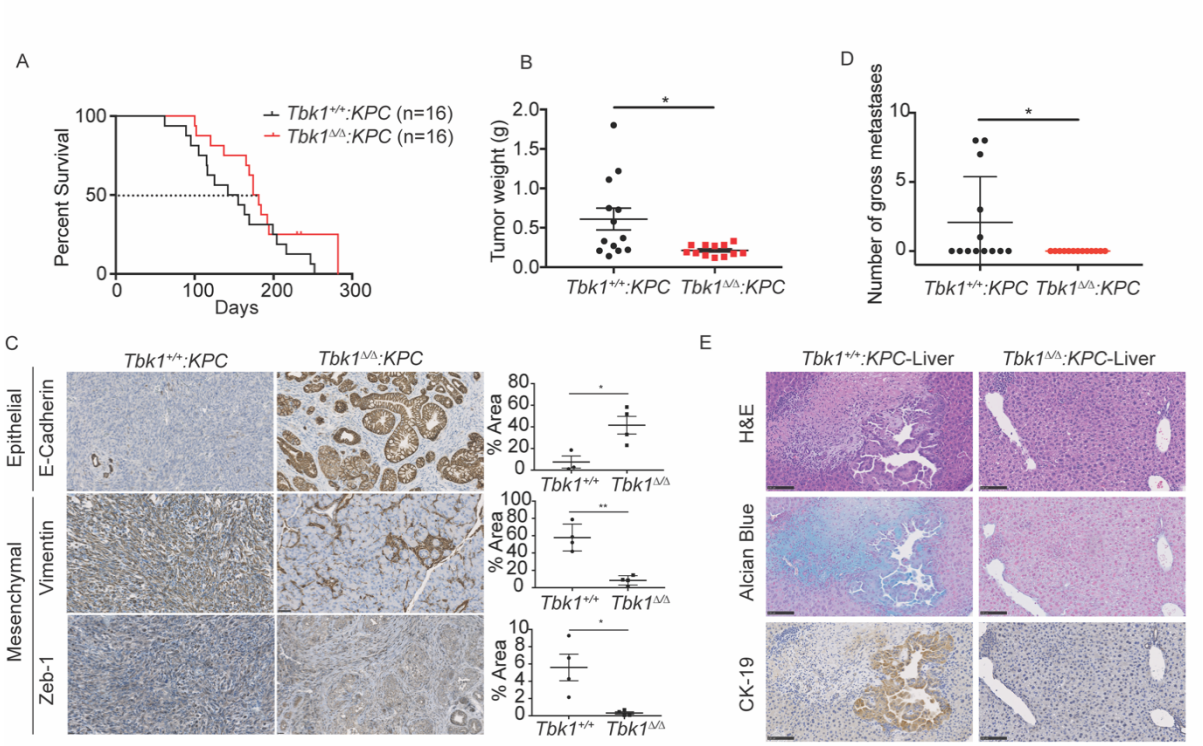

Figure 11. Loss of functional Tbk1 reduces metastasis. A) Kaplan-Meier survival curve of Tbk1Δ/Δ: KPC and Tbk1+/+: KPC mice (n = 16 mice/group). A log-rank Mantel-Cox test was used for survival comparison, p = 0.15. **B)** Tumor weights of Tbk1Δ/Δ: KPC and Tbk1+/+: KPC mice. **C)** Representative 20X images from E-Cadherin, Vimentin, and Zeb-1 stained tumors from Tbk1Δ/Δ: KPC and Tbk1+/+: KPC mice. Images were quantified by percent DAB divided by percent hematoxylin area; n ≥ 4 mice/group. **D)** Number of gross metastases in Tbk1Δ/Δ: KPC and Tbk1+/+: KPC mice (n=13 mice/group). **(E)** Representative liver histology in Tbk1Δ/Δ: KPC and Tbk1+/+: KPC mice including H&E, alcian blue, and CK19 immunohistochemical staining. Scale bar indicates 100 µm, images were taken at 20X magnification. Unpaired two-tailed t test, *p < 0.05, ***p < 0.001, ****p < 0.0001.

KPC animals relative to *Tbk1*$^{+/+}$: *KPC* animals **(Figure 11B)**. While we did not investigate the immune landscape of the PDA GEMMs, we did find via gene expression analysis that *Tbk1*$^{\Delta/\Delta}$*: KIC* tumors displayed a higher expression of a number of pro-inflammatory genes relative to *Tbk1*$^{+/+}$*: KIC* tumors **(Figure 12)**. The elevated pro-inflammatory gene expression in *Tbk1*$^{\Delta/\Delta}$*: KIC* tumors could be indicative of a heighted antitumor immune response to some degree, resulting in smaller tumors.

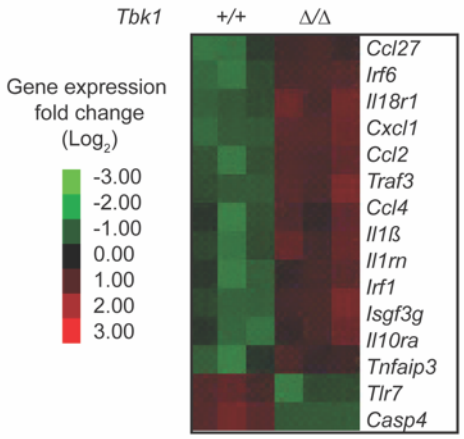

Figure 12. Tbk1Δ/Δ: KIC tumors contain higher pro-inflammatory gene expression than Tbk1+/+: KIC tumors. Heatmap representing gene expression fold change (log2) of inflammatory genes from Tbk1Δ/Δ: KIC and Tbk1+/+: KIC tumors. Color key indicates gene expression fold change; n = 3 tumors/genotype, $p < 0.05$ for all genes between Tbk1Δ/Δ: KIC and Tbk1+/+: KIC tumors.

Like the *KIC* model, *Tbk1*$^{\Delta/\Delta}$: *KPC* tumors showed significantly greater levels of E-cadherin, whereas *Tbk1*$^{+/+}$: *KPC* tumors showed significantly higher expression of mesenchymal markers such as Vimentin and Zeb-1, indicating *Tbk1*$^{\Delta/\Delta}$: *KPC* tumors to be more epithelial

relative to *Tbk1*$^{+/+}$: *KPC* tumors (**Figure 11C**). Liver and lung metastases were evaluated grossly (**Figure 11D)** and by H&E, alcian blue, and CK19 immunohistochemical staining **(Figure 11E)**. As expected, ~40% of *Tbk1*$^{+/+}$: *KPC* mice were positive for metastasis, but strikingly, no metastatic lesions were detected in *Tbk1*$^{\Delta/\Delta}$: *KPC* mice. To confirm the EMT phenotype of the tumor cells, we again isolated single cell clones from individual *Tbk1*$^{+/+}$: *KPC* and *Tbk1*$^{\Delta/\Delta}$: *KPC* tumors. Consistent with gene expression data from *Tbk1*$^{+/+}$: *KIC* tumor cell lines, evaluation of EMT-related markers revealed higher expression of the epithelial protein, ZO-1 and lower expression of the mesenchymal proteins Slug and Zeb-1 in *Tbk1*$^{\Delta/\Delta}$: *KPC* cell lines **(Figure 13)**. These data suggest loss of functional *Tbk1* in the *KPC* GEMM restricts tumor cell metastases.

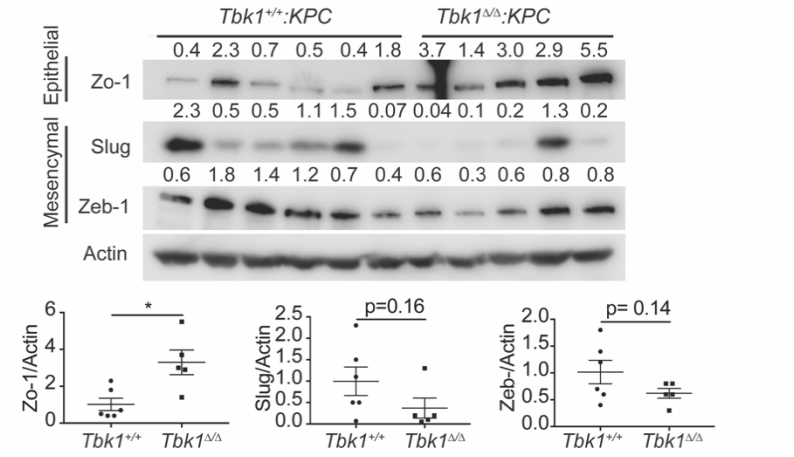

Figure 13. Tbk1 promotes mesenchymal protein expression in KPC cell lines. Protein lysates isolated from Tbk1+/+: KPC and Tbk1Δ/Δ: KPC cell lines were immunoblotted for indicated epithelial and mesenchymal markers. Actin was used as a loading control. Signal intensity of each sample was quantified and normalized to the mean Tbk1+/+: KPC signal. Results are representative of mean +/- SEM. Unpaired two-tailed t test, *p < 0.05.

Re-expression of *Tbk1* in *Tbk1$^{\Delta/\Delta}$*: *KIC* cells

To confirm that TBK1 promotes pancreatic tumor cell motility, we stably re-expressed full-length human *TBK1* by lentiviral infection in *Tbk1$^{\Delta/\Delta}$: KIC* tumor cells and assayed them for invasive and migratory activity. Re-expression of *TBK1* in *Tbk1$^{\Delta/\Delta}$: KIC* tumor cells was confirmed by Western blot **(Figure 14A)**. Though the level of *TBK1* re-expression in *Tbk1$^{\Delta/\Delta}$: KIC* tumor cell lines was substantially lower than endogenous TBK1 levels in *Tbk1$^{+/+}$*: *KIC* cell lines, we did detect a rescue of the mesenchymal morphology in *Tbk1$^{\Delta/\Delta}$: KIC* cells infected with TBK1-expressing lentivirus (pCDH-TBK1) compared to empty vector-expressing (pCDH-empty vector) cells **(Figure 14B, Figure 15)**. Further, *Tbk1$^{\Delta/\Delta}$: KIC* cell lines rescued with pCDH-TBK1 formed 2-3x as many lung tumor nodules, resulting in greater diseased lung burden than pCDH-empty vector-infected cells after i.v. injection **(Figure 14C-E**). These results demonstrate that *Tbk1* loss is responsible for the migratory and invasive deficiency in *Tbk1$^{\Delta/\Delta}$*: *KIC* cells and highlight a novel function for TBK1 in promoting a migratory program in tumor cells.

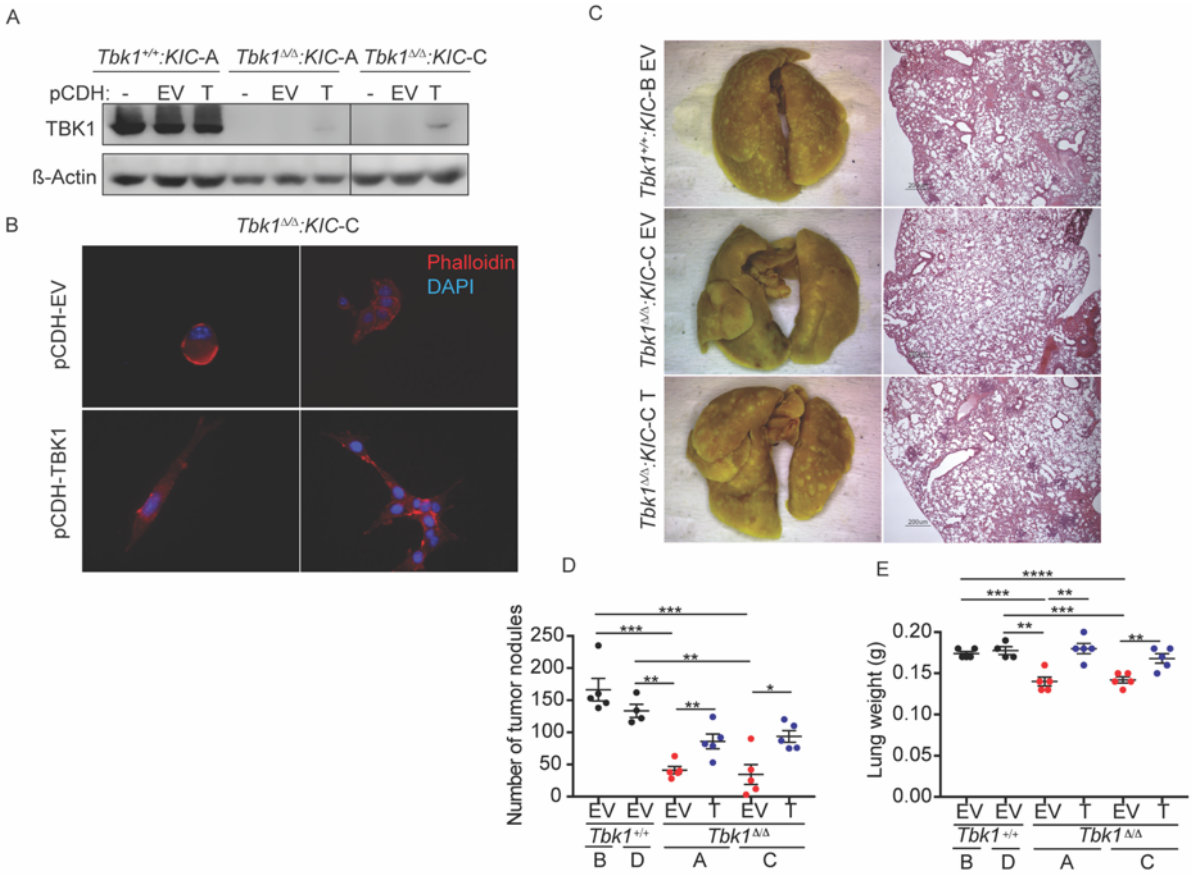

Figure 14. Re-expression of Tbk1 partially reverses colonization deficit in Tbk1Δ/Δ: KIC cells. **A)** Protein lysates from Tbk1Δ/Δ: KIC and Tbk1+/+: KIC cell lines infected with pCDH-empty vector (EV) or pCDH-TBK1 (T) were immunoblotted for TBK1. β-actin was used as a loading control. Solid line indicates where blot was cropped; however, all samples were run on the same gel and exposed simultaneously. **B)** Representative images of Tbk1Δ/Δ: KIC-C cells infected with EV or T plated on a mixed layer of collagen and Matrigel. Cells were fixed and Nuclei were labeled with DAPI (blue); actin was labeled with phalloidin (red). **C)** Representative images of lungs and 20X H&E from NOD SCID mice sacrificed 7 days after i.v. injection with Tbk1: KIC EV and T-cell lines (100,000 cells injected per mouse, n = 4-5 mice/group). **D)** Number of tumor nodules from **(C)**. **E)** Lung weights from **(C)**. Results are representative of mean +/- SEM. Unpaired two-tailed t test, *$p < 0.05$, **$p < 0.01$, ****$p < 0.0001$.

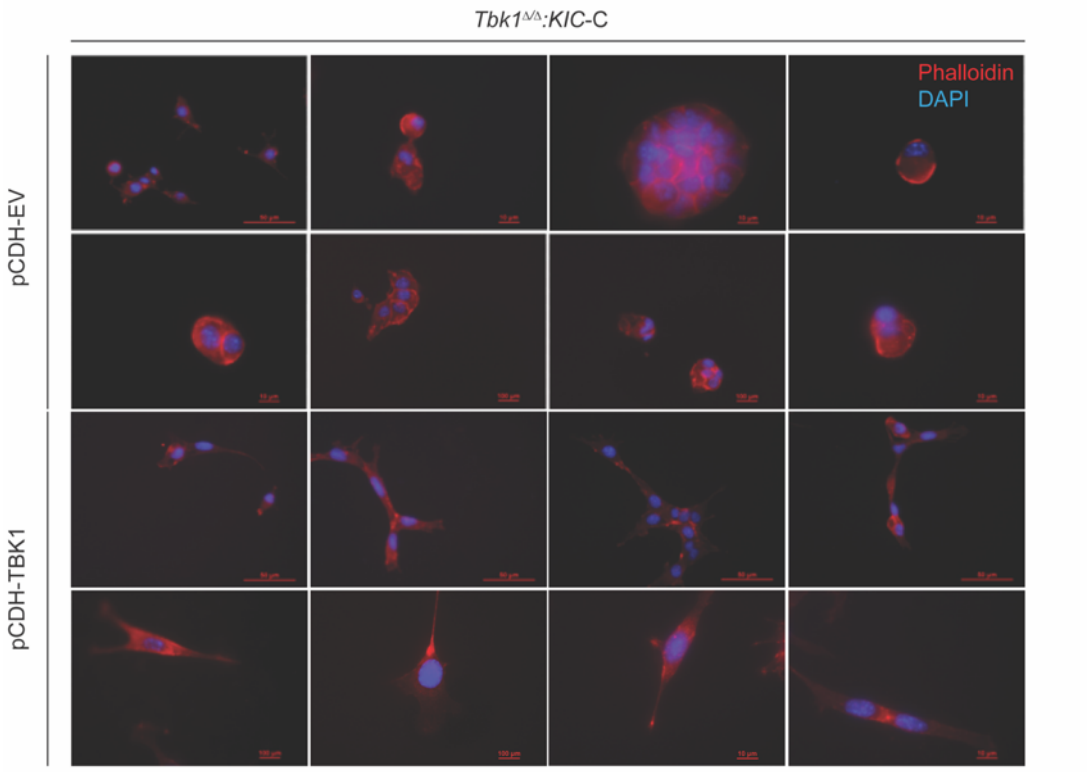

Figure 15. TBK1 re-expression drives a mesenchymal morphology in Tbk1Δ/Δ: KIC cell lines. Representative images of Tbk1Δ/Δ: KIC-C cells infected with lentiviral empty vector (EV) or full-length TBK1 (T) plated on a mixed layer of collagen and Matrigel. Cells are fixed and nuclei are labeled with DAPI (blue) and F-actin is labeled with phalloidin (red).

TBK1 is central to AXL-driven epithelial plasticity

Pancreatic tumor cells frequently exploit EMT programs during metastatic dissemination (Krebs et al., 2017; Ostapoff et al., 2014). However, the absence of functional TBK1 in pancreatic tumor cells limits EMT, invasion, and metastases. We recently reported that TBK1 is downstream of the receptor tyrosine kinase AXL, a receptor associated with EMT in PDA (Kirane et al., 2015; Ludwig et al., 2018). Pharmacological inhibition of AXL led to a concentration-dependent decrease of TBK1 activity while the stimulation of AXL with its ligand, Gas6, resulted in TBK1 activation (Ludwig et al., 2018). To determine if TBK1 is

central to AXL-driven EMT, we evaluated AXL signaling in *Tbk1$^{\Delta/\Delta}$: KIC* tumor cells. AXL was stimulated in *Tbk1$^{\Delta/\Delta}$: KIC* and *Tbk1$^{+/+}$: KIC* cells with AF854, an activating anti-AXL antibody (Zagorska et al., 2014), and the resulting cell lysates were probed for epithelial (E-cadherin, claudin-1), mesenchymal (N-cadherin, Slug) and AXL signaling targets (AKT). AXL activation induced N-Cadherin and Slug protein by 2–3-fold in *Tbk1$^{+/+}$: KIC* tumor cells while having no effect on mesenchymal markers in *Tbk1$^{\Delta/\Delta}$: KIC* tumor cells **(Figure 16A)**.

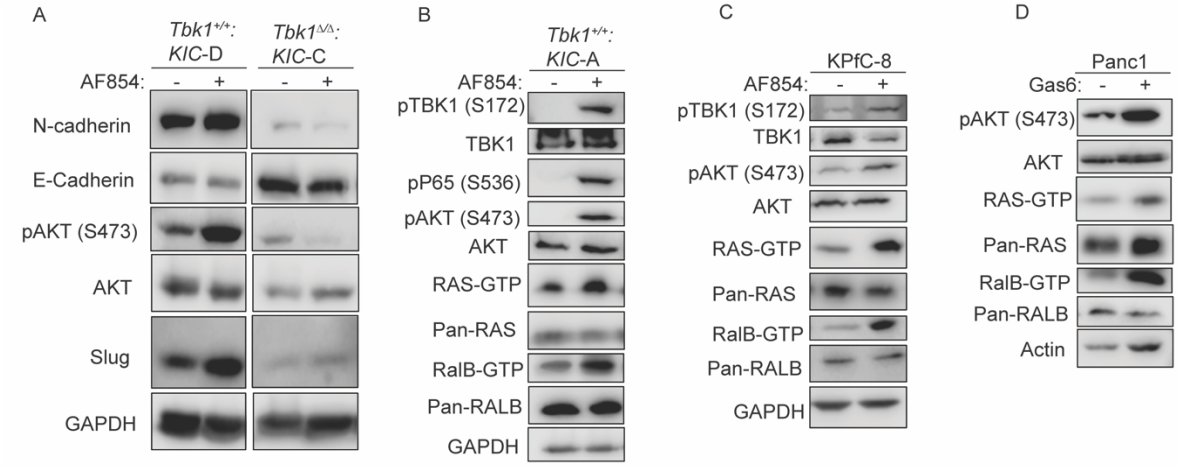

Figure 16. Tbk1 promotes epithelial plasticity downstream of Axl. A) Protein lysates from Tbk1: KIC cell lines treated with PBS or AF854 (6 nM) for 30 min were immunoblotted for indicated proteins and quantified. **B)** Protein lysates from Tbk1: KIC-A cells treated with PBS or AF854 (6 nM) for 30 min were assayed for active Ras and active RalB and immunoblotted for indicated proteins and quantified. **C)** Protein lysates isolated from KPfC-8 cells treated with PBS or AF854 (6 nM) for 30 min were assayed for active Ras, active RalB, and immunoblotted for indicated proteins and quantified. **D)** Protein lysates from Panc-1 cells treated with PBS or 200ng/mL Gas6 for 30 min were assayed for active Ras, active RalB, and immunoblotted for indicated proteins and quantified. GAPDH and actin were used as loading controls. Western blots displayed are representative of n > 3 repeats for each activation assay.

Furthermore, pAKT levels increased 5-fold in *Tbk1*$^{+/+}$*: KIC* cells and remained unaltered in *Tbk1*$^{\Delta/\Delta}$*: KIC* tumor cells upon AF854 treatment, indicating that TBK1 may be upstream of AKT. Next, we investigated AXL-induced RAS activation in *Tbk1*$^{+/+}$*: KIC* cell lines as a possible link between the AXL and TBK1 signaling cascade. *Tbk1*$^{+/+}$*: KIC-A* cells treated with AF854 showed a substantial increase of GTP-bound RAS, demonstrating that RAS activity is augmented by AXL activation **(Figure 16B)**. These results were confirmed by using GTP and GDP loading as positive and negative controls, respectively (**Figure 17A**). The activation of RAS with AF854 was also confirmed by inhibiting AXL, using BGB324, an established inhibitor of AXL activity (Ludwig et al., 2018) (**Figure 17B**). Previous work has shown a RalB GTPase-mediated activation of TBK1 (Chien et al., 2006); therefore, we tested if AXL-

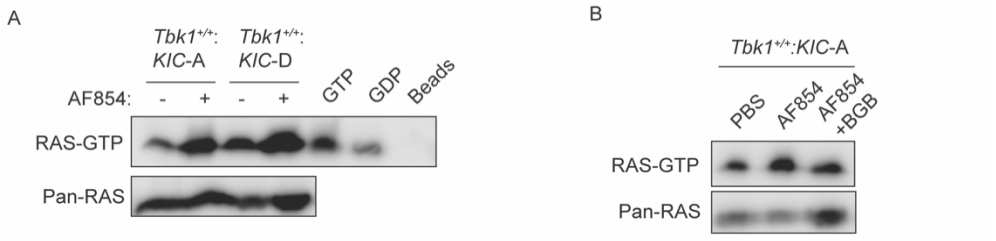

Figure 17. Axl-activating antibody AF854 stimulates Ras activity. A) Protein lysates from Tbk1+/+: KIC-A and Tbk1+/+: KIC-D cells treated with PBS or AF854 (6nM) for 30 min were assayed for active Ras and Pan-Ras. GTP and GDP protein loading were used as positive and negative controls, respectively. **B)** Protein lysates isolated from Tbk1+/+: KIC-A cells treated with either PBS, AF854 (6nM), or AF854 (6nM) + BGB324 (BGB, 2 μM) for 30 min were assayed for active Ras and Pan-Ras.

induced activation of RAS could increase GTP-bound RalB, mediating the activation of TBK1. *Tbk1*$^{+/+}$*: KIC-A* cells treated with AF854 showed a 3-fold increase in RalB-GTP, demonstrating that RalB activity is increased upon AXL activation **(Figure 16B)**. AXL-induced Ras and RalB activation was validated in an additional murine PDA cell line, KPfC-8, derived from a spontaneous tumor in the *KPfC (Kras*$^{LSL\text{-}G12D/+}$; *Trp53*$^{lox/lox}$*; Ptf1a*$^{Cre/+}$) GEMM of PDA **(Figure 16C)**. To extend and confirm these findings in human pancreatic cancer, we stimulated Panc-1 cells with Gas6, which we previously demonstrated increases TBK1 activity (Ludwig et al., 2018), and detected an increase in GTP-bound Ras and RalB **(Figure 16D)**. These results are the first to show that AXL activates RAS and RalB, which leads to downstream activation of TBK1 and AKT, ultimately resulting in increased EMT and a more aggressive and metastatic tumor cell phenotype.

CHAPTER FOUR
Results

AXL-TBK1 DRIVEN NUCLEAR AKT3 STABILIZES SNAIL/SLUG TO DRIVE EMT

AKT3 promotes EMT via TBK1

AXL activation promotes tumor cell migration and invasion (H. J. Lee et al., 2014). Consistent with this, *AXL* mRNA expression correlates with EMT and stem cell-related gene expression in breast cancer cell lines and patient breast carcinoma biopsies, but not normal breast tissue **(Figure 18A-C)**. Furthermore, IHC analysis of patient primary breast tumor biopsies revealed AXL protein expression correlates with expression of mesenchymal markers N-cadherin and twist2 **(Figure 18D)**. Interestingly, analysis of publicly available GEO RNA sequencing data of breast cancer cell lines showed that while *AXL* and *AKT3* correlate significantly, *AXL* and *AKT1* or *AKT2* do not **(Figure 19A)**. Similar results were found by analyzing the correlation of AKT isoforms and AXL in human breast cancer using gene expression profiling interactive analysis (GEPIA) in invasive breast carcinoma (BRCA) from the TCGA database **(Figure 20A)** (Tang et al., 2017). *AKT1* and *AKT2* showed no correlation with *AXL*, whereas *AKT3* correlated significantly with *AXL* expression in BRCA (*p*-value = 4.4e-110, R = 0.61).

AKT is a key regulator of many cellular phenotypes associated with cancer, including cell survival, proliferation, and metastasis (Bellacosa, Testa, Staal, & Tsichlis, 1991). Activation of AKT can drive EMT via the induction of EMT transcription factors (EMT-TFs) including

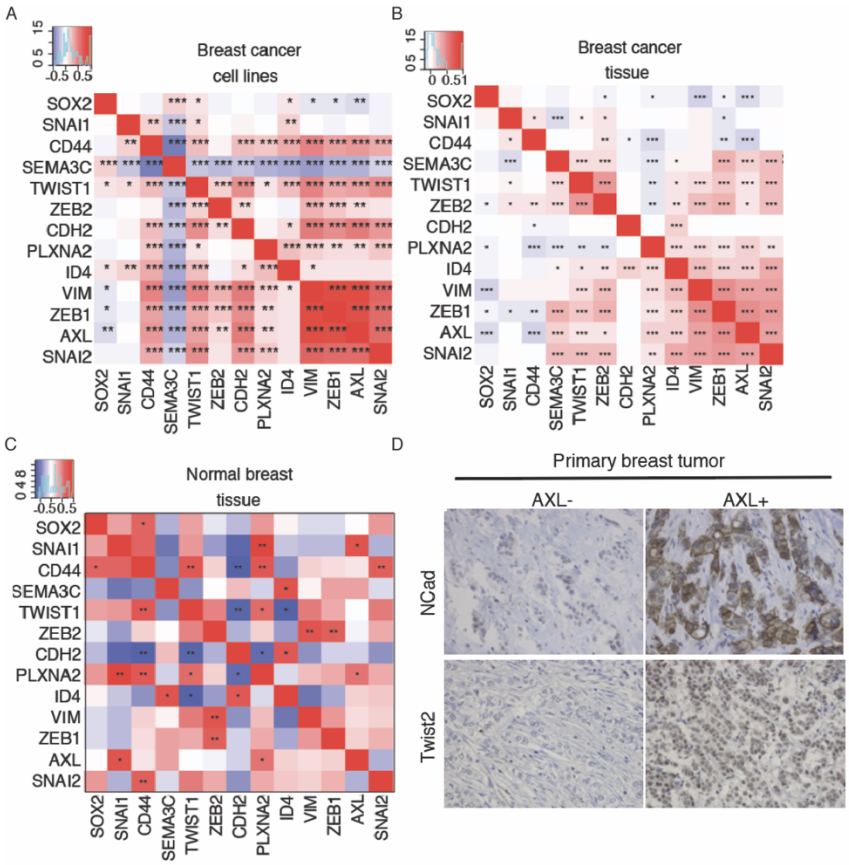

Figure 18. AXL signaling is required for EMT in breast cancer.
A-C) AXL mRNA correlates with EMT and stem cell-related gene expression in breast cancer cell lines **(A)**, breast carcinoma biopsies **(B)** and normal breast tissue **(C)**. Positive correlation values are demarcated as red and negative correlation values are shown as blue (* $p<0.045$, ** $p<0.009$, *** $p <2x10\text{-}5$; Spearman's correlation test). D) IHC of patient primary breast tumor biopsies with strong AXL expression correlate with EMT marker N-cadherin and twist2 expression.

snail and slug, which transcriptionally repress E-cadherin and induce vimentin, twist1, MMP-2, and MMP-9 that promote tumor cell invasion (Grille et al., 2003; Larue & Bellacosa, 2005; Xu et al., 2015). There are three mammalian AKT isoforms (AKT1, AKT2, and AKT3). While each isoform is encoded by distinct genes, there is ~80% amino acid sequence identity and are activated by similar mechanisms (Irie et al., 2005; Woodgett, 2005). Although the function of AKT in cancer cell survival and growth has been well

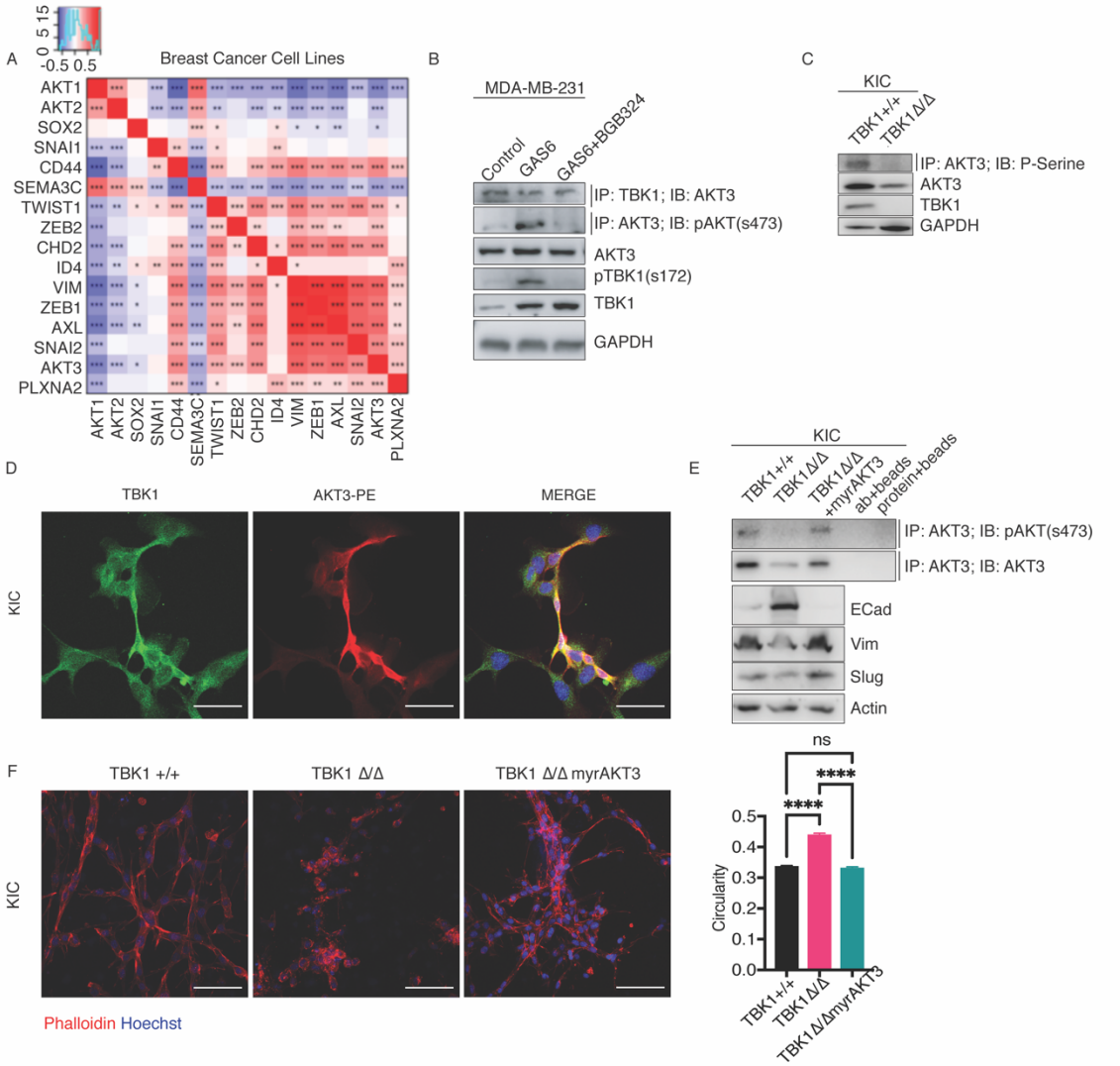

Figure 19. AKT3 promotes EMT via TBK1. A) Correlation of AKT1, AKT2, and AKT3 mRNA with EMT and stem genes in breast cancer cell lines. Positive correlation values are demarcated as red and negative correlation values are shown as blue (* p<0.045, ** p<0.009, *** p <2x10-5; Spearman's correlation test). **B)** MDA-MB-231 cells were stimulated with DMSO, GAS6 (200 ng/ml) +/- 2 μM BGB324. Immunoprecipitation of AKT3 was probed for pAKT(s473) and immunoprecipitation of TBK1 was probed for AKT3. Total lysates were probed for AKT3, pTBK1 (s172), TBK1 and GAPDH (loading control). **C)** Immunoprecipitation of AKT3 in primary TBK1 WT and deficient KIC PDA cells probed for total phospho-serine. Total lysates were probed for AKT3, TBK1 and Actin (loading control). **D)** Immunofluorescence of TBK1 (green), AKT3 (Red), and DAPI (blue) in TBK1 WT KIC PDA cells. Cells were imaged at 20X using confocal microscopy. Scale bar, 50 μm. **E)** Immunoprecipitation of AKT3 in TBK1+/+, TBK1Δ/Δ, and TBK1Δ/Δ KIC PDA cell lines transduced with myrAKT3 (TBK1Δ/Δ-myrAKT3). AKT3 immunoprecipitation was probed for pAKT (s473) and total AKT3. Cell lysates were probed for E-Cadherin, vimentin, slug and actin (loading control). Immunoprecipitation controls without protein or antibody are shown. **F)** TBK1+/+, TBK1Δ/Δ, and TBK1Δ/Δ-myrAKT3 cells were plated in Collagen/Matrigel and stained for Phalloidin (red) and hoechst (blue). Z-stack (1 μm) Images were taken by confocal microscopy at 20X magnification. Scale bar, 100 μm. Circularity of cells was calculated using ImageJ. n > 500 cells/condition. All statistics were done using one-way ANOVA; * p<0.05, ** p<0.01, *** p <0.001, **** p <0.0001. All representative results shown were reproduced in at least three independent experiments.

characterized, the contribution of different AKT isoforms has not been investigated as intensely and is often under appreciated. Based on a phosphoproteomics screen, AKT isoforms have specific expression patterns and serve different functions in cell signaling and cancer (Sanidas et al., 2014). Although it is the less studied of the isoforms, AKT3 has been implicated in various aspects of EMT, including tumor progression, DNA damage repair response, and drug resistance (Chin et al., 2014; F. M. Lin et al., 2019; Toulany et al., 2017; Turner et al., 2015).

Consistent with AXL and AKT3 correlation, forced expression of slug in the epithelial breast line, MCF10a, drives EMT and induces AXL and AKT3 expression, while AKT1 and AKT2 levels were not elevated **(Figure 20B)**. Additionally, when AXL was knocked down in these cells, AKT3 was no longer expressed **(Figure 20B)**, supporting the correlation between AXL and AKT3.

To investigate the function of AKT isoforms in EMT, MCF10a cells were treated with TGFβ, a potent EMT inducer, for 4 days, after which each AKT isoform was immunoprecipitated and probed for phosphorylation (S473). We found that TGFβ-induced EMT results in phosphorylation of AKT3, but not AKT1 or AKT2, supporting that AKT3 is selectively associated with EMT **(Figure 20C**). Given the correlation of AKT3 with AXL and EMT, we sought to determine if AKT3 contributes to AXL-mediated EMT. To mimic constitutively active AKT1 or 3, MCF10a cells were transduced with retroviral vectors expressing myristoylated AKT1 (myrAKT1) or myristoylated AKT3 (myrAKT3) and

analyzed for changes associated with EMT (protein expression and morphology, **Figure 20D, E**). Transduction of myrAKT1 did not alter cellular phenotype. However, myrAKT3 transduction resulted in robust changes in cell phenotype as well as EMT protein changes. Expression of AXL and mesenchymal markers vimentin and N-cadherin were elevated and the cells displayed a more invasive and mesenchymal-like morphology in 2D and 3D (embedded in matrigel), suggesting constitutively active AKT3 can drive EMT **(Figure 20D, E)**. To investigate if AKT3 is activated downstream of AXL, PANC1 cells were treated with DMSO, GAS6, or GAS6 and a neutralizing monoclonal anti-AXL antibody, tilvestamab. Probing for pAKT3 indicated that AKT3 can be activated in an AXL specific manner **(Figure 20F)**.

Our prior studies established that TBK1 promotes EMT downstream of AXL in PDA (Cruz et al., 2019). Although the mechanism by which TBK1 drives EMT remains unclear, prior evidence shows that TBK1 can directly activate AKT (Bellacosa et al., 1991; Ou et al., 2011). Given our previous findings that AKT is activated downstream of AXL in a TBK1-dependent manner (Cruz et al., 2019) we hypothesized that TBK1 binds to and activates AKT3 to drive EMT downstream of AXL. To test this, we treated MDA-MB-231 cells with DMSO, GAS6, or GAS6 plus BGB324 (R428; bemcentinib), a small molecular inhibitor of AXL (Holland et al., 2010; Ludwig et al., 2018). Immunoprecipitation of AKT3 revealed that TBK1 binds to AKT3, and that AXL stimulation results in AKT3 phosphorylation **(Figure 19B)**. Furthermore, BGB324 inhibited GAS6-induced activation of TBK1 and AKT3. To investigate TBK1-AKT3 interaction further, we used primary cell lines developed from

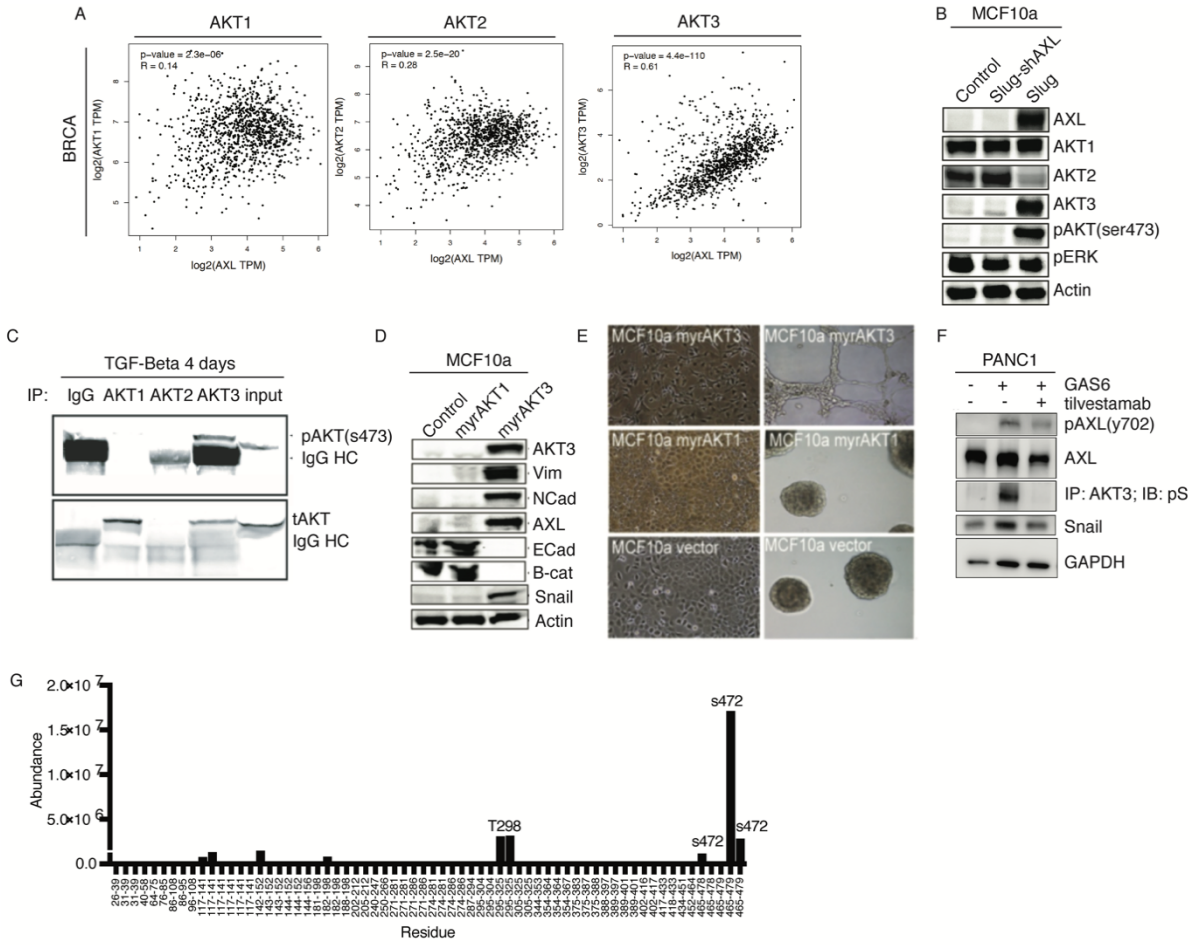

Figure 20. AKT3 is associated with EMT and breast tumor initiation. A) Gene expression correlation of AKT isoforms and AXL using GEPIA (Gene expression profiling interactive analysis) in invasive breast carcinoma (BRCA) and pancreatic adenocarcinoma (PAAD) tumors from the TCGA and GTEx databases. **B)** Protein level of AKT isoforms (AKT-1,-2,-3), Axl, total phosphorylated AKT S473 (pAKT) and ERK1/2 (pERK) in MCF10a -expressing slug, or control vector, and MCF10a/slugand HMLER/slug cells transduced with shAXL or shLuc retroviral vector. **C)** Immunoprecipitation of AKT isoforms (AKT-1,-2,-3) from MCF10a cell extracts after TGF-treatment (10 ng/ml, 4 days) followed by Western blot for phospho-AKT S473 show that AKT3 is the main phosphorylated AKT isoform. **D)** MCF10a cells were transduced with retroviral vectors that express myrAKT1 or myrAKT3 and analyzed for AXL, epithelial (E-cadherin) and mesenchymal (vimentin, N-cadherin) marker expression, AKT1/3 and pAKT levels. **E)** Phase contrast images of MCF10a cells in 2D tissue culture plates (left) and matrigel (right). **F)** PANC1 cells were stimulated with DMSO, GAS6 (200 ng/ml) +/- anti-AXL tilvestamab. Immunoprecipitation of AKT3 was probed for total phosphorylated serine. Total lysates were probed for pAXL y702, total AXL, snail, and GAPDH (loading control). **G)** In-vitro kinase activity assay of human recombinant TBK1 and AKT3 using cold ATP. PTM mass-spec analysis revealed that TBK1 phosphorylates AKT3 at serine 472. Residue abundance of recombinant AKT3 alone was subtracted from residue abundance of activated AKT3. All representative results shown were reproduced in at least three independent experiments.

genetically engineered mouse models (GEMMs) of pancreatic cancer, *TBK1*$^{+/+}$ *KIC* (*Kras*$^{LSL-G12D/+}$ *; Cdkn2a*$^{Lox/Lox}$ *; Ptf1a*$^{Cre/}$) or *TBK1-mutant* (*TBK1*$^{\Delta/\Delta}$) *KIC* mice (Cruz et al., 2019). We found that AKT3 is phosphorylated in *TBK1*$^{+/+}$ *KIC* cells but not in *TBK1*$^{\Delta/\Delta}$ *KIC* cells **(Figure 19C)**, supporting the hypothesis that TBK1 can activate AKT3. We next assessed the co-expression of AKT3 and TBK1 in *KIC* PDA cell lines using immunofluorescence and confocal microscopy **(Figure 19D)**. To investigate if TBK1 can directly bind to and activate AKT3 we performed an in vitro kinase activity assay with human recombinant active TBK1 and AKT3 using cold ATP. Mass-spectrometry analysis confirmed that TBK1 directly phosphorylates AKT3 at serine 472 **(Figure 20G)**.

To investigate if AKT3 induces EMT downstream of TBK1, we transduced *KIC TBK1*$^{\Delta/\Delta}$ cells with myrAKT3 (*TBK1*$^{\Delta/\Delta}$/myrAKT3) and found that myrAKT3 rescues expression of mesenchymal markers, vimentin and slug, and decreases the expression of E-cadherin **(Figure 19E)**, demonstrating that myrAKT3 induces a mesenchymal-like phenotype in TBK1-mutant PDA cells. To evaluate if the protein changes seen in Figure 19E result in a phenotypic change, we cultured *TBK1*$^{+/+}$, *TBK1*$^{\Delta/\Delta}$, and *TBK1*$^{\Delta/\Delta}$/myrAKT3 *KIC* cells in collagen/matrigel and found that *TBK1*$^{+/+}$ cells were invasive with elongated morphology while *TBK1*$^{\Delta/\Delta}$ cells were epithelial and less elongated **(Figure 19F)**. Interestingly, *TBK1*$^{\Delta/\Delta}$/myrAKT3 cells reverted to a mesenchymal-like morphology, similar to *TBK1*$^{+/+}$ cells, suggesting constitutively active AKT3 is sufficient to drive EMT, even in the absence

of TBK1. These data support that AKT3 is downstream of TBK1 and is required for TBK1 driven EMT.

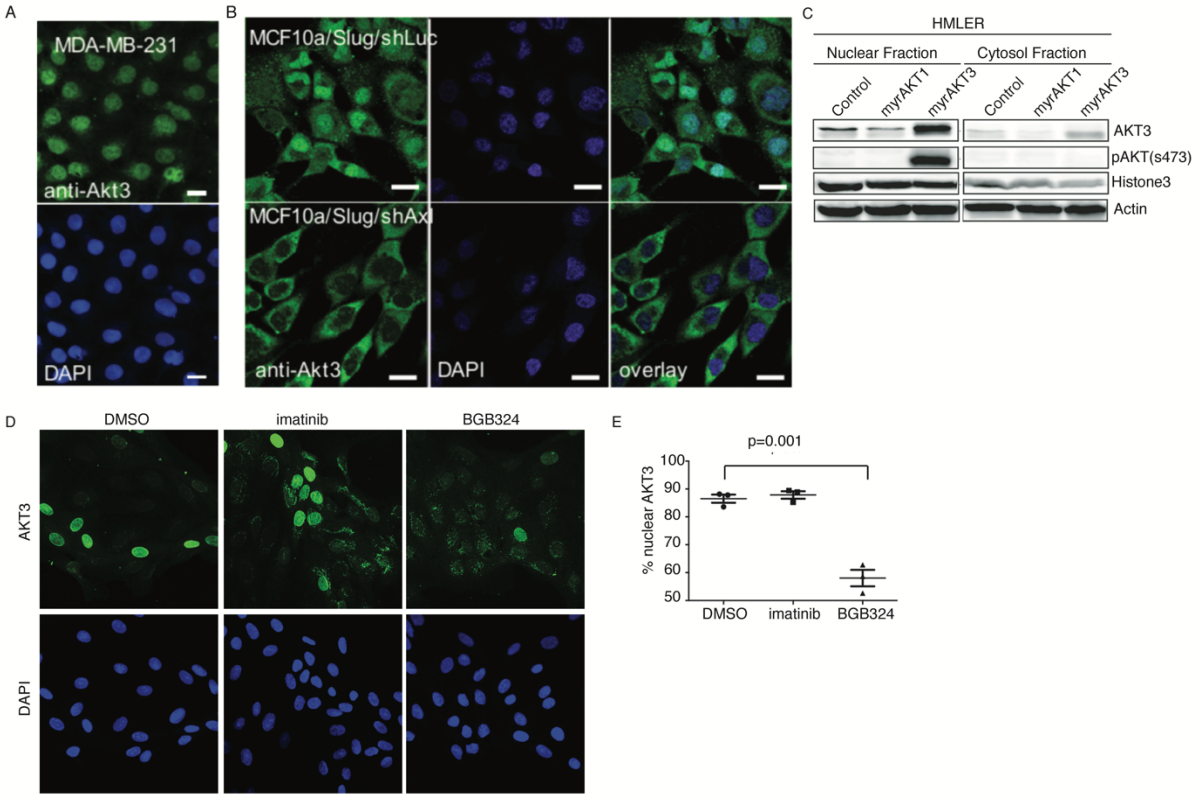

Figure 21. EMT requires AXL dependent activation of nuclear localized AKT3. A) Subcellular localization of endogenous AKT3 (anti-AKT-FITC, green) in MDA-MB231 by immunofluorescence. Nucleus: DAPI (blue). Scale bar, 50 µm. **B)** Immunofluorescence analysis of AKT3 (anti-AKT3-FITC, green) MCF10a/slug cells after transfection with shAXL or shLuc retroviral vectors. Scale bar, 20 µm. **C)** Western blot analysis of AKT1/3, pAKT levels and nuclear marker protein histone 3 in nuclear and cytoplasmic cell fractions from HMLER cells transduced with retroviral vectors encoding myrAKT1, myrAKT3 or control vector. **D, E)** Nuclear localization **(D)** and quantification **(E)** of AKT3 in AXL-expressing mammary epithelial progenitor cells requires AXL but not ABL/CKIT/PDGFR activity. cKit+ AXL+ HMEC cells treated with vehicle (DMSO), 1 µM imatinib, or 600 nM BGB324 for 24 hrs and analyzed by immunofluorescence (anti-AKT3-FITC, green). Nucleus: DAPI (blue). Scale bar, 50 µm. %nuclear AKT3 shown as mean ± S.E.M. from 3 x 25,000 cells/coverslip, in triplicate; p=0.001, t-test. All representative results shown were reproduced in at least three independent experiments.

AXL-TBK1 is required for AKT3 nuclear localization.

It has been reported that while AKT1 and AKT2 are found in the cytoplasm and mitochondria, respectively, AKT3 is often found in the nucleus (Santi & Lee, 2010). We observed clear nuclear localization of AKT3 in MDA-MB-231 and MCF10a/slug cells

(Figure 21A, B). Interestingly, AXL silencing in MCF10a/slug cells reduced AKT3 nuclear localization, suggesting that AXL mediates the nuclear localization of AKT3 **(Figure 21B)**. These data were validated further with cell fractionation experiments where AKT3 was detected in nuclear fractions of MDA-MB-231 cells **(Figure 22A)** and HMLER cells transduced with myrAKT3 **(Figure 21C)**.

To determine if TBK1 contributes to the nuclear localization of AKT3 immunofluorescence of AKT3 in *TBK1*$^{+/+}$, *TBK1*$^{\Delta/\Delta}$, and *TBK1*$^{\Delta/\Delta}$/myrAKT3 *KIC* and MDA-MB-231 cells **(Figure 22B, C)** was performed. The percentage of cells with nuclear AKT3 was reduced ~80% in the absence of functional TBK1 in *KIC* cells. This effect was partially rescued by myrAKT3, suggesting that AKT3 activation by TBK1 contributes to AKT3 nuclear localization. Furthermore, when MDA-MB-231/GFP cells were treated with BGB324 to inactivate AXL, thereby preventing TBK1 activation, AKT3 did not translocate to the nucleus **(Figure 22D)**. To investigate how AXL affects nuclear localization of AKT3, MDA-MB-231 **(Figure 22E)** and PANC1 **(Figure 22F)** cells were treated with serum free media (SFM), GAS6, or GAS6 + BGB324 for 12 hrs **(Figure 22G)**. Immunocytochemistry for AKT3 in MDA-MB-231 cells demonstrated that AKT3 was nuclear localized in 15.9% of cells treated with serum free media (SFM) while GAS6 treatment resulted in 47.1% of cells showing nuclear AKT3 **(Figure 22E)**. In contrast, AXL inhibition with BGB324, decreased nuclear AKT3 to only 2.9% of cells, supporting that AXL stimulation induces the nuclear localization of AKT3. Similar effects were observed in PANC1 cells **(Figure 22F)**. To demonstrate that inhibition of AKT3 nuclear localization is not a general phenomenon

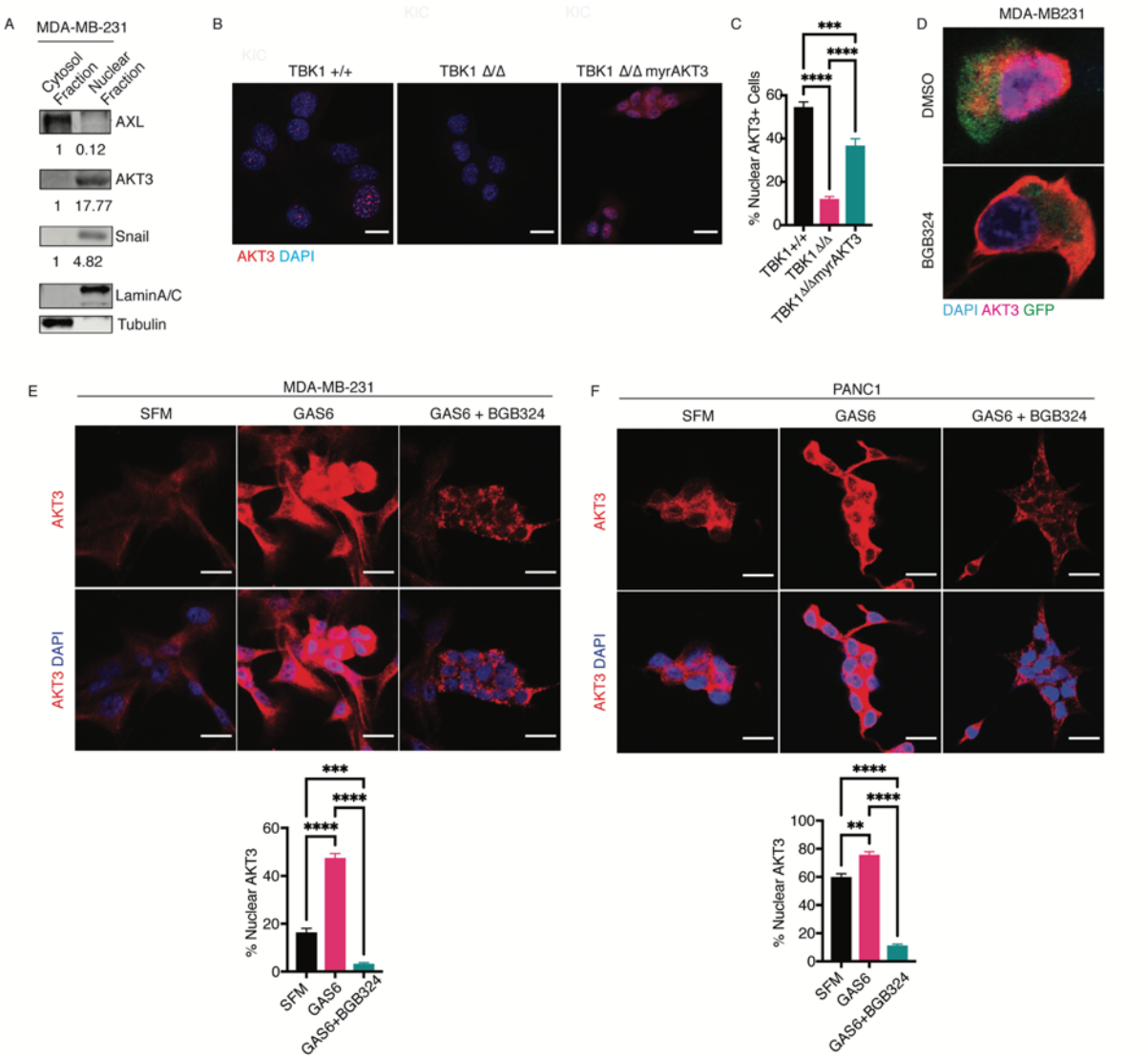

Figure 22. AXL-TBK1 is required for AKT3 nuclear localization. A) Western blot analysis of AXL, AKT3, snail, lamin A/C and tubulin in MDA-MB-231 nuclear and cytoplasmic cell fractions. Protein expression was quantified and normalized to protein in the cytosol. **B-C)** Immunofluorescence of AKT3 (Red) and DAPI (blue) in TBK1+/+, TBK1Δ/Δ, and TBK1Δ/Δ-myrAKT3 KIC PDA cells. Percent of cells with nuclear AKT3 is graphed in **(C)**. Scale bar, 20 µm. **D)** Immunofluorescence of MDA-MB-231/GFP cells treated with DMSO or BGB324. Cells are stained with AKT3 (red) and nuclei are stained with DAPI (blue). **E-F)** Immunofluorescence of TBK1 (green), AKT3 (Red), and DAPI (blue) in MDA-MB-231 **(E)** and PANC1 **(F)** cells treated with SFM, 200 ng/mL GAS6 +/- 2 µM BGB324 for 12hrs. Cells were imaged at 20X using confocal microscopy. Scale bar, 20 µm. Percent of cells with nuclear AKT3 are graphed below each cell type, n>200 cells. All representative results shown were reproduced in at least three independent experiments. All statistics were done use one-way ANOVA; * $p<0.05$, ** $p<0.01$, *** $p<0.001$, **** $p<0.0001$

associated with RTK inhibition, HMECs were treated with imatinib, an inhibitor of ABL/CKIT/PDGFR. BGB324 reduced nuclear AKT3 but the imatinib did not **(Figure 21D, E)**.

Proteins over 40 kDa must be actively transported through the nuclear membrane by importins, which recognize and bind nuclear location sequences (NLS) (Wente & Rout, 2010). We used a web-based NLS mapper (Kosugi, Hasebe, Tomita, & Yanagawa, 2009) and identified a weak bipartite NLS in the AKT3 amino acid sequence (accession number: Q9Y243) located in a flexible linker region between the PH-domain and kinase domain **(Figure 23A)**. Based on these *in silico* findings we created two AKT3 mutant overexpression constructs: AKT3-NLS1 and AKT3-NLS2. AKT3-NLS1 carries two point-mutations (K141R and R142A) that alter the leucine rich NLS region to the sequence that resembles the

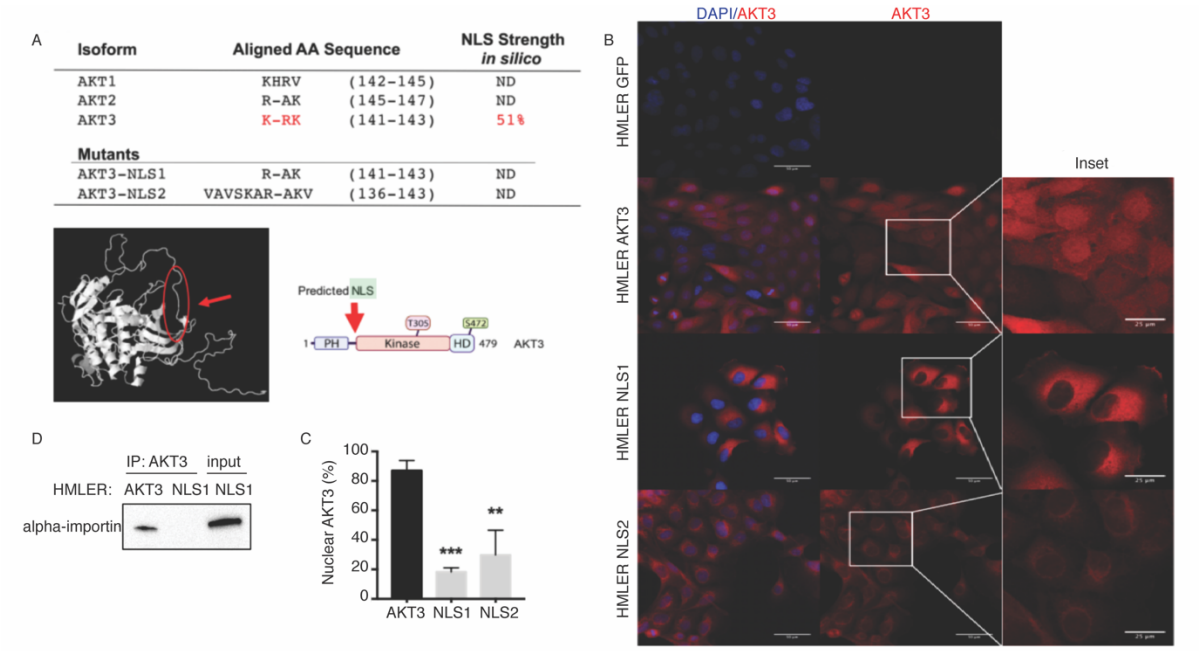

Figure 23. Nuclear Localization of AKT3 is dependent on NLS sequence. A) Display of predicted nuclear localization sequence (NLS) in AKT3 with calculated in silico NLS score (100% indicates predominantly nuclear, 0% indicates predominantly cytoplasmic). **B)** Confocal images of HMLER cells that overexpress AKT3 and AKT3-NLS mutants (red) with quantitation of subcellular location shown in **(C)**. At least 60 cells per condition were analyzed. Data shown as percent of cells with predominant nuclear AKT3. **D)** Immunoprecipitation using anti-AKT3 of HMLER-AKT3 and AKT3-NLS1 lysate and blotting for α-importin (lane 1-2). Whole lysate of HMLER AKT3-NLS1 as expression control (lane 3). All representative results shown were reproduced in at least three independent experiments.

linker area in AKT2 **(Figure 23A)**. For AKT3-NLS2, a 10 amino acid sequence flanking the NLS was replaced to mimic a longer part of the linker region as coded in AKT2. Wildtype AKT3 and the mutants were retrovirally delivered and expressed in HMLER cells **(Figure 23B)**. Immunocytochemical analyses showed clear subcellular localization differences between control, AKT3, AKT3-NLS1 and AKT3-NLS2 transfected cells **(Figure 23C)**. Wildtype AKT3 was predominantly (87%) nuclear localized; however, AKT3-NLS1 and AKT3-NLS2 mutants were largely restricted to the cytoplasm with 18% and 29% nuclear localization, respectively. Immunoprecipitation of AKT3 in HMLER lysates and probing with α-importin showed that the AKT3-NLS1 mutant had impaired interaction with α-importin **(Figure 23D)**.

Snail and slug are AXL-TBK1 dependent substrates of AKT3

EMT is orchestrated by a limited number of transcription factors, considered to be the ultimate inducers of EMT (EMT-TFs). These transcription factors include the zinc finger transcription repressors snail (*SNAI1*) and slug (*SNAI2*) (Ansieau, Collin, & Hill, 2014; Diaz, Vinas-Castells, & Garcia de Herreros, 2014; D. D. Tran, Corsa, Biswas, Aft, & Longmore, 2011). Previously, we found that the activation of TBK1 in AXL-driven metastasis drives the engagement of slug and snail (Cruz et al., 2019). We used GEPIA analysis to evaluate the correlation between the mRNA expression levels of SNAI2 and the different *AKT* isoforms in BRCA **(Figure 24)**. Indeed, while *AKT3* correlated with *SNAI2* expression, *AKT1* and *AKT2* did not.

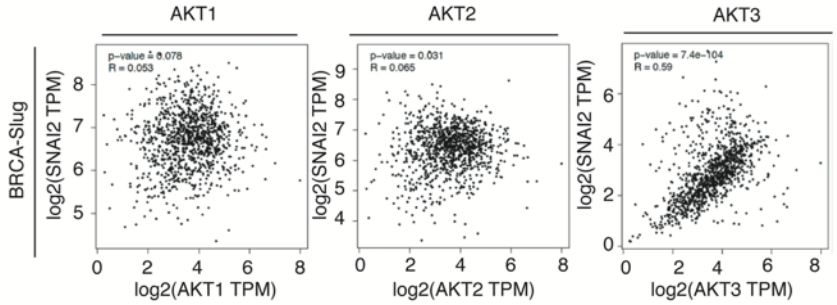

Figure 24. AKT3 correlates with Slug in Invasive Breast Carcinoma. Gene expression correlation of AKT isoforms and SNAI2 using GEPIA (Gene expression profiling interactive analysis) in invasive breast carcinoma tumors (BRCA) from the TCGA and GTEx databases.

Given the presence of AKT3 in the nucleus, we sought to determine if AKT3 interacts with EMT-TFs. Immunoprecipitation of AKT3 in PANC1 cells revealed that AKT3 associated with snail **(Figure 25A)**. Furthermore, this complex remained intact in *KIC* PDA lines only when TBK1 was functional **(Figure 25B)**, suggesting TBK1 is required for the interaction between AKT3 and snail. When MDA-MB-231 **(Figure 25C)** and PANC1 **(Figure 25D)** cells were treated with SFM or GAS6 for 12 hrs, slug/snail was found to be in the nucleus and cytoplasm of the cells. However, when AXL was inhibited with BGB324, snail/slug translocation to the nucleus was significantly reduced, suggesting that the AXL-TBK1-AKT3 pathway is involved in snail/slug nuclear translocation. This phenomenon was confirmed using imaging flow cytometry (Amnis Imagestream®), which clearly showed an ~80% reduction of cells that display nuclear slug after AXL inhibition **(Figure 25E, F)**. Consistent with these observations in vitro, co-IHC of slug and AKT3 in *KPC GEMM* PDA tumors revealed that slug positive areas coincided with AKT3 positive ones, but not vice versa **(Figure 25G)**, suggesting a dependence of slug on AKT3 for expression.

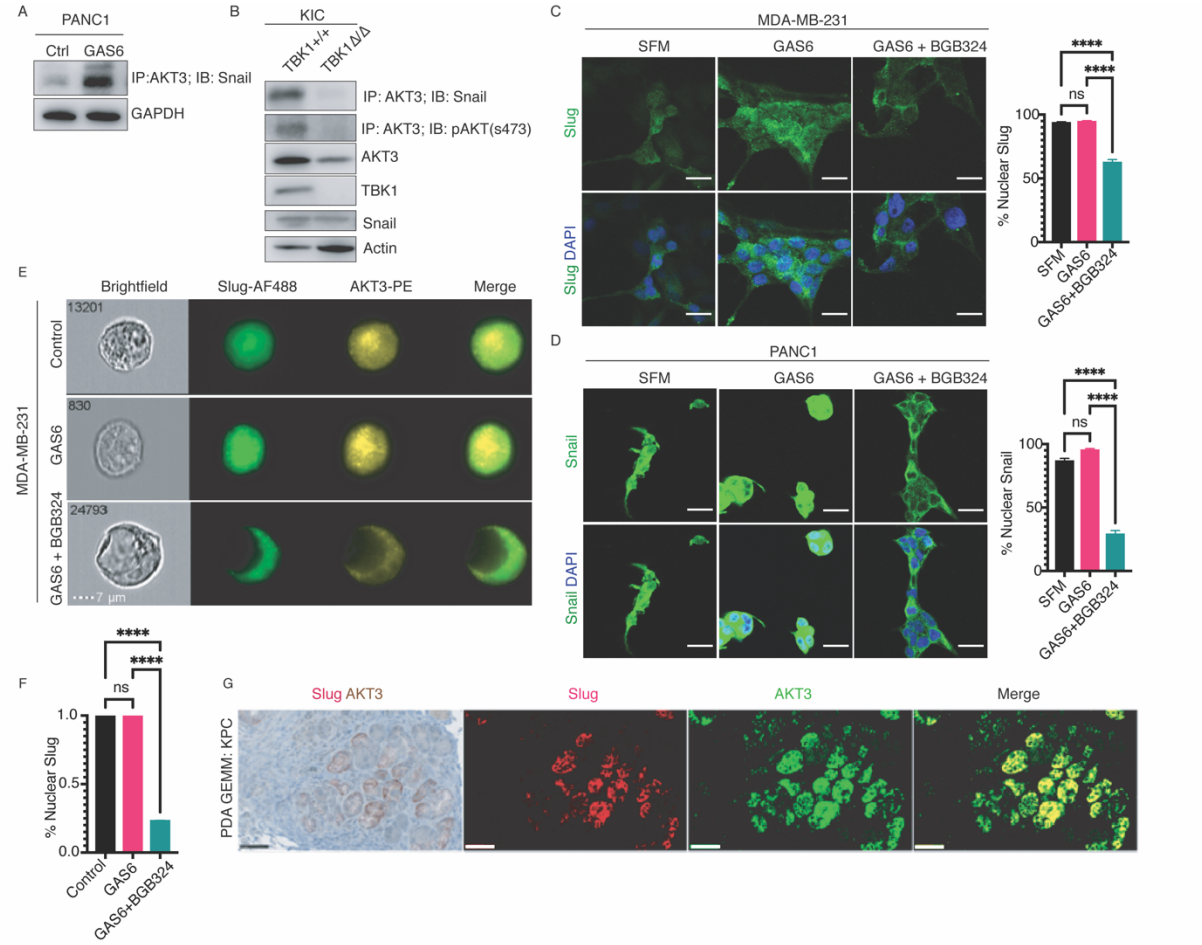

Figure 25. Snail/Slug is a TBK1-dependent substrate of AKT3. A) PANC1 cells were stimulated with DMSO or GAS6 (200 ng/mL). Immunoprecipitation of AKT3 was probed for Snail. GAPDH was used as a loading control. **B)** Immunoprecipitation of AKT3 in primary TBK1 WT and deficient PDA cell lines were probed for Snail and pAKT (s473). Lysates were probed for total snail, AKT3, TBK1, and Actin. **C-D)** Immunofluorescence of slug or snail (green) and DAPI (blue) in MDA-MB-231 **(C)** and PANC1 **(D)** cells treated with SFM, 200 ng/mL GAS6 +/- 2 μM BGB324 for 12hrs. Cells were imaged at 20X using confocal microscopy (scale bar,20 μm) and nuclear slug/snail was quantified, n>200 cells. **E)** Representative images from Imaging Flow cytometry (Amnis Imagestream®) of Slug-AF488 (green) and AKT3-PE (yellow) in MDA-MB-231 cells treated with 200 ng/mL GAS6 +/- 2 μM BGB324 for 6hrs. Scale bar, 7 μm. **F)** Nuclear localization of slug was quantified in each condition from **(E)**; Control, n=549, GAS6, n=6781, GAS6 + BGB324, n=7730. Location of slug and AKT3 co-localization was also quantified. **G)** IHC of KPC PDA tumor for slug (red) and AKT3 (brown). Staining was then pseudo-colored using ImageJ: slug is red, AKT3 is green, and yellow is slug and AKT3 co-localized. All representative results shown were reproduced in at least three independent experiments. All statistics were done use one-way ANOVA; * $p<0.05$, ** $p<0.01$, *** $p<0.001$, **** $p<0.0001$

AXL activity stabilizes snail/slug via TBK1-AKT3

Given the finding that slug expression in *KPC* tumors strongly correlated with AKT3, we hypothesized that slug/snail activity is dependent on AKT3 providing a stabilizing effect on

slug/snail protein. To test this hypothesis, MCF10a/slug cells were transfected with siAKT3. Even though slug was overexpressed to drive EMT in these cells, when AKT3 was not present vimentin and AXL expression were substantially reduced **(Figure 26A)**, supporting the hypothesis that AKT3 is required for slug/snail EMT-inducing activity.

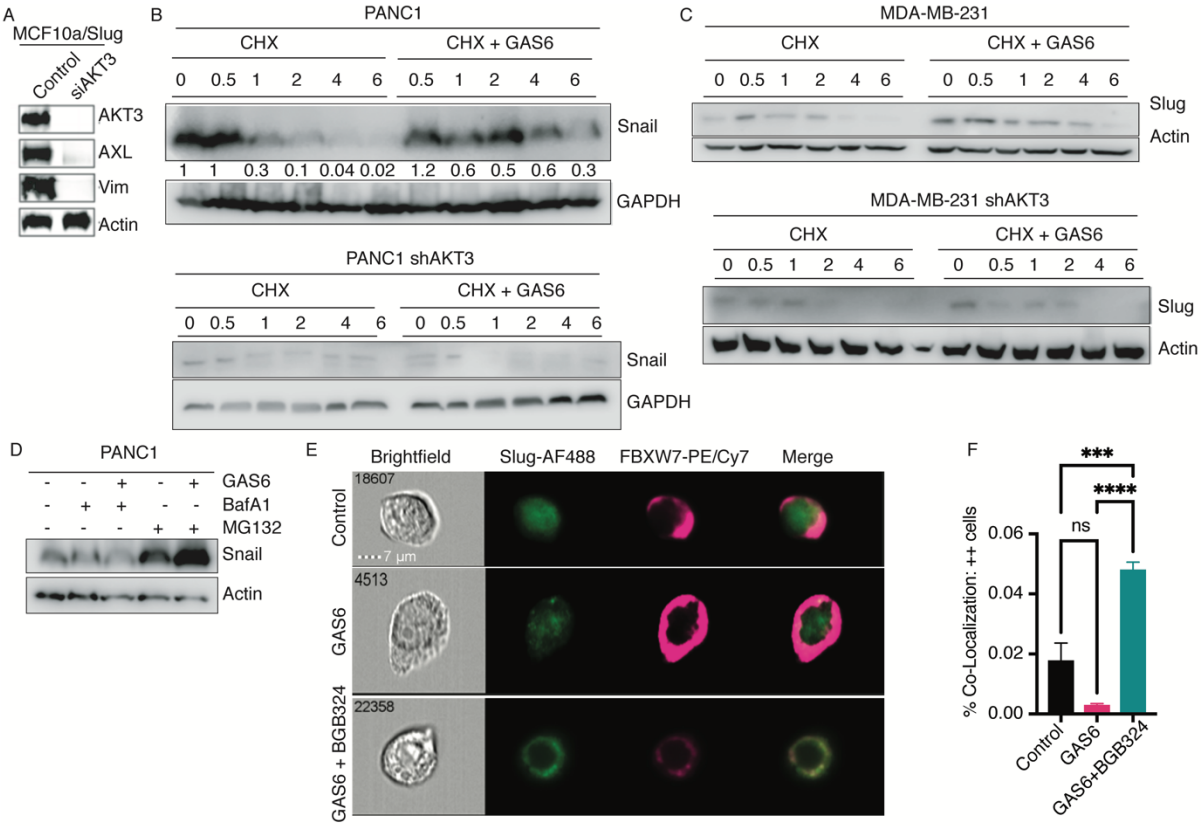

Figure 26. AXL activity stabilizes Snail/Slug via TBK1-AKT3. A) MCF10a/slug cells transfected with siAKT3 or control. Lysates were probed for AKT3, AXL, vimentin, and actin. **B,C)** PANC1 **(B)** and MDA-MB-231 **(C)** cells transduced with shAKT3 were treated with cycloheximide (0.5 µg/mL) or cycloheximide + GAS6 (200 ng/mL) and harvested at 30 min, 1, 2, 4, and 6 hrs of treatment. Lysates were probed for snail/slug and GAPDH/actin. **D)** PANC1 cells were treated for 8 hrs with DMSO, BafA1 (0.5 µM) +/- GAS6 or MG-132 (10 µM) +/- GAS6. Cells were lysed and probed for snail and actin (loading control). **E)** Representative images from imaging flow cytometry (Amnis Imagestream®) of Slug-AF488 (green) and FBXW7-Pe/Cy7 (pink) in MDA-MB-231 cells untreated or treated with 200 ng/mL GAS6 +/- 2 µM BGB324 for 6hrs. Scale bar, 7 µm. **F)** Co-localization of slug and FBXW7 in cells that were double positive (++) for both markers from **(E)** was quantified and displayed as percentage in each condition; Control, n=8/457, GAS6, n=14/5133, GAS6 + BGB324, n=276/5778. All representative results shown were reproduced in at least three independent experiments. All statistics were done use one-way ANOVA; * $p<0.05$, ** $p<0.01$, *** $p<0.001$, **** $p<0.0001$

To determine if AXL-AKT3 activity influences the protein stability of snail/slug, we treated PANC1 **(Figure 26B)** and MDA-MB-231 (Figure 26C) cells with cycloheximide (CHX), a protein synthesis inhibitor, +/- GAS6 over a time course of 6 hrs. , Consistent with previous findings (S. P. Wang et al., 2009) snail had a half-life of 1 hr when treated with CHX. Interestingly, when AXL was activated with GAS6, the half-life of snail was prolonged to 4 hrs, suggesting AXL activity stabilizes slug/snail protein. To determine AKT3 involvement, we repeated the experiment in cells transduced with shAKT3 and found that the addition of GAS6 no longer had a stabilizing effect on snail. AKT3 was similarly required for AXL-induced slug stability in MDA-MB-231 cells **(Figure 26C)**. To determine whether snail protein is degraded by the proteasome or the lysosome, PANC1 cells were treated with a lysosome inhibitor (BafA1) or a proteasome inhibitor (MG-132) +/- GAS6 for 8 hrs **(Figure 26D)**. Although BafA1 had no effect on snail expression levels, when cells were treated with MG-132, there was a robust increase of snail protein, indicating snail is degraded via the proteasome.

The F-box E3 ubiquitin ligase FBWX7 has been implicated in the degradation of snail/slug in multiple cancers (Cuevas et al., 2019; G. Xiao et al., 2018; H. Yang et al., 2015). Xiao and colleagues showed when FBXW7 was targeted with shRNA in two different lung cancer cell lines, the expression of snail increased markedly (G. Xiao et al., 2018). This finding was recapitulated in ovarian cancer cells (Cuevas et al., 2019). To evaluate if AXL-AKT3 protects slug from FBXW7 and therefore degradation, we used Imaging flow cytometry

(Amnis Imagestream®) of MDA-MB-231 cells and scored co-expression of FBXW7 and slug **(Figure 26E, F)**. Interestingly, when MDA-MB-231 cells were treated with GAS6, FBXW7 and slug were rarely overlapping, but when AXL was inhibited, overlap of the two proteins increased significantly, suggesting that perhaps AXL-TBK1-AKT3 protects slug from FBXW7 mediated degradation.

Selective targeting of AKT3 with a novel allosteric small molecule inhibitor inhibits metastasis.

Several drugs targeting pan-AKT activity (e.g. GDC0068, AXD5363, MK-2206) are currently in various stages of clinical testing. However, many of these trials report toxicity such as hyperglycemia and hyperinsulinemia due to the essential functions of AKT1 and AKT2 in tissue homeostasis (Hudis et al., 2013; Jansen, Mayer, & Arteaga, 2016; Ma et al., 2015; Yap et al., 2014). An AKT3 selective inhibitor has the potential to overcome these issues. The similarity between AKT1, 2 and 3 in the kinase domain precludes selective kinase inhibition. However, an allosteric site located in a cleft between the PH domain and the kinase domain has been used to identify AKT1, AKT2 and AKT1/2-selective inhibitors (Barnett et al., 2005; Lindsley et al., 2005; W. I. Wu et al., 2010). Sequence alignment around this allosteric site suggested that there are exploitable differences in this region **(Figure 27A)**. Based on a structural model produced by comparison of the crystal structures of AKT1 (W. I. Wu et al., 2010) and the AKT2 kinase domain suggested that a single amino acid deletion in AKT2 and AKT3 compared to AKT1 leads to a change in the path that the protein backbone follows, opening up a pocket at the front of the allosteric binding site

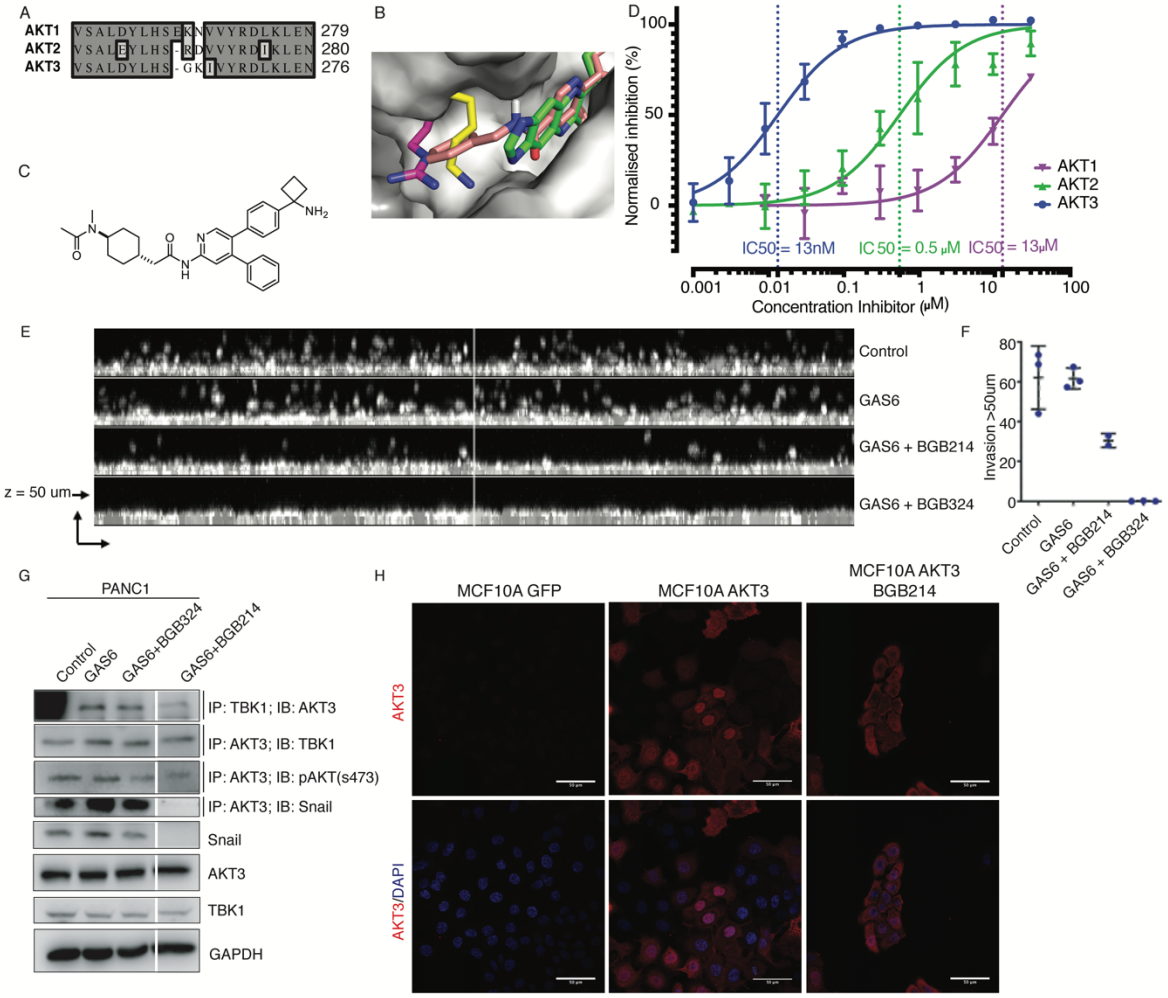

Figure 27. Efficacy of selective targeting of AKT3 with a novel allosteric small molecule inhibitor.
A) Exploitable differences in sequence between AKT1, AKT2 and AKT3 around the allosteric site include a deletion in AKT2 and AKT3 compared to AKT1, implying that the backbone may follow a different path in these proteins. **B)** Surface view of the front of the allosteric binding site of AKT3, including bound allosteric inhibitor AKT VIII (green). Homology model of AKT3 based on crystal structures of AKT1 bound to AKT VIII (PDB 3o96) and AKT2 kinase domain (PDB 1o6k). Side chains from the AKT1 crystal structure (Lys268, yellow) and the AKT2 crystal structure (Arg269, magenta) are superimposed, showing how they impinge on the space made available by the smaller Glycine present at this location in AKT3 (Gly265). A molecule with similar structure to BGB214 (pink) docked at the allosteric site clashes with Lys268 of AKT1 (yellow). **C)** Structure of BGB214. **D)** Inhibition of AKT1, AKT2 and AKT3 enzymatic activity on GSK3α-derived Ultra UlightTM-labelled crosstide substrate (n>3). **E)** MDA-MB-231 cells plated in collagen/matrigel and treated with GAS6 +/- 3 μM BGB214 or 2 μM BGB324 for 48hrs. Z-stack images were taken using confocal microscopy over 50 μm. **F)** Invasion greater than 50 μm was quantified. **G)** PANC1 cells were stimulated with DMSO, GAS6 (200 ng/mL) +/- 2 μM BGB324 or 3 μM BGB214. Immunoprecipitation of AKT3 was probed for pAKT(s473), TBK1, and snail. Immunoprecipitation of TBK1 was probed for AKT3. Lysates were probed for AKT3, snail, TBK1 and GAPDH (loading control). Lanes were run on same blot but space indicates they are not continuous. **H)** Analysis of nuclear localization of AKT3 (anti-AKT3, red; DAPI, blue) in MCF10a cells after AKT3 overexpression and treatment with 600 nM BGB214 for 24 hrs.

(Figure 27B). This pocket is small in the case of AKT2 due to the protrusion of the large side chain of Arg269, but larger in AKT3 due to the presence of a glycine at this site. A series of novel allosteric small molecule inhibitors of AKT3 were developed (WO/2016/102672) with backbones that bind to the allosteric site via the right hand side of the molecule with the group on the left making a bend to access the additional space, causing the molecule to clash with AKT1 Lysine 268. One example of these is BGB214 (N-(5-(4-(1-aminocyclobutyl)phenyl)-4-phenylpyridin-2-yl)-2-((1r,4r)-4-(N-methylacetamido)cyclohexyl)acetamide), a potent and selective AKT3 inhibitor **(Figure 27C)**. In biochemical assays using purified tag-free enzymes, BGB214 had an IC_{50} of 13 nM for AKT3 with approximately 1000-fold selectivity against AKT1 and >35-fold selectivity against AKT2 **(Figure 27D)**.

To evaluate the efficacy of BGB214 to prevent aggressive cancer traits such as migration and 3D growth, MDA-MB-231 cells were plated in collagen/matrigel and treated with GAS6, GAS6 + BGB214, or GAS6 + BGB324 for 48 hrs **(Figure 27E, F)**. Invasion over 50 μm was determined and quantified revealing that inhibition of AXL or AKT3 substantially reduced cell migration/invasion **(Figure 27F)**. Similarly, in an organotypic 3D growth assay, BGB214 dose-dependently prevented MDA-MB-231 growth **(Figure 28A)**, but did not significantly affect cell growth in 2D proliferation assays **(Figure 28B, C)**. Interestingly, BGB214 mediated inhibition of pAKT3 S472 in PANC1 cells resulted in decreased expression of total snail **(Figure 27G)**.

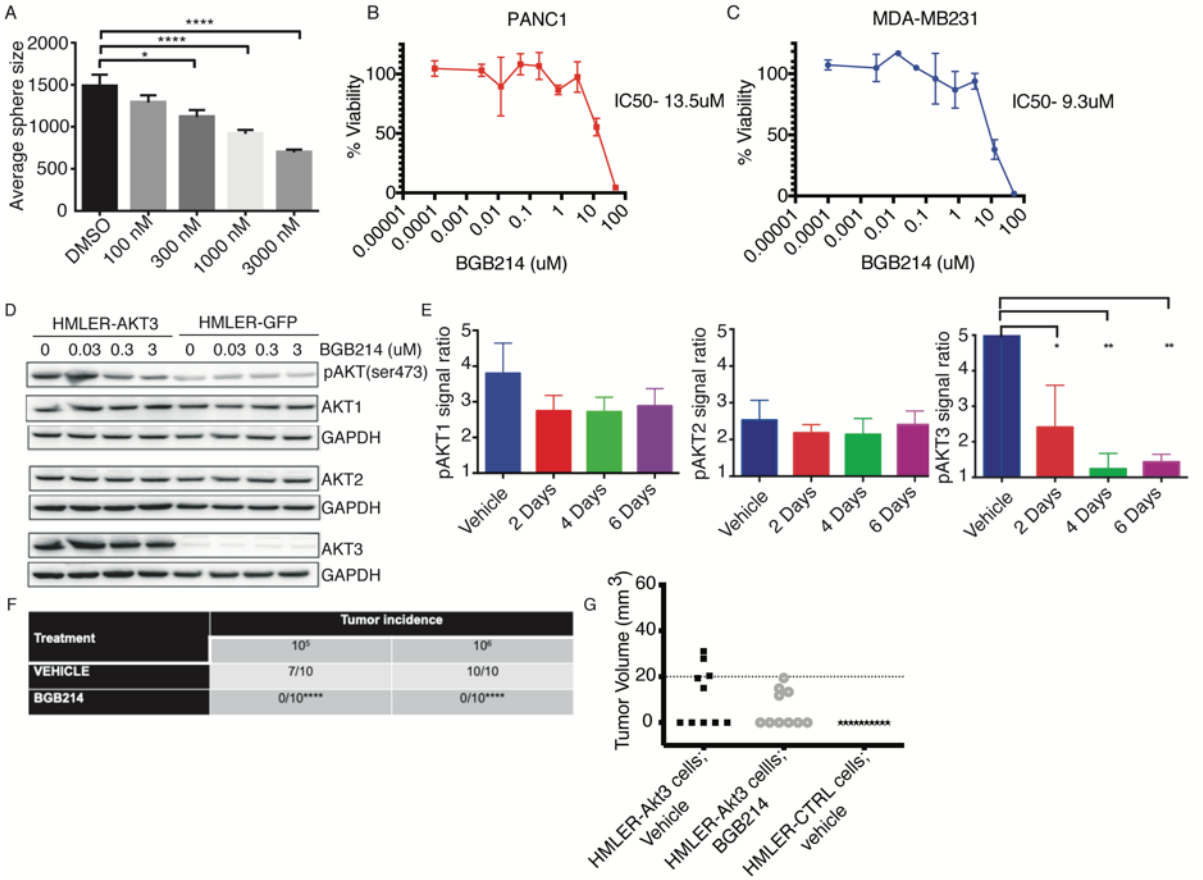

Figure 28. Evaluation of BGB214 in vitro and in vivo. A) MDA-MB-231 cells were seeded in 3D Matrigel cultures and treated for 9 days with the indicated dose of BGB214. Spheres were quantified. Histograms show average sphere size for each treatment. Mean + SE is shown, n=3. Statistical analysis by one-way ANOVA, Tukey's multiple comparisons test. *p < 0.05, ****p<0.0001. **B)** PANC1 **(C)** or MDA-MB-231 cells were plated on day 0 and BGB214 was added on day 1 in 4-fold dilutions. For each assay, 8 different drug concentrations were tested with 8 replicates per concentration. Relative cell number was determined by adding MTS incubating for 1 to 3 hrs at 37°C. Drug sensitivity curves and IC50s were calculated using in-house software. Response was validated in replicate plates ($n \geq 4$). Assays have been repeated in 4 biological replicates, with 16 technical replicates each in total. **D)** HMLER-AKT3 or HMLER-GFP cells were treated with increasing concentration of BGB214 (AKT3i). Lysates were harvested and probed for pAKT(s473), AKT1, -2, or -3. GAPDH was used as a loading control. **E)** MCF10A-DCIS cells were transplanted subcutaneously into mice, treated with 25 mg/kg BGB214 for 2-6 days. pAKT1, 2, and 3 levels were subsequently evaluated. **F)** Tumor incidence of HMLER/IRES-GFP and HMLER/Akt3 cells injected subcutaneously into host NSG mice at limiting dilutions (between 105-106 cells) following treatment with BGB214 (150 mg/kg, orally once daily in a 5 days on 2 days off regime). Cells were treated in vitro for 24 hrs with BGB214 at a concentration close to observed IC90 (0.54 µM). Tumor incidence was evaluated 14 days post implantation and tumor size cut off value was set at 20 mm3. **G)** Tumor incidence of HMLER/IRES-GFP and HMLER/Akt3 cells injected subcutaneously into host NSG mice at limiting dilution (106 cells) and treated with BGB214 (50 mg/kg, orally twice daily). Tumor incidence was evaluated 14 post implantation and tumor size cut off value of 20 mm3 is indicated.**** p 0.0001 by unpaired Student two tailed test

The specificity of BGB214 for pAKT3 was confirmed in a panel of cell lines in vitro and in vivo. HMLER-AKT3 or HMLER-GFP cells were treated with increasing concentrations of BGB214 **(Figure 28D)**. HMLER-GFP cells have very low levels of AKT3 endogenously. pAKT levels were only reduced when AKT3 was overexpressed, indicating that BGB214 selectively inhibits AKT3. In addition, MCF10-DCIS subcutaneous tumors treated with 25 mg/kg BGB214 for 2-6 days specifically resulted in decreased pAKT3 with little effect on pAKT1 and pAKT2 **(Figure 28E)**.

To investigate the potential of BGB214 to prevent tumor initiation **(Figure 28F)**, HMLER cells transduced with control vector or AKT3 were pre-treated in vitro with BGB214 for 24 hours and then injected subcutaneously into NOD SCID mice at limiting dilutions ($1x10^5$-$1x10^6$ cells) and mice treated with BGB214 for 14 days. AKT3 inhibition by BGB214 significantly reduced the tumor initiation capacity of HMLER-AKT3 cells **(Figure 28F)**. The same reduction in tumor initiating capacity was observed following injection of HMLER-AKT3 cells without in vitro treatment with BGB214 preceding injection **(Figure 28G)**.

Finally, we investigated the potential of BGB214 to modulate nuclear localization of AKT3 in MCF10a cells. AKT3 was overexpressed in MCF10a cells and nuclear localization was evaluated following treatment with BGB214. AKT3 localized to the nucleus in control treated cells however, treatment with BGB214 prevented nuclear localization of AKT3

(Figure 27H). We conclude that inhibition of p-AKT3 with the allosteric inhibitor BGB214 prevents pAKT3 mediated tumorigenic features such as invasion, 3D growth, EMT transcription factor stability and tumor initiation. Interestingly, BGB214 also prevented nuclear localization of AKT3, indicating inhibition of phosphorylation as a feasible way to prevent nuclear localization driven oncogenic features of AKT3.

Nuclear AKT3 is associated with aggressive breast cancer and metastasis.

To evaluate the relevance of AKT3 in human cancer patients, IHC analysis of patient samples from triple negative breast cancer patients revealed that AXL, AKT3, and the mesenchymal marker vimentin correlated in matched sections at the tumor periphery, with little expression in the center of the tumor, supporting the correlation of AXL and AKT3 with EMT in human breast cancer patients **(Figure 29A)**.

To assess the biologic consequence of nuclear AKT3, luciferase-HMLER cells overexpressing GFP control, AKT3, and AKT3-NLS1 were injected intravenously into NSG mice **(Figure 29B, C)**. The AKT3 overexpressing cells seeded the lung at a higher rate compared to the AKT3-NLS1 and GFP control, suggesting that nuclear AKT3 contributes to metastatic seeding of breast cancer cells.

To assess the effect of AKT3 expression in breast epithelial cells we retrovirally overexpressed AKT3 in MCF10A cells and compared the mRNA expression pattern via RNA sequencing with MCF10A cells transduced with GFP control vector. We found 46

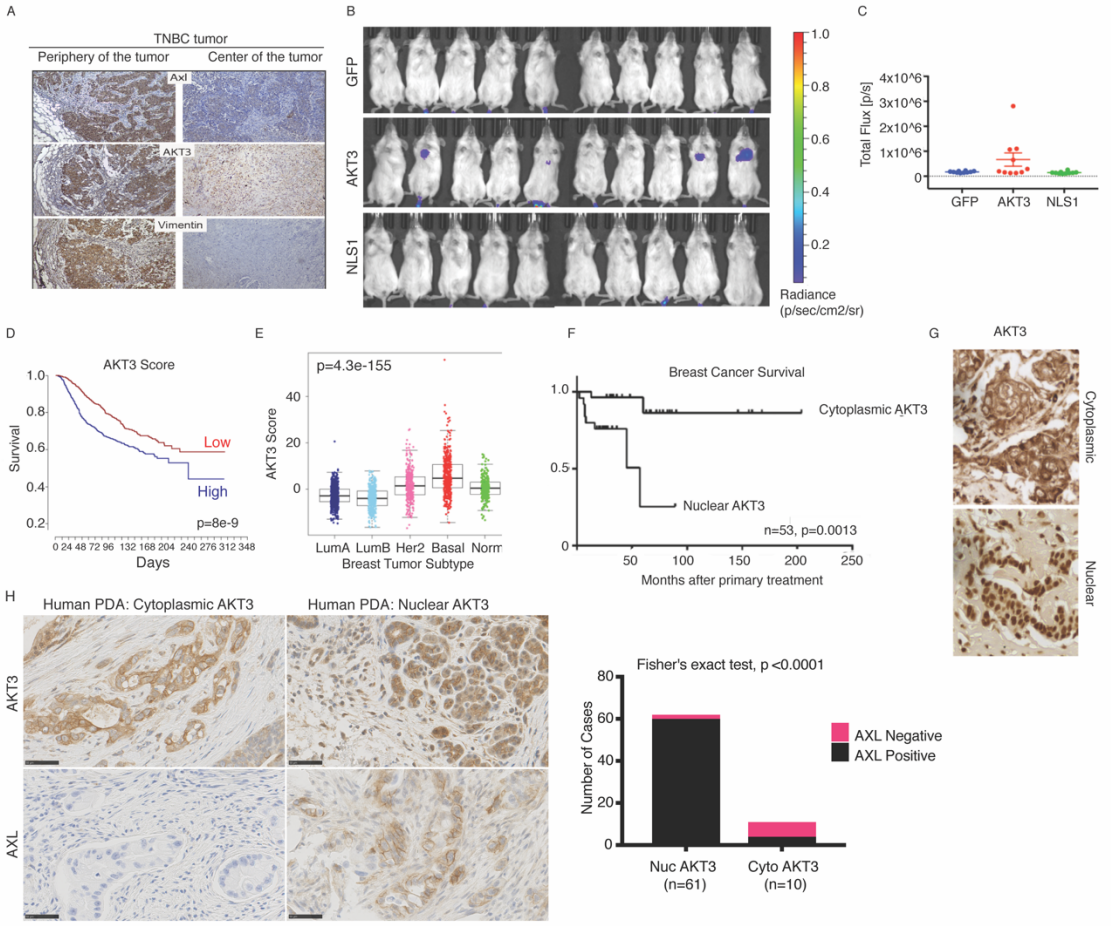

Figure 29. Nuclear AKT3 is required for metastasis and is associated with aggressive cancer. A) Representative images of IHC for AXL, AKT3, and vimentin in human triple negative breast cancer in matched sections at the periphery and center of the tumor. All representative results shown were reproduced in at least three independent experiments. **B, C)** In vivo imaging of 5x105 HMLER cells (GFP-Luc, AKT3-Luc, and NLS1-Luc) injected i.v. into NSG mice with quantification of Luciferase activity **(C)**. Animals were intraperitoneally injected with 150 mg/kg D-luciferin 10-15 min prior to imaging. Quantification of lung signal as standardized flux unit. **D)** Kaplan Meier plot indicating that high AKT3 induced expression (AKT3 score) correlated with worse outcome (p=8e-9) based on the METABRIT database. **E)** Significant different distribution of the AKT3 score between the PAM50 subtypes (p=4.3e-115, Kruskal–Wallis test); ER negative tumors were in general enriched for the AKT3 score, particularly in Basal like tumors. **F)** Survival analyses of 53 breast cancer patients based on nuclear or cytoplasmic AKT3 localization (p=0.0013 Log rank (Mantel-Cox) test. **G)** Representative images of IHC staining for AKT3 in human breast cancer samples in (F). AKT3 localization predominantly cytoplasmic (left) or nuclear (right). **H)** Representative images of IHC staining for AKT3 and AXL in human PDA (n=71). Fisher's exact contingency test was used to calculate if there was a correlation between nuclear AKT3 and AXL positive expression within the tumor.

differentially expressed (DE) genes (FC≥2, FDR<0.05) **(Table 2)**. The DE genes and their directionality were used to calculate an "AKT3 score" which was then mapped against probes in the Metabric database, which is composed of gene expression patterns from 1980 breast cancer patients. The patients were divided into two groups depending upon if the AKT3 score was above or below the mean. Plotting the AKT3 score against patient survival indicates that a high AKT3 score correlates with a significantly worse overall outcome (KM, p=8e-9) **(Figure 29D)**. Further, we found a significantly different distribution between breast cancer subtypes (based on PAM50 intrinsic subtypes) and AKT3 scores (p=4.3e-155, Kruskal–Wallis test) **(Figure 29E)**. ER negative tumors are in general enriched for the AKT3 score, particularly basal-like tumors **(Figure 29E)**. That high levels of AKT3 associated gene expression correlates with more aggressive forms of breast cancer, worse overall outcome, and a higher hazard ratio is consistent with previous reports of AKT3 high copy number alterations in TNBC patients (Anwar et al., 2020; Meric-Bernstam et al., 2014) and reports that AKT3 expression is associated with higher grade breast cancer tumors (Bonin et al., 2019). To validate our previous findings, we sought to determine if nuclear AKT3 was associated with worse overall survival. To evaluate this, we performed IHC for AKT3 in clinical breast cancer samples **(Figure 29F, G)**. Grouping patients based on AKT3 subcellular localization revealed that nuclear AKT3 predicted a worse overall outcome (n=53 patients, p=0.0013 Log-rank test) in this cohort of patients.

Lastly, to assess the location of AKT3 in pancreatic tumors from patients, IHC for AKT3 and AXL (**Figure 29H**) demonstrated that AXL^+ tumors displayed single cells outside epithelial

ducts that expressed nuclear AKT3. However, in AXL^- tumors, AKT3 was cytoplasmic, supporting our findings that AXL is associated with nuclear localization of AKT3 and this localization results in a less differentiated (more mesenchymal-like) tumor cell phenotype (**Figure 29H**). Together, these results suggest that nuclear AKT3 may be a therapeutic target that avoids toxicity associated with pan-AKT inhibition and a biomarker for worse overall survival and aggressive cancers.

Symbol	logFC	Pvalue	FDR
AKT3	4.96	1.40E-27	2.12E-23
TGFBI	1.78	4.53E-15	2.30E-11
CD24	1.89	2.91E-14	1.10E-10
SERPINE1	1.6	5.67E-12	1.72E-08
A2ML1	1.49	1.18E-11	3.00E-08
SPRR1B	1.73	2.77E-11	6.01E-08
KLHL4	4.26	8.05E-11	1.53E-07
IGFBP3	1.84	1.05E-10	1.78E-07
ZBED2	1.91	1.50E-10	2.28E-07
OVOL1	2.51	7.09E-10	9.80E-07
KRT6A	1.31	9.94E-10	1.26E-06
F3	1.66	1.51E-09	1.77E-06
IL1A	1.84	2.34E-09	2.54E-06
IVL	2.3	1.07E-08	1.09E-05
IL7R	1.95	2.24E-08	2.13E-05
SDK2	-5.3	4.58E-08	4.09E-05
S100P	1.41	6.26E-08	5.28E-05
PI3	1.44	7.71E-08	6.16E-05
LAMB3	1.22	1.24E-07	9.13E-05
UCA1	2.3	3.47E-07	2.39E-04
KRT6C	1.8	4.26E-07	2.70E-04
LAMC2	1.24	4.19E-07	2.70E-04
CPA4	1.4	8.50E-07	5.16E-04
WNT7B	1.55	1.33E-06	7.77E-04
SPINK6	2	1.60E-06	9.00E-04
CEACAM5	3.29	1.67E-06	9.06E-04
SERPINB2	2.59	2.19E-06	1.11E-03
LTBP1	1.45	5.43E-06	2.66E-03
ANGPTL4	1.21	6.17E-06	2.93E-03
IL1B	1.75	7.20E-06	3.31E-03
ADGRF4	1.58	7.64E-06	3.41E-03
NA	1.27	7.97E-06	3.46E-03
RYR2	1.45	1.35E-05	5.56E-03
INHBA	1.32	1.72E-05	6.90E-03
SPRR2D	1.52	2.04E-05	7.93E-03
KCNJ15	3.29	2.38E-05	9.04E-03
BMP2	1.69	2.69E-05	9.95E-03
AC007879.7	1.39	3.19E-05	1.15E-02
SERPINB10	3.01	4.16E-05	1.47E-02
SERPINB13	1.41	4.36E-05	1.51E-02
ZNF114	2.33	4.59E-05	1.55E-02
PTHLH	1.38	5.36E-05	1.77E-02
MYLK	1.4	6.61E-05	2.09E-02
PCDH7	1.59	6.95E-05	2.15E-02
PSCA	1.25	1.11E-04	3.38E-02

Table 2. Differentially expressed (DE) genes determined by RNA sequencing in MCF10A cells after AKT3 overexpression compared to GFP control vector (DE genes with fold change ≥2, and FDR<0.05).

CHAPTER FIVE
Conclusions and Recommendations

CONCLUSIONS

TBK1 as a driver of epithelial plasticity

Our results show that tumors and isogenic cell lines from multiple pancreatic GEMMs that lack functional TBK1 are more epithelial in gene expression and morphology than PDA GEMM tumors containing wild-type *Tbk1*. These findings, in combination with mechanistic studies demonstrating that TBK1 is downstream of the EMT driver AXL, indicate that EMT in pancreatic tumor cells is halted by *Tbk1* loss. Our findings expand the spectrum of biological activities of TBK1 and suggest that the therapeutic inhibition of TBK1 may be a useful strategy to control tumor cell invasion and resulting metastases in RAS-driven cancers.

AXL-TBK1 driven nuclear activation of AKT3 promotes EMT

Additionally, we report a novel mechanism in which nuclear AKT3 is vital to AXL-TBK1 driven EMT by stabilizing the EMT transcription factors slug and snail **(Figure 30)**. To validate AKT3 as a therapeutic target, we used the first AKT isoform specific small molecule inhibitor, BGB214, which is an AKT3-isoform selective allosteric small molecule inhibitor. BGB214 inhibits AKT3 nuclear translocation, EMT-TF stability, AKT3-mediated invasion, and tumor initiation in vivo. Lastly, we show that nuclear AKT3 expression is relevant in human cancer and correlates with worse outcome in

aggressive breast cancer. Our findings suggest that nuclear AKT3 activity is an important feature of AXL-driven epithelial plasticity and that selective AKT3 targeting represents a novel therapeutic avenue for treating aggressive cancer.

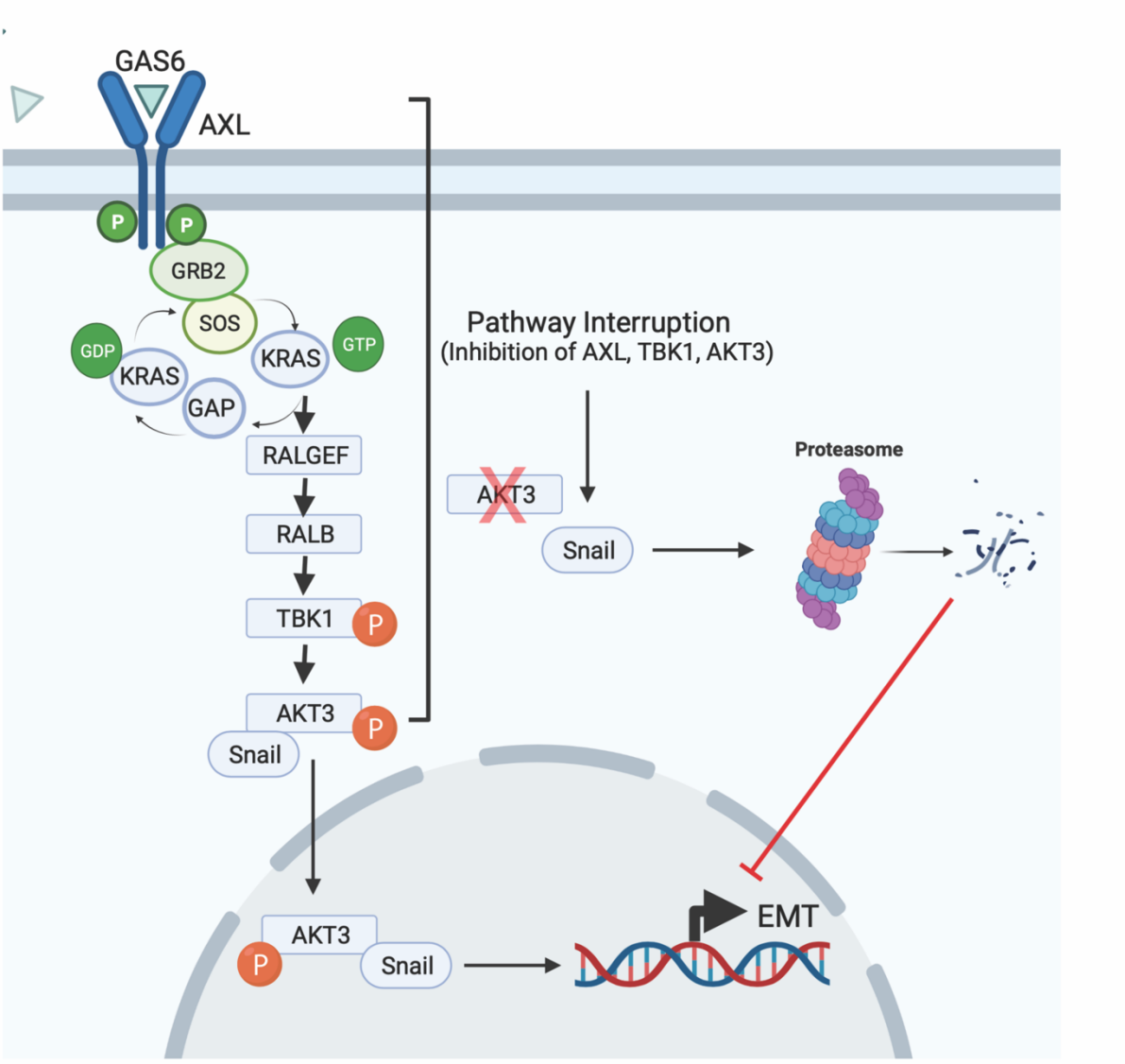

Figure 30. AXL-TBK1 driven nuclear AKT3 stabilizes snail/slug. AXL activation by its ligand GAS6 leads to the stimulation of TBK1 and subsequent activation of AKT3. Activation of AKT3 drives the binding of AKT3 to slug/snail, where they are translocated into the nucleus. The binding of AKT3 to slug/snail protects the EMT-TFs from proteasomal degradation. When this pathway is interrupted and AKT3 is not activated, AKT3 can no longer bind to s lug/snail thus leading to proteasomal degradation of the EMT-TFs and a decrease in EMT.

UNANSWERED QUESTIONS AND FUTURE DIRECTIONS

Are TBK1 and AKT3 pro- or anti- tumorigenic? Controversies in the field.

TBK1 has been linked to EMT in other cancer types. In contrast to our results, knockdown of TBK1 in ERα-positive breast cancer cells reportedly induced EMT and enhanced tumor growth and lung metastasis by suppressing ERα expression (K. M. Yang et al., 2013). However, in two separate recent studies, gene expression analysis revealed that a mesenchymal gene signature in melanoma and non-small cell lung cancer (NSCLC) cell lines was associated with sensitivity to TBK1 inhibition (TBK1i) (Cooper et al., 2017; Eskiocak et al., 2017). Further analysis revealed mutations in *RAS* family members as a common feature of NSCLC cell lines that showed sensitivity to TBK1i while NSCLC cells that were resistant to TBK1i had a more epithelial gene expression profile and less frequent activating RAS mutations (Cooper et al., 2017). The mesenchymal gene signature in TBK1i-sensitive NSCLC lines is consistent with our observations in KRAS-driven $Tbk1^{+/+}$*: KIC* tumors that have undergone EMT. Moreover, the epithelial gene expression profile of TBK1-resistant NSCLC cells lines matches the epithelial phenotype of $Tbk1^{\Delta/\Delta}$*: KIC* tumors that grew independent of TBK1.

AKT activation is linked to fundamental signaling pathways underlying cancer development and progression. Many investigations have focused on the function of AKT1, AKT2, or panAKT, but have largely ignored AKT3. This may be because AKT3 is the least expressed of the three isoforms (Konishi et al., 1995) and prior results on the

function of AKT3 in tumorigenesis are inconsistent (Chin et al., 2014; Chung et al., 2013; Grottke et al., 2016; Li et al., 2017; Santi & Lee, 2011; Stottrup, Tsang, & Chin, 2016). Regardless, a few reports have suggested that AKT3 contributes to cancer progression, including breast cancer (Mure et al., 2010; Nakatani, Sakaue, Thompson, Weigel, & Roth, 1999; Nakatani, Thompson, et al., 1999; Stahl et al., 2004). We predict that the inconsistency of AKT3 studies may be due to differential genetic contexts of the studies as well as to the fact that AKT3 can be expressed as two alternatively spliced variants, one which lacks S472 (Suyama et al., 2018). In the study by Suyama et al., overexpression of the AKT3 variant lacking S472 was associated with improved overall survival and reduced lung metastasis in preclinical models of breast cancer, whereas when AKT3 had the S472 phosphorylation site they saw increased tumorigenesis (Suyama et al., 2018). This is consistent with our findings that phosphorylation on serine 472 via TBK1 is needed for AKT3 nuclear localization to promote EMT and metastasis. In summary, our data support that nuclear AKT3 has utility as a potential biomarker for aggressive cancers that express AXL, and that AKT3 is a specific mediator of EMT signaling downstream of AXL. Additionally, as there are ongoing clinical trials targeting AXL in multiple cancer types, analyses of these tumors for AXL expression and AKT3 localization after treatment may provide clinicians with a much-needed read-out for treatment efficacy. Lastly, we propose that selective inhibition of AKT3 may represent a novel therapeutic avenue for treating aggressive and recurrent cancer that avoids toxicity associated with pan-AKT inhibition.

In what genetic contexts does the AXL-TBK1-AKT3 pathway promote EMT?

EMT is a key cellular program that contributes to tumor progression by enhancing tumor cell survival, tumor cell dissemination, and therapy resistance and has a strong association with worse clinical prognosis in many KRAS-driven cancers. Because KRAS is not currently an amenable target for many of these KRAS-driven cancers, targeting KRAS effector signaling is an attractive alternative. With this in mind, pharmacologically targeting the pathways that contribute to KRAS-driven EMT is worth considering as a strategy to improve response to standard therapy and reduce clinical progression, therapy resistance, and metastasis.

Activating mutations in *KRAS* are the dominant oncogenic drivers of pancreatic cancer (Hingorani et al., 2003; Karnoub & Weinberg, 2008). No other common epithelial cancer has a single gene with comparable mutation frequency, yet efforts to therapeutically target mutant RAS proteins have not been successful (Gysin, Salt, Young, & McCormick, 2011). However, targeting signaling components downstream of RAS that are required for RAS-mediated oncogenesis presents a viable therapeutic alternative (Engelman et al., 2008). TBK1 is a crucial effector of mutant active KRAS that we found to be expressed abundantly in *KRAS*-mutant PDA tumors and cell lines. Additionally, recent evidence suggests TBK1 expression correlates negatively with survival in human pancreatic cancer patients (Cruz & Brekken, 2018). The assessment of *Tbk1* loss in multiple clinically relevant GEMMs of PDA revealed that PDA mice lacking kinase active TBK1 have

significantly smaller and more epithelial tumors. Although survival was not significantly impacted by the loss of *Tbk1*, Tbk1 loss resulted in fewer metastatic lesions relative to PDA mice with wild-type *Tbk1*. Mechanistic studies established that TBK1 promotes EMT downstream of AXL in PDA, providing insight into a novel function for TBK1. Further, these studies suggest that therapies targeting TBK1 could be used to exploit *KRAS*-mutant tumors.

Additionally, it is important to note that in our studies we only interrogated this pathway in the context of AXL and AXL stimulation. It is possible that this mechanism may only be relevant in cell lines that contain high levels of AXL, which is supported by our finding that AXL is expressed in human PDAC tumors that display the nuclear localization of AKT3. Further studies are needed to understand if other RTKs can activate TBK1-AKT3 to stabilize snail/slug.

How is slug/snail protected by AKT3 binding?

In our study we find that the binding of AKT3 to slug/snail protects the EMT-TFs from proteasomal degradation, although more studies are needed to determine if FBXW7 is required for the degradation of slug/snail. It is possible that AKT3 does not directly stabilize EMT-TFs, but perhaps other proteins such as deubiquitinating enzymes (DUBs) promote the stability of these EMT-TFs in an AXL-TBK1 dependent manner. For example, the DUB USP10 has been shown to promote the stability of slug and snail in

breast, ovarian, and lung cancer cell lines (Ouchida et al., 2018). Other potential candidate proteins that might be involved in the degradation of snail are the F-box ligases, of which FBX15 and FBXO11 have been shown to ubiquitinate and support the degradation of Snail (Yu, Zhou, & Wu, 2017). Another protein that has been implicated in regulating the expression of slug and AXL is the transcription factor ΔNp63a, which has been shown to drive the migration of basal breast cancer cells in part through elevation of the expression of AXL and slug, as well as miR-205 to silence ZEB1/2 (Dang, Esparza, Maine, Westcott, & Pearson, 2015). ΔNp63a drives breast cancer invasion by selectively engaging certain proponents of the EMT program while still promoting the retention of epithelial characteristics to drive collective migration. Further studies are needed to evaluate the exact pathway by which slug/snail is degraded in an AXL-TBK1-AKT3 dependent manner. Additionally, as all of our cell lines only had slug or snail, it would be useful to interrogate the differences between slug and snail and if AKT3 has a preference of either of the transcription factors when both are present. Additionally, our previous studies have shown an increase in other EMT-TFs, such as ZEB1, downstream of AXL-TBK1 (Cruz et al., 2019). Further studies are needed to evaluate if the AXL-TBK1-AKT3 signaling cascade only influences protein expression of snail/slug or multiple EMT-TFs.

Does AXL-TBK1-AKT3 have an influence on more than just metastasis?

Interestingly, *Tbk1*-mutant KPC tumors were smaller than *Tbk1* wild-type tumors, indicating that *Tbk1* loss affects primary tumor growth in addition to tumor cell motility.

In the *KIC* GEMMs, endpoint tumor weights at 6 and 8 weeks were significantly smaller in the $Tbk1^{\Delta/\Delta}$ compared to the $Tbk1^{+/+}$ mice. In contrast, at 10 weeks there was no difference in endpoint tumor weights. Our results suggest $Tbk1^{\Delta/\Delta}$ tumor cells proliferate more quickly than $Tbk1^{+/+}$ tumor cells as evidence by in vitro cell proliferation assays and Ki67 immunohistochemistry of the *KIC* tumors. It is possible that this enhanced proliferation underlies the fact that $Tbk1^{\Delta/\Delta}$ tumors eventually catch up to the $Tbk1^{+/+}$ tumors, in terms of tumor weight.

TBK1 is central to numerous biological processes that could affect the growth of the primary tumor, including cell division, autophagy, innate immune response, and AKT/mTOR signaling (Cooper et al., 2017; Cruz & Brekken, 2018; Eskiocak et al., 2017; Helgason, Phung, & Dueber, 2013; J. Y. Kim et al., 2013; Pillai et al., 2015; Y. Xiao et al., 2017; S. Yang et al., 2016; Z. Zhu et al., 2014). In the context of pancreatic cancer, TBK1 has been reported to promote basal levels of autophagy as a means of silencing cytokine production (S. Yang et al., 2016). These findings imply that the inhibition or loss of TBK1 in PDA could increase cytokine production, ultimately driving immune activation and potentially an antitumor immune response. As previously mentioned, gene expression analysis revealed that $Tbk1^{\Delta/\Delta}$*: KIC* tumors displayed a higher expression of pro-inflammatory cytokines including *Cxcl1, Ccl2, Ccl4, Ccl27*, *Irf1,* and *Il1b*. While these results are not sufficient to conclude that *Tbk1* loss promotes antitumor immunity in PDA, the idea is not unreasonable given that $Tbk1^{\Delta/\Delta}$ mice have been shown to produce higher levels of pro-inflammatory cytokines in response to

immune challenge (Marchlik et al., 2010). In agreement with the notion that *Tbk1* loss produces antitumor immunity, two recent studies reported that immune evasion and metastatic behavior are highly associated with the engagement of the cGAS-STING-TBK1 innate immune pathway in cancer cells (Bakhoum & Cantley, 2018; Bakhoum et al., 2018; Canadas et al., 2018). In the first study, Backhoum et al. (Bakhoum et al., 2018) found that chromosomal instability in cancer cells, caused by errors in chromosomal segregation during mitosis, promoted cellular invasion and metastasis through the introduction of double-stranded DNA into the cytosol, engaging the cGAS-STING-TBK1 antiviral pathway. In the second report, Cañadas et al. (Canadas et al., 2018) characterized an interferon-stimulated positive feedback loop of antisense endogenous retroviruses (ERVs) present in a number of human cancer cell lines that produced hyperactive innate immune signaling, myeloid cell infiltration, and immune checkpoint activation. Additionally, they discovered that high ERV-expressing cancer cells correlate with an AXL-positive mesenchymal state, which is consistent with our observations (Canadas et al., 2018).

An important consideration with our $Tbk1^{\Delta/\Delta}$ PDA models is that the global *Tbk1* mutation eliminates TBK1 kinase activity and significantly reduces *Tbk1* expression in all cell types, including immune cells, which could impact immune responses to tumor challenge. In fact, a recent study demonstrated that dendritic cell conditional *Tbk1* knockout mice (*Tbk1-DKO*) injected subcutaneously with B16 melanoma cells lived longer and had smaller tumors compared to wild-type *Tbk1* control mice (Y. Xiao et al.,

2017). An assessment of B16 melanoma tumors from *Tbk1-DKO* animals revealed enhanced interferon-responsive gene expression and greater T-effector cell infiltration into tumors and lymph nodes, confirming antitumor immunity conferred by dendritic cell *Tbk1* loss. Collectively, these observations support a pro-tumor immune function for TBK1 that could contribute to the larger tumor sizes in *Tbk1* wild-type PDA mice. Going forward, it will be important to understand the unique function of TBK1 in each relevant cell type within a tumor.

In addition to TBK1, our studies do not rule out that AKT3 affects other cell types such as macrophages. In fact, it has been reported that 7-DHC, a cholesterol precursor, regulates type I interferon production via AKT3 activation, where AKT3 directly binds and phosphorylates IRF3 on S385 (J. Xiao et al., 2020). Additionally, AKT3 (pS473) in macrophages has been shown to promote migration, proliferation, wound healing, and collagen organization (Gu, Dai, Zhao, Gui, & Gui, 2020). Interestingly, a recent study showed that AKT3 phosphorylated RNA processing proteins that regulate the alternative splicing of fibroblast growth factor receptors (FGFR), consistent with an importance of nuclear targeting of AKT3 in EMT maintenance (Sanidas et al., 2014).

Is EMT necessary for metastasis?

Despite significant evidence that EMT directly contributes to tumor progression, several studies have suggested EMT is not required for the metastatic spread of PDAC and breast

cancer (Y. Chen et al., 2018; Fischer et al., 2015; Z. Zhao et al., 2016; Zheng et al., 2015). For example, most metastatic lesions are known to exhibit epithelial features, an observation that seems to be at odds with EMT as a prerequisite for metastasis (T. Brabletz et al., 2001; Savagner, 2001; Ye & Weinberg, 2015). As such, the importance of EMT in cancer biology has long been questioned (Tarin, Thompson, & Newgreen, 2005).

Epithelial plasticity not only includes the process of EMT, but also the reverse, mesenchymal-to-epithelial transition or MET. Recent evidence suggests that MET is required for successful metastatic colonization, although it remains unknown whether the tissue-specific adaptations are acquired thorough epigenetic or genetic means. Distant metastases in carcinoma patients often present with epithelial features having a similar histology as the tissue of origin (Malanchi et al., 2011; Thiery, 2002). These observations support that epithelial plasticity lies at the heart of tumor development and progression, and that such plasticity is necessary for tumor cell survival and colonization. It has become increasingly evident that EMT encompasses a range of hybrid plastic states, a phenotype coined as “partial EMT” (Aiello et al., 2018; Grigore, Jolly, Jia, Farach-Carson, & Levine, 2016; Jolly, Ware, Gilja, Somarelli, & Levine, 2017). Because partial EMT is not well-defined, it is unclear whether this hybrid status signifies a transitional phase during EMT or represents its own state. Similarly, using a mouse model of PDAC, the Stanger group has shown that individual tumors can activate different plasticity programs, such as “classical EMT” which involves transcriptional repression and an alternative program in which the epithelial state is lost post-transcriptionally (Aiello et

al., 2018). These plasticity programs were associated with either single-cell invasion or collective invasion, respectively (Aiello et al., 2018). It is unclear what underlies this phenotypic heterogeneity, considering the tumors investigated in this study had the same oncogenic drivers (TP53 and KRAS). Perhaps the only difference between the states is the tumor microenvironment, as Aiello et al. found that when partial EMT cells are exposed to TGFβ, they execute a classic EMT program (Aiello et al., 2018; Giampieri et al., 2009). This constant plastic state may partially explain the intratumoral heterogeneity that is often seen in carcinomas such as PDAC (Chaffer et al., 2011; Chaffer et al., 2013; Gupta et al., 2011).

The chronic activation of an EMT program within a tumor may depend on paracrine signals within the tumor microenvironment, dictating whether the tumor cells undergo EMT or MET. Because these cells exist in a plastic state, it is possible that these tumor cells readily revert their phenotype based on a microenvironment-specific context and factors (Aiello et al., 2018; Bissell, Radisky, Rizki, Weaver, & Petersen, 2002; Jechlinger, Grunert, & Beug, 2002; Thiery, 2002). One challenge impeding current in vivo studies is the difficulty of distinguishing carcinoma cells that have undergone EMT from fibroblasts or other mesenchymal cells that are normally found in the tumor stroma. To combat this, many labs have begun to use single-cell sequencing technology in KRAS-driven cancers such as PDAC to investigate EMT in vivo (Hosein AN, 2019). Additionally, current in vivo lineage-tracing technology has not settled the debate between the importance of collective migration and/or EMT for metastatic dissemination.

Additionally, the mechanisms of invasion and metastatic potential and their correlation with clinical outcome has yet to be defined. Regardless, epithelial plasticity remains as an indispensable feature in multiple phases of human cancer in an oncogene- and tissue-specific manner.

BIBLIOGRAPHY

Abe, T., & Barber, G. N. (2014). Cytosolic-DNA-mediated, STING-dependent proinflammatory gene induction necessitates canonical NF-kappaB activation through TBK1. *J Virol, 88*(10), 5328-5341. doi:10.1128/JVI.00037-14

Aguilera, K. Y., Rivera, L. B., Hur, H., Carbon, J. G., Toombs, J. E., Goldstein, C. D., . . . Brekken, R. A. (2014). Collagen signaling enhances tumor progression after anti-VEGF therapy in a murine model of pancreatic ductal adenocarcinoma. *Cancer Res, 74*(4), 1032-1044. doi:10.1158/0008-5472.CAN-13-2800

Aguirre, A. J., Bardeesy, N., Sinha, M., Lopez, L., Tuveson, D. A., Horner, J., . . . DePinho, R. A. (2003). Activated Kras and Ink4a/Arf deficiency cooperate to produce metastatic pancreatic ductal adenocarcinoma. *Genes Dev, 17*(24), 3112-3126. doi:10.1101/gad.1158703

Ahn, Y. H., Gibbons, D. L., Chakravarti, D., Creighton, C. J., Rizvi, Z. H., Adams, H. P., . . . Kurie, J. M. (2012). ZEB1 drives prometastatic actin cytoskeletal remodeling by downregulating miR-34a expression. *J Clin Invest, 122*(9), 3170-3183. doi:10.1172/JCI63608

Aiello, N. M., Maddipati, R., Norgard, R. J., Balli, D., Li, J., Yuan, S., . . . Stanger, B. Z. (2018). EMT Subtype Influences Epithelial Plasticity and Mode of Cell Migration. *Dev Cell, 45*(6), 681-695 e684. doi:10.1016/j.devcel.2018.05.027

Alfarouk, K. O. (2016). Tumor metabolism, cancer cell transporters, and microenvironmental resistance. *J Enzyme Inhib Med Chem, 31*(6), 859-866. doi:10.3109/14756366.2016.1140753

Ansieau, S., Collin, G., & Hill, L. (2014). EMT or EMT-Promoting Transcription Factors, Where to Focus the Light? *Front Oncol, 4*, 353. doi:10.3389/fonc.2014.00353

Antony, J., Tan, T. Z., Kelly, Z., Low, J., Choolani, M., Recchi, C., . . . Huang, R. Y. (2016). The GAS6-AXL signaling network is a mesenchymal (Mes) molecular subtype-specific therapeutic target for ovarian cancer. *Sci Signal, 9*(448), ra97. doi:10.1126/scisignal.aaf8175

Anwar, T., Rufail, M. L., Djomehri, S. I., Gonzalez, M. E., Lazo de la Vega, L., Tomlins, S. A., . . . Kleer, C. G. (2020). Next-generation sequencing identifies recurrent copy number variations in invasive breast carcinomas from Ghana. *Mod Pathol*. doi:10.1038/s41379-020-0515-2

Arumugam, T., Ramachandran, V., Fournier, K. F., Wang, H., Marquis, L., Abbruzzese, J. L., . . . Choi, W. (2009). Epithelial to mesenchymal transition contributes to drug resistance in pancreatic cancer. *Cancer Res, 69*(14), 5820-5828. doi:10.1158/0008-5472.CAN-08-2819

Asiedu, M. K., Beauchamp-Perez, F. D., Ingle, J. N., Behrens, M. D., Radisky, D. C., & Knutson, K. L. (2014). AXL induces epithelial-to-mesenchymal transition and regulates the function of breast cancer stem cells. *Oncogene, 33*(10), 1316-1324. doi:10.1038/onc.2013.57

Aveic, S., Corallo, D., Porcu, E., Pantile, M., Boso, D., Zanon, C., . . . Tonini, G. P. (2018). TP-0903 inhibits neuroblastoma cell growth and enhances the sensitivity

to conventional chemotherapy. *Eur J Pharmacol, 818*, 435-448. doi:10.1016/j.ejphar.2017.11.016

Bae, S. S., Cho, H., Mu, J., & Birnbaum, M. J. (2003). Isoform-specific regulation of insulin-dependent glucose uptake by Akt/protein kinase B. *J Biol Chem, 278*(49), 49530-49536. doi:10.1074/jbc.M306782200

Bailey, P., Chang, D. K., Nones, K., Johns, A. L., Patch, A. M., Gingras, M. C., . . . Grimmond, S. M. (2016). Genomic analyses identify molecular subtypes of pancreatic cancer. *Nature, 531*(7592), 47-52. doi:10.1038/nature16965

Bakhoum, S. F., & Cantley, L. C. (2018). The Multifaceted Role of Chromosomal Instability in Cancer and Its Microenvironment. *Cell, 174*(6), 1347-1360. doi:10.1016/j.cell.2018.08.027

Bakhoum, S. F., Ngo, B., Laughney, A. M., Cavallo, J. A., Murphy, C. J., Ly, P., . . . Cantley, L. C. (2018). Chromosomal instability drives metastasis through a cytosolic DNA response. *Nature, 553*(7689), 467-472. doi:10.1038/nature25432

Barbie, D. A., Tamayo, P., Boehm, J. S., Kim, S. Y., Moody, S. E., Dunn, I. F., . . . Hahn, W. C. (2009). Systematic RNA interference reveals that oncogenic KRAS-driven cancers require TBK1. *Nature, 462*(7269), 108-112. doi:10.1038/nature08460

Bardeesy, N., & DePinho, R. A. (2002). Pancreatic cancer biology and genetics. *Nat Rev Cancer, 2*(12), 897-909. doi:10.1038/nrc949

Barnett, S. F., Defeo-Jones, D., Fu, S., Hancock, P. J., Haskell, K. M., Jones, R. E., . . . Huber, H. E. (2005). Identification and characterization of pleckstrin-homology-domain-dependent and isoenzyme-specific Akt inhibitors. *Biochem J, 385*(Pt 2), 399-408. doi:10.1042/BJ20041140

Bellacosa, A., Testa, J. R., Staal, S. P., & Tsichlis, P. N. (1991). A retroviral oncogene, akt, encoding a serine-threonine kinase containing an SH2-like region. *Science, 254*(5029), 274-277. Retrieved from https://www.ncbi.nlm.nih.gov/pubmed/1833819

Ben-Batalla, I., Erdmann, R., Jorgensen, H., Mitchell, R., Ernst, T., von Amsberg, G., . . . Loges, S. (2017). Axl Blockade by BGB324 Inhibits BCR-ABL Tyrosine Kinase Inhibitor-Sensitive and -Resistant Chronic Myeloid Leukemia. *Clin Cancer Res, 23*(9), 2289-2300. doi:10.1158/1078-0432.CCR-16-1930

Biancur, D. E., & Kimmelman, A. C. (2018). The plasticity of pancreatic cancer metabolism in tumor progression and therapeutic resistance. *Biochim Biophys Acta Rev Cancer, 1870*(1), 67-75. doi:10.1016/j.bbcan.2018.04.011

Biankin, A. V., Waddell, N., Kassahn, K. S., Gingras, M. C., Muthuswamy, L. B., Johns, A. L., . . . Grimmond, S. M. (2012). Pancreatic cancer genomes reveal aberrations in axon guidance pathway genes. *Nature, 491*(7424), 399-405. doi:10.1038/nature11547

Bissell, M. J., Radisky, D. C., Rizki, A., Weaver, V. M., & Petersen, O. W. (2002). The organizing principle: microenvironmental influences in the normal and malignant breast. *Differentiation, 70*(9-10), 537-546. doi:10.1046/j.1432-0436.2002.700907.x

Bond, M. R., & Hanover, J. A. (2015). A little sugar goes a long way: the cell biology of O-GlcNAc. *J Cell Biol, 208*(7), 869-880. doi:10.1083/jcb.201501101

Bonin, S., Pracella, D., Barbazza, R., Dotti, I., Boffo, S., & Stanta, G. (2019). PI3K/AKT Signaling in Breast Cancer Molecular Subtyping and Lymph Node Involvement. *Dis Markers, 2019*, 7832376. doi:10.1155/2019/7832376

Brabletz, S., & Brabletz, T. (2010). The ZEB/miR-200 feedback loop--a motor of cellular plasticity in development and cancer? *EMBO Rep, 11*(9), 670-677. doi:10.1038/embor.2010.117

Brabletz, T. (2012). MiR-34 and SNAIL: another double-negative feedback loop controlling cellular plasticity/EMT governed by p53. *Cell Cycle, 11*(2), 215-216. doi:10.4161/cc.11.2.18900

Brabletz, T., Jung, A., Reu, S., Porzner, M., Hlubek, F., Kunz-Schughart, L. A., . . . Kirchner, T. (2001). Variable beta-catenin expression in colorectal cancers indicates tumor progression driven by the tumor environment. *Proc Natl Acad Sci U S A, 98*(18), 10356-10361. doi:10.1073/pnas.171610498

Brabletz, T., Kalluri, R., Nieto, M. A., & Weinberg, R. A. (2018). EMT in cancer. *Nat Rev Cancer, 18*(2), 128-134. doi:10.1038/nrc.2017.118

Brand, T. M., Iida, M., Stein, A. P., Corrigan, K. L., Braverman, C. M., Coan, J. P., . . . Wheeler, D. L. (2015). AXL Is a Logical Molecular Target in Head and Neck Squamous Cell Carcinoma. *Clin Cancer Res, 21*(11), 2601-2612. doi:10.1158/1078-0432.CCR-14-2648

Braunger, J., Schleithoff, L., Schulz, A. S., Kessler, H., Lammers, R., Ullrich, A., . . . Janssen, J. W. (1997). Intracellular signaling of the Ufo/Axl receptor tyrosine kinase is mediated mainly by a multi-substrate docking-site. *Oncogene, 14*(22), 2619-2631. doi:10.1038/sj.onc.1201123

Bryant, D. M., Wylie, F. G., & Stow, J. L. (2005). Regulation of endocytosis, nuclear translocation, and signaling of fibroblast growth factor receptor 1 by E-cadherin. *Mol Biol Cell, 16*(1), 14-23. doi:10.1091/mbc.e04-09-0845

Buck, E., Eyzaguirre, A., Barr, S., Thompson, S., Sennello, R., Young, D., . . . Haley, J. D. (2007). Loss of homotypic cell adhesion by epithelial-mesenchymal transition or mutation limits sensitivity to epidermal growth factor receptor inhibition. *Mol Cancer Ther, 6*(2), 532-541. doi:10.1158/1535-7163.MCT-06-0462

Burk, U., Schubert, J., Wellner, U., Schmalhofer, O., Vincan, E., Spaderna, S., & Brabletz, T. (2008). A reciprocal repression between ZEB1 and members of the miR-200 family promotes EMT and invasion in cancer cells. *EMBO Rep, 9*(6), 582-589. doi:10.1038/embor.2008.74

Byers, L. A., Diao, L., Wang, J., Saintigny, P., Girard, L., Peyton, M., . . . Heymach, J. V. (2013). An epithelial-mesenchymal transition gene signature predicts resistance to EGFR and PI3K inhibitors and identifies Axl as a therapeutic target for overcoming EGFR inhibitor resistance. *Clin Cancer Res, 19*(1), 279-290. doi:10.1158/1078-0432.CCR-12-1558

Campbell, P. J., Yachida, S., Mudie, L. J., Stephens, P. J., Pleasance, E. D., Stebbings, L. A., . . . Futreal, P. A. (2010). The patterns and dynamics of genomic instability in metastatic pancreatic cancer. *Nature, 467*(7319), 1109-1113. doi:10.1038/nature09460

Canadas, I., Thummalapalli, R., Kim, J. W., Kitajima, S., Jenkins, R. W., Christensen, C. L., . . . Barbie, D. A. (2018). Tumor innate immunity primed by specific interferon-stimulated endogenous retroviruses. *Nat Med, 24*(8), 1143-1150. doi:10.1038/s41591-018-0116-5

Caramel, J., Papadogeorgakis, E., Hill, L., Browne, G. J., Richard, G., Wierinckx, A., . . . Tulchinsky, E. (2013). A switch in the expression of embryonic EMT-inducers drives the development of malignant melanoma. *Cancer Cell, 24*(4), 466-480. doi:10.1016/j.ccr.2013.08.018

Cates, J. M., Byrd, R. H., Fohn, L. E., Tatsas, A. D., Washington, M. K., & Black, C. C. (2009). Epithelial-mesenchymal transition markers in pancreatic ductal adenocarcinoma. *Pancreas, 38*(1), e1-6. doi:10.1097/MPA.0b013e3181878b7f

Cerami, E., Gao, J., Dogrusoz, U., Gross, B. E., Sumer, S. O., Aksoy, B. A., . . . Schultz, N. (2012). The cBio cancer genomics portal: an open platform for exploring multidimensional cancer genomics data. *Cancer Discov, 2*(5), 401-404. doi:10.1158/2159-8290.CD-12-0095

Chaffer, C. L., Brueckmann, I., Scheel, C., Kaestli, A. J., Wiggins, P. A., Rodrigues, L. O., . . . Weinberg, R. A. (2011). Normal and neoplastic nonstem cells can spontaneously convert to a stem-like state. *Proc Natl Acad Sci U S A, 108*(19), 7950-7955. doi:10.1073/pnas.1102454108

Chaffer, C. L., Marjanovic, N. D., Lee, T., Bell, G., Kleer, C. G., Reinhardt, F., . . . Weinberg, R. A. (2013). Poised chromatin at the ZEB1 promoter enables breast cancer cell plasticity and enhances tumorigenicity. *Cell, 154*(1), 61-74. doi:10.1016/j.cell.2013.06.005

Chen, G., Bradford, W. D., Seidel, C. W., & Li, R. (2012). Hsp90 stress potentiates rapid cellular adaptation through induction of aneuploidy. *Nature, 482*(7384), 246-250. doi:10.1038/nature10795

Chen, Y., LeBleu, V. S., Carstens, J. L., Sugimoto, H., Zheng, X., Malasi, S., . . . Kalluri, R. (2018). Dual reporter genetic mouse models of pancreatic cancer identify an epithelial-to-mesenchymal transition-independent metastasis program. *EMBO Mol Med, 10*(10). doi:10.15252/emmm.201809085

Cheng, Q., Chang, J. T., Gwin, W. R., Zhu, J., Ambs, S., Geradts, J., & Lyerly, H. K. (2014). A signature of epithelial-mesenchymal plasticity and stromal activation in primary tumor modulates late recurrence in breast cancer independent of disease subtype. *Breast Cancer Res, 16*(4), 407. doi:10.1186/s13058-014-0407-9

Cheng, Z. X., Sun, B., Wang, S. J., Gao, Y., Zhang, Y. M., Zhou, H. X., . . . Bai, X. W. (2011). Nuclear factor-kappaB-dependent epithelial to mesenchymal transition induced by HIF-1alpha activation in pancreatic cancer cells under hypoxic conditions. *PLoS One, 6*(8), e23752. doi:10.1371/journal.pone.0023752

Cheng, Z. X., Wang, D. W., Liu, T., Liu, W. X., Xia, W. B., Xu, J., . . . Zhong, Z. H. (2014). Effects of the HIF-1alpha and NF-kappaB loop on epithelial-mesenchymal transition and chemoresistance induced by hypoxia in pancreatic cancer cells. *Oncol Rep, 31*(4), 1891-1898. doi:10.3892/or.2014.3022

Chien, Y., Kim, S., Bumeister, R., Loo, Y. M., Kwon, S. W., Johnson, C. L., . . . White, M. A. (2006). RalB GTPase-mediated activation of the IkappaB family kinase

TBK1 couples innate immune signaling to tumor cell survival. *Cell, 127*(1), 157-170. doi:10.1016/j.cell.2006.08.034

Chin, Y. R., Yoshida, T., Marusyk, A., Beck, A. H., Polyak, K., & Toker, A. (2014). Targeting Akt3 signaling in triple-negative breast cancer. *Cancer Res, 74*(3), 964-973. doi:10.1158/0008-5472.CAN-13-2175

Choi, Y. J., Kim, S. Y., So, K. S., Baek, I. J., Kim, W. S., Choi, S. H., . . . Choi, C. M. (2015). AUY922 effectively overcomes MET- and AXL-mediated resistance to EGFR-TKI in lung cancer cells. *PLoS One, 10*(3), e0119832. doi:10.1371/journal.pone.0119832

Chung, S., Yao, J., Suyama, K., Bajaj, S., Qian, X., Loudig, O. D., . . . Hazan, R. B. (2013). N-cadherin regulates mammary tumor cell migration through Akt3 suppression. *Oncogene, 32*(4), 422-430. doi:10.1038/onc.2012.65

Collisson, E. A., Sadanandam, A., Olson, P., Gibb, W. J., Truitt, M., Gu, S., . . . Gray, J. W. (2011). Subtypes of pancreatic ductal adenocarcinoma and their differing responses to therapy. *Nat Med, 17*(4), 500-503. doi:10.1038/nm.2344

Cooper, J. M., Ou, Y. H., McMillan, E. A., Vaden, R. M., Zaman, A., Bodemann, B. O., . . . White, M. A. (2017). TBK1 Provides Context-Selective Support of the Activated AKT/mTOR Pathway in Lung Cancer. *Cancer Res, 77*(18), 5077-5094. doi:10.1158/0008-5472.CAN-17-0829

Cox, A. D., & Der, C. J. (2010). Ras history: The saga continues. *Small GTPases, 1*(1), 2-27. doi:10.4161/sgtp.1.1.12178

Cox, A. D., Fesik, S. W., Kimmelman, A. C., Luo, J., & Der, C. J. (2014). Drugging the undruggable RAS: Mission possible? *Nat Rev Drug Discov, 13*(11), 828-851. doi:10.1038/nrd4389

Creighton, C. J., Li, X., Landis, M., Dixon, J. M., Neumeister, V. M., Sjolund, A., . . . Chang, J. C. (2009). Residual breast cancers after conventional therapy display mesenchymal as well as tumor-initiating features. *Proc Natl Acad Sci U S A, 106*(33), 13820-13825. doi:10.1073/pnas.0905718106

Cruz, V. H., Arner, E. N., Du, W., Bremauntz, A. E., & Brekken, R. A. (2019). Axl-mediated activation of TBK1 drives epithelial plasticity in pancreatic cancer. *JCI Insight, 5*. doi:10.1172/jci.insight.126117

Cruz, V. H., & Brekken, R. A. (2018). Assessment of TANK-binding kinase 1 as a therapeutic target in cancer. *J Cell Commun Signal, 12*(1), 83-90. doi:10.1007/s12079-017-0438-y

Cuevas, I. C., Sahoo, S. S., Kumar, A., Zhang, H., Westcott, J., Aguilar, M., . . . Castrillon, D. H. (2019). Fbxw7 is a driver of uterine carcinosarcoma by promoting epithelial-mesenchymal transition. *Proc Natl Acad Sci U S A, 116*(51), 25880-25890. doi:10.1073/pnas.1911310116

Curtis, C., Shah, S. P., Chin, S. F., Turashvili, G., Rueda, O. M., Dunning, M. J., . . . Aparicio, S. (2012). The genomic and transcriptomic architecture of 2,000 breast tumours reveals novel subgroups. *Nature, 486*(7403), 346-352. doi:10.1038/nature10983

Dang, T. T., Esparza, M. A., Maine, E. A., Westcott, J. M., & Pearson, G. W. (2015). DeltaNp63alpha Promotes Breast Cancer Cell Motility through the Selective

Activation of Components of the Epithelial-to-Mesenchymal Transition Program. *Cancer Res, 75*(18), 3925-3935. doi:10.1158/0008-5472.CAN-14-3363

Davoli, T., Uno, H., Wooten, E. C., & Elledge, S. J. (2017). Tumor aneuploidy correlates with markers of immune evasion and with reduced response to immunotherapy. *Science, 355*(6322). doi:10.1126/science.aaf8399

De La, O. J., Emerson, L. L., Goodman, J. L., Froebe, S. C., Illum, B. E., Curtis, A. B., & Murtaugh, L. C. (2008). Notch and Kras reprogram pancreatic acinar cells to ductal intraepithelial neoplasia. *Proc Natl Acad Sci U S A, 105*(48), 18907-18912. doi:10.1073/pnas.0810111105

Del Pozo Martin, Y., Park, D., Ramachandran, A., Ombrato, L., Calvo, F., Chakravarty, P., . . . Malanchi, I. (2015). Mesenchymal Cancer Cell-Stroma Crosstalk Promotes Niche Activation, Epithelial Reversion, and Metastatic Colonization. *Cell Rep, 13*(11), 2456-2469. doi:10.1016/j.celrep.2015.11.025

Denecker, G., Vandamme, N., Akay, O., Koludrovic, D., Taminau, J., Lemeire, K., . . . Berx, G. (2014). Identification of a ZEB2-MITF-ZEB1 transcriptional network that controls melanogenesis and melanoma progression. *Cell Death Differ, 21*(8), 1250-1261. doi:10.1038/cdd.2014.44

Diaz, V. M., Vinas-Castells, R., & Garcia de Herreros, A. (2014). Regulation of the protein stability of EMT transcription factors. *Cell Adh Migr, 8*(4), 418-428. doi:10.4161/19336918.2014.969998

Dongre, A., Rashidian, M., Reinhardt, F., Bagnato, A., Keckesova, Z., Ploegh, H. L., & Weinberg, R. A. (2017). Epithelial-to-Mesenchymal Transition Contributes to Immunosuppression in Breast Carcinomas. *Cancer Res, 77*(15), 3982-3989. doi:10.1158/0008-5472.CAN-16-3292

Dontu, G., Abdallah, W. M., Foley, J. M., Jackson, K. W., Clarke, M. F., Kawamura, M. J., & Wicha, M. S. (2003). In vitro propagation and transcriptional profiling of human mammary stem/progenitor cells. *Genes Dev, 17*(10), 1253-1270. doi:10.1101/gad.1061803

Dou, Z., Ghosh, K., Vizioli, M. G., Zhu, J., Sen, P., Wangensteen, K. J., . . . Berger, S. L. (2017). Cytoplasmic chromatin triggers inflammation in senescence and cancer. *Nature, 550*(7676), 402-406. doi:10.1038/nature24050

Du, W., & Brekken, R. A. (2018). Does Axl have potential as a therapeutic target in pancreatic cancer? *Expert Opin Ther Targets, 22*(11), 955-966. doi:10.1080/14728222.2018.1527315

Du, W., Huang, H., Sorrelle, N., & Brekken, R. A. (2018). Sitravatinib potentiates immune checkpoint blockade in refractory cancer models. *JCI Insight, 3*(21). doi:10.1172/jci.insight.124184

Engelman, J. A., Chen, L., Tan, X., Crosby, K., Guimaraes, A. R., Upadhyay, R., . . . Wong, K. K. (2008). Effective use of PI3K and MEK inhibitors to treat mutant Kras G12D and PIK3CA H1047R murine lung cancers. *Nat Med, 14*(12), 1351-1356. doi:10.1038/nm.1890

Eskiocak, B., McMillan, E. A., Mendiratta, S., Kollipara, R. K., Zhang, H., Humphries, C. G., . . . White, M. A. (2017). Biomarker Accessible and Chemically

Addressable Mechanistic Subtypes of BRAF Melanoma. *Cancer Discov, 7*(8), 832-851. doi:10.1158/2159-8290.cd-16-0955

Fan, B., Malato, Y., Calvisi, D. F., Naqvi, S., Razumilava, N., Ribback, S., . . . Willenbring, H. (2012). Cholangiocarcinomas can originate from hepatocytes in mice. *J Clin Invest, 122*(8), 2911-2915. doi:10.1172/JCI63212

Farmer, P., Bonnefoi, H., Anderle, P., Cameron, D., Wirapati, P., Becette, V., . . . Delorenzi, M. (2009). A stroma-related gene signature predicts resistance to neoadjuvant chemotherapy in breast cancer. *Nat Med, 15*(1), 68-74. doi:10.1038/nm.1908

Fischer, K. R., Durrans, A., Lee, S., Sheng, J., Li, F., Wong, S. T., . . . Gao, D. (2015). Epithelial-to-mesenchymal transition is not required for lung metastasis but contributes to chemoresistance. *Nature, 527*(7579), 472-476. doi:10.1038/nature15748

Gaianigo, N., Melisi, D., & Carbone, C. (2017). EMT and Treatment Resistance in Pancreatic Cancer. *Cancers (Basel), 9*(9). doi:10.3390/cancers9090122

Galluzzi, L., Buque, A., Kepp, O., Zitvogel, L., & Kroemer, G. (2015). Immunological Effects of Conventional Chemotherapy and Targeted Anticancer Agents. *Cancer Cell, 28*(6), 690-714. doi:10.1016/j.ccell.2015.10.012

Galluzzi, L., Vanpouille-Box, C., Bakhoum, S. F., & Demaria, S. (2018). SnapShot: CGAS-STING Signaling. *Cell, 173*(1), 276-276 e271. doi:10.1016/j.cell.2018.03.015

Garbe, J. C., Pepin, F., Pelissier, F. A., Sputova, K., Fridriksdottir, A. J., Guo, D. E., . . . Labarge, M. A. (2012). Accumulation of multipotent progenitors with a basal differentiation bias during aging of human mammary epithelia. *Cancer Res, 72*(14), 3687-3701. doi:10.1158/0008-5472.CAN-12-0157

Genovese, G., Carugo, A., Tepper, J., Robinson, F. S., Li, L., Svelto, M., . . . Chin, L. (2017). Synthetic vulnerabilities of mesenchymal subpopulations in pancreatic cancer. *Nature, 542*(7641), 362-366. doi:10.1038/nature21064

Gheldof, A., & Berx, G. (2013). Cadherins and epithelial-to-mesenchymal transition. *Prog Mol Biol Transl Sci, 116*, 317-336. doi:10.1016/B978-0-12-394311-8.00014-5

Giampieri, S., Manning, C., Hooper, S., Jones, L., Hill, C. S., & Sahai, E. (2009). Localized and reversible TGFbeta signalling switches breast cancer cells from cohesive to single cell motility. *Nat Cell Biol, 11*(11), 1287-1296. doi:10.1038/ncb1973

Gibbons, D. L., Lin, W., Creighton, C. J., Rizvi, Z. H., Gregory, P. A., Goodall, G. J., . . . Kurie, J. M. (2009). Contextual extracellular cues promote tumor cell EMT and metastasis by regulating miR-200 family expression. *Genes Dev, 23*(18), 2140-2151. doi:10.1101/gad.1820209

Gjerdrum, C., Tiron, C., Hoiby, T., Stefansson, I., Haugen, H., Sandal, T., . . . Lorens, J. B. (2010). Axl is an essential epithelial-to-mesenchymal transition-induced regulator of breast cancer metastasis and patient survival. *Proc Natl Acad Sci U S A, 107*(3), 1124-1129. doi:10.1073/pnas.0909333107

Gluck, S., Guey, B., Gulen, M. F., Wolter, K., Kang, T. W., Schmacke, N. A., . . . Ablasser, A. (2017). Innate immune sensing of cytosolic chromatin fragments through cGAS promotes senescence. *Nat Cell Biol, 19*(9), 1061-1070. doi:10.1038/ncb3586

Gomez, L. S., Zancan, P., Marcondes, M. C., Ramos-Santos, L., Meyer-Fernandes, J. R., Sola-Penna, M., & Da Silva, D. (2013). Resveratrol decreases breast cancer cell viability and glucose metabolism by inhibiting 6-phosphofructo-1-kinase. *Biochimie, 95*(6), 1336-1343. doi:10.1016/j.biochi.2013.02.013

Greten, F. R., Weber, C. K., Greten, T. F., Schneider, G., Wagner, M., Adler, G., & Schmid, R. M. (2002). Stat3 and NF-kappaB activation prevents apoptosis in pancreatic carcinogenesis. *Gastroenterology, 123*(6), 2052-2063. doi:10.1053/gast.2002.37075

Grigore, A. D., Jolly, M. K., Jia, D., Farach-Carson, M. C., & Levine, H. (2016). Tumor Budding: The Name is EMT. Partial EMT. *J Clin Med, 5*(5). doi:10.3390/jcm5050051

Grille, S. J., Bellacosa, A., Upson, J., Klein-Szanto, A. J., van Roy, F., Lee-Kwon, W., . . . Larue, L. (2003). The protein kinase Akt induces epithelial mesenchymal transition and promotes enhanced motility and invasiveness of squamous cell carcinoma lines. *Cancer Res, 63*(9), 2172-2178. Retrieved from https://www.ncbi.nlm.nih.gov/pubmed/12727836

Grippo, P. J., Nowlin, P. S., Demeure, M. J., Longnecker, D. S., & Sandgren, E. P. (2003). Preinvasive pancreatic neoplasia of ductal phenotype induced by acinar cell targeting of mutant Kras in transgenic mice. *Cancer Res, 63*(9), 2016-2019. Retrieved from https://www.ncbi.nlm.nih.gov/pubmed/12727811

Grottke, A., Ewald, F., Lange, T., Norz, D., Herzberger, C., Bach, J., . . . Jucker, M. (2016). Downregulation of AKT3 Increases Migration and Metastasis in Triple Negative Breast Cancer Cells by Upregulating S100A4. *PLoS One, 11*(1), e0146370. doi:10.1371/journal.pone.0146370

Gu, S., Dai, H., Zhao, X., Gui, C., & Gui, J. (2020). AKT3 deficiency in M2 macrophages impairs cutaneous wound healing by disrupting tissue remodeling. *Aging (Albany NY), 12*. doi:10.18632/aging.103051

Guest, R. V., Boulter, L., Kendall, T. J., Minnis-Lyons, S. E., Walker, R., Wigmore, S. J., . . . Forbes, S. J. (2014). Cell lineage tracing reveals a biliary origin of intrahepatic cholangiocarcinoma. *Cancer Res, 74*(4), 1005-1010. doi:10.1158/0008-5472.CAN-13-1911

Gupta, P. B., Fillmore, C. M., Jiang, G., Shapira, S. D., Tao, K., Kuperwasser, C., & Lander, E. S. (2011). Stochastic state transitions give rise to phenotypic equilibrium in populations of cancer cells. *Cell, 146*(4), 633-644. doi:10.1016/j.cell.2011.07.026

Gupta, P. B., Onder, T. T., Jiang, G., Tao, K., Kuperwasser, C., Weinberg, R. A., & Lander, E. S. (2009). Identification of selective inhibitors of cancer stem cells by high-throughput screening. *Cell, 138*(4), 645-659. doi:10.1016/j.cell.2009.06.034

Gysin, S., Salt, M., Young, A., & McCormick, F. (2011). Therapeutic strategies for targeting ras proteins. *Genes Cancer, 2*(3), 359-372. doi:10.1177/1947601911412376

Haigis, K. M. (2017). KRAS Alleles: The Devil Is in the Detail. *Trends Cancer, 3*(10), 686-697. doi:10.1016/j.trecan.2017.08.006

Halbrook, C. J., & Lyssiotis, C. A. (2017). Employing Metabolism to Improve the Diagnosis and Treatment of Pancreatic Cancer. *Cancer Cell, 31*(1), 5-19. doi:10.1016/j.ccell.2016.12.006

Hamad, N. M., Elconin, J. H., Karnoub, A. E., Bai, W., Rich, J. N., Abraham, R. T., . . . Counter, C. M. (2002). Distinct requirements for Ras oncogenesis in human versus mouse cells. *Genes Dev, 16*(16), 2045-2057. doi:10.1101/gad.993902

Hanover, J. A., Krause, M. W., & Love, D. C. (2012). Bittersweet memories: linking metabolism to epigenetics through O-GlcNAcylation. *Nat Rev Mol Cell Biol, 13*(5), 312-321. doi:10.1038/nrm3334

Harma, V., Schukov, H. P., Happonen, A., Ahonen, I., Virtanen, J., Siitari, H., . . . Nees, M. (2014). Quantification of dynamic morphological drug responses in 3D organotypic cell cultures by automated image analysis. *PLoS One, 9*(5), e96426. doi:10.1371/journal.pone.0096426

Helgason, E., Phung, Q. T., & Dueber, E. C. (2013). Recent insights into the complexity of Tank-binding kinase 1 signaling networks: the emerging role of cellular localization in the activation and substrate specificity of TBK1. *FEBS Lett, 587*(8), 1230-1237. doi:10.1016/j.febslet.2013.01.059

Hill, L., Browne, G., & Tulchinsky, E. (2013). ZEB/miR-200 feedback loop: at the crossroads of signal transduction in cancer. *Int J Cancer, 132*(4), 745-754. doi:10.1002/ijc.27708

Hill, M. A., Alexander, W. B., Guo, B., Kato, Y., Patra, K., O'Dell, M. R., . . . Hezel, A. F. (2018). Kras and Tp53 Mutations Cause Cholangiocyte- and Hepatocyte-Derived Cholangiocarcinoma. *Cancer Res, 78*(16), 4445-4451. doi:10.1158/0008-5472.CAN-17-1123

Hingorani, S. R., Petricoin, E. F., Maitra, A., Rajapakse, V., King, C., Jacobetz, M. A., . . . Tuveson, D. A. (2003). Preinvasive and invasive ductal pancreatic cancer and its early detection in the mouse. *Cancer Cell, 4*(6), 437-450. Retrieved from https://www.ncbi.nlm.nih.gov/pubmed/14706336

Hingorani, S. R., Wang, L., Multani, A. S., Combs, C., Deramaudt, T. B., Hruban, R. H., . . . Tuveson, D. A. (2005). Trp53R172H and KrasG12D cooperate to promote chromosomal instability and widely metastatic pancreatic ductal adenocarcinoma in mice. *Cancer Cell, 7*(5), 469-483. doi:10.1016/j.ccr.2005.04.023

Hoesel, B., & Schmid, J. A. (2013). The complexity of NF-kappaB signaling in inflammation and cancer. *Mol Cancer, 12*, 86. doi:10.1186/1476-4598-12-86

Holland, S. J., Pan, A., Franci, C., Hu, Y., Chang, B., Li, W., . . . Hitoshi, Y. (2010). R428, a selective small molecule inhibitor of Axl kinase, blocks tumor spread and prolongs survival in models of metastatic breast cancer. *Cancer Res, 70*(4), 1544-1554. doi:10.1158/0008-5472.CAN-09-2997

Hosein AN, H. H., Wang Z, Parmar K, Du W, Huang J, Maitra A, Olson E, Verma U, Brekken RA. (2019). Cellular heterogeneity during mouse pancreatic ductal adenocarcinoma progression at single-cell resolution. *bioRxiv*. doi:https://doi.org/10.1101/539874

Hotz, B., Arndt, M., Dullat, S., Bhargava, S., Buhr, H. J., & Hotz, H. G. (2007). Epithelial to mesenchymal transition: expression of the regulators snail, slug, and twist in pancreatic cancer. *Clin Cancer Res, 13*(16), 4769-4776. doi:10.1158/1078-0432.CCR-06-2926

Hudis, C., Swanton, C., Janjigian, Y. Y., Lee, R., Sutherland, S., Lehman, R., . . . Han, H. S. (2013). A phase 1 study evaluating the combination of an allosteric AKT inhibitor (MK-2206) and trastuzumab in patients with HER2-positive solid tumors. *Breast Cancer Res, 15*(6), R110. doi:10.1186/bcr3577

Hugo, W., Zaretsky, J. M., Sun, L., Song, C., Moreno, B. H., Hu-Lieskovan, S., . . . Lo, R. S. (2016). Genomic and Transcriptomic Features of Response to Anti-PD-1 Therapy in Metastatic Melanoma. *Cell, 165*(1), 35-44. doi:10.1016/j.cell.2016.02.065

Ikenoue, T., Terakado, Y., Nakagawa, H., Hikiba, Y., Fujii, T., Matsubara, D., . . . Furukawa, Y. (2016). A novel mouse model of intrahepatic cholangiocarcinoma induced by liver-specific Kras activation and Pten deletion. *Sci Rep, 6*, 23899. doi:10.1038/srep23899

Irie, H. Y., Pearline, R. V., Grueneberg, D., Hsia, M., Ravichandran, P., Kothari, N., . . . Brugge, J. S. (2005). Distinct roles of Akt1 and Akt2 in regulating cell migration and epithelial-mesenchymal transition. *J Cell Biol, 171*(6), 1023-1034. doi:10.1083/jcb.200505087

Janda, E., Lehmann, K., Killisch, I., Jechlinger, M., Herzig, M., Downward, J., . . . Grunert, S. (2002). Ras and TGF[beta] cooperatively regulate epithelial cell plasticity and metastasis: dissection of Ras signaling pathways. *J Cell Biol, 156*(2), 299-313. doi:10.1083/jcb.200109037

Jansen, V. M., Mayer, I. A., & Arteaga, C. L. (2016). Is There a Future for AKT Inhibitors in the Treatment of Cancer? *Clin Cancer Res, 22*(11), 2599-2601. doi:10.1158/1078-0432.CCR-16-0100

Jechlinger, M., Grunert, S., & Beug, H. (2002). Mechanisms in epithelial plasticity and metastasis: insights from 3D cultures and expression profiling. *J Mammary Gland Biol Neoplasia, 7*(4), 415-432. Retrieved from https://www.ncbi.nlm.nih.gov/pubmed/12882526

Jolly, M. K., Ware, K. E., Gilja, S., Somarelli, J. A., & Levine, H. (2017). EMT and MET: necessary or permissive for metastasis? *Mol Oncol, 11*(7), 755-769. doi:10.1002/1878-0261.12083

Jones, J., Bentas, W., Blaheta, R. A., Makarevic, J., Hudak, L., Wedel, S., . . . Juengel, E. (2008). Modulation of adhesion and growth of colon and pancreatic cancer cells by the histone deacetylase inhibitor valproic acid. *Int J Mol Med, 22*(3), 293-299. Retrieved from https://www.ncbi.nlm.nih.gov/pubmed/18698487

Kamei, T., Matozaki, T., Sakisaka, T., Kodama, A., Yokoyama, S., Peng, Y. F., . . . Takai, Y. (1999). Coendocytosis of cadherin and c-Met coupled to disruption of

cell-cell adhesion in MDCK cells--regulation by Rho, Rac and Rab small G proteins. *Oncogene, 18*(48), 6776-6784. doi:10.1038/sj.onc.1203114

Karin, M. (2006). Nuclear factor-kappaB in cancer development and progression. *Nature, 441*(7092), 431-436. doi:10.1038/nature04870

Karnoub, A. E., & Weinberg, R. A. (2008). Ras oncogenes: split personalities. *Nat Rev Mol Cell Biol, 9*(7), 517-531. doi:10.1038/nrm2438

Keil, C., Leach, Robert William, Faizaan, Shaik Mohammed, Bezawada, Srikanth, Parsons, Lance, & Baryshnikova, Anastasia. (2016, October 13). Treeview 3.0 (alpha 3) - Visualization and analysis of large data matrices. Zenodo. http://doi.org/10.5281/zenodo.160573.

Kim, D., Paggi, J. M., Park, C., Bennett, C., & Salzberg, S. L. (2019). Graph-based genome alignment and genotyping with HISAT2 and HISAT-genotype. *Nat Biotechnol, 37*(8), 907-915. doi:10.1038/s41587-019-0201-4

Kim, H. N., Narayanan, N. K., Lasano, S., & Narayanan, B. (2011). Modulation of PGE2-induced EP4 expression on snail signaling and the impact on epithelial-mesenchymal transition: significance of EP4 antagonism. *Anticancer Res, 31*(12), 4347-4357. Retrieved from https://www.ncbi.nlm.nih.gov/pubmed/22199300

Kim, J. Y., Welsh, E. A., Oguz, U., Fang, B., Bai, Y., Kinose, F., . . . Haura, E. B. (2013). Dissection of TBK1 signaling via phosphoproteomics in lung cancer cells. *Proc Natl Acad Sci U S A, 110*(30), 12414-12419. doi:10.1073/pnas.1220674110

Kirane, A., Ludwig, K. F., Sorrelle, N., Haaland, G., Sandal, T., Ranaweera, R., . . . Brekken, R. A. (2015). Warfarin Blocks Gas6-Mediated Axl Activation Required for Pancreatic Cancer Epithelial Plasticity and Metastasis. *Cancer Res, 75*(18), 3699-3705. doi:10.1158/0008-5472.CAN-14-2887-T

Konishi, H., Kuroda, S., Tanaka, M., Matsuzaki, H., Ono, Y., Kameyama, K., . . . Kikkawa, U. (1995). Molecular cloning and characterization of a new member of the RAC protein kinase family: association of the pleckstrin homology domain of three types of RAC protein kinase with protein kinase C subspecies and beta gamma subunits of G proteins. *Biochem Biophys Res Commun, 216*(2), 526-534. doi:10.1006/bbrc.1995.2654

Koorstra, J. B., Karikari, C. A., Feldmann, G., Bisht, S., Rojas, P. L., Offerhaus, G. J., . . . Maitra, A. (2009). The Axl receptor tyrosine kinase confers an adverse prognostic influence in pancreatic cancer and represents a new therapeutic target. *Cancer Biol Ther, 8*(7), 618-626. doi:10.4161/cbt.8.7.7923

Kopp, J. L., Dubois, C. L., Schaeffer, D. F., Samani, A., Taghizadeh, F., Cowan, R. W., . . . Sander, M. (2018). Loss of Pten and Activation of Kras Synergistically Induce Formation of Intraductal Papillary Mucinous Neoplasia From Pancreatic Ductal Cells in Mice. *Gastroenterology, 154*(5), 1509-1523 e1505. doi:10.1053/j.gastro.2017.12.007

Kopp, J. L., von Figura, G., Mayes, E., Liu, F. F., Dubois, C. L., Morris, J. P. t., . . . Sander, M. (2012). Identification of Sox9-dependent acinar-to-ductal reprogramming as the principal mechanism for initiation of pancreatic ductal adenocarcinoma. *Cancer Cell, 22*(6), 737-750. doi:10.1016/j.ccr.2012.10.025

Korherr, C., Gille, H., Schafer, R., Koenig-Hoffmann, K., Dixelius, J., Egland, K. A., . . . Brinkmann, U. (2006). Identification of proangiogenic genes and pathways by high-throughput functional genomics: TBK1 and the IRF3 pathway. *Proc Natl Acad Sci U S A, 103*(11), 4240-4245. doi:10.1073/pnas.0511319103

Kosugi, S., Hasebe, M., Tomita, M., & Yanagawa, H. (2009). Systematic identification of cell cycle-dependent yeast nucleocytoplasmic shuttling proteins by prediction of composite motifs. *Proc Natl Acad Sci U S A, 106*(25), 10171-10176. doi:10.1073/pnas.0900604106

Krebs, A. M., Mitschke, J., Lasierra Losada, M., Schmalhofer, O., Boerries, M., Busch, H., . . . Brabletz, T. (2017). The EMT-activator Zeb1 is a key factor for cell plasticity and promotes metastasis in pancreatic cancer. *Nat Cell Biol, 19*(5), 518-529. doi:10.1038/ncb3513

Kudo-Saito, C., Shirako, H., Takeuchi, T., & Kawakami, Y. (2009). Cancer metastasis is accelerated through immunosuppression during Snail-induced EMT of cancer cells. *Cancer Cell, 15*(3), 195-206. doi:10.1016/j.ccr.2009.01.023

Labarge, M. A., Garbe, J. C., & Stampfer, M. R. (2013). Processing of human reduction mammoplasty and mastectomy tissues for cell culture. *J Vis Exp*(71). doi:10.3791/50011

Lamouille, S., Xu, J., & Derynck, R. (2014). Molecular mechanisms of epithelial-mesenchymal transition. *Nat Rev Mol Cell Biol, 15*(3), 178-196. doi:10.1038/nrm3758

Larsen, J. E., Nathan, V., Osborne, J. K., Farrow, R. K., Deb, D., Sullivan, J. P., . . . Minna, J. D. (2016). ZEB1 drives epithelial-to-mesenchymal transition in lung cancer. *J Clin Invest, 126*(9), 3219-3235. doi:10.1172/JCI76725

Larue, L., & Bellacosa, A. (2005). Epithelial-mesenchymal transition in development and cancer: role of phosphatidylinositol 3' kinase/AKT pathways. *Oncogene, 24*(50), 7443-7454. doi:10.1038/sj.onc.1209091

Laughney, A. M., Elizalde, S., Genovese, G., & Bakhoum, S. F. (2015). Dynamics of Tumor Heterogeneity Derived from Clonal Karyotypic Evolution. *Cell Rep, 12*(5), 809-820. doi:10.1016/j.celrep.2015.06.065

Leconet, W., Larbouret, C., Chardes, T., Thomas, G., Neiveyans, M., Busson, M., . . . Robert, B. (2014). Preclinical validation of AXL receptor as a target for antibody-based pancreatic cancer immunotherapy. *Oncogene, 33*(47), 5405-5414. doi:10.1038/onc.2013.487

Lee, H. J., Jeng, Y. M., Chen, Y. L., Chung, L., & Yuan, R. H. (2014). Gas6/Axl pathway promotes tumor invasion through the transcriptional activation of Slug in hepatocellular carcinoma. *Carcinogenesis, 35*(4), 769-775. doi:10.1093/carcin/bgt372

Lee, K. M., Yasuda, H., Hollingsworth, M. A., & Ouellette, M. M. (2005). Notch 2-positive progenitors with the intrinsic ability to give rise to pancreatic ductal cells. *Lab Invest, 85*(8), 1003-1012. doi:10.1038/labinvest.3700298

Li, Y., Cai, B., Shen, L., Dong, Y., Lu, Q., Sun, S., . . . Chen, J. (2017). MiRNA-29b suppresses tumor growth through simultaneously inhibiting angiogenesis and

tumorigenesis by targeting Akt3. *Cancer Lett, 397*, 111-119. doi:10.1016/j.canlet.2017.03.032

Li, Y., Wang, Y., Li, L., Kong, R., Pan, S., Ji, L., . . . Sun, B. (2016). Hyperoside induces apoptosis and inhibits growth in pancreatic cancer via Bcl-2 family and NF-kappaB signaling pathway both in vitro and in vivo. *Tumour Biol, 37*(6), 7345-7355. doi:10.1007/s13277-015-4552-2

Liao, Y., Smyth, G. K., & Shi, W. (2014). featureCounts: an efficient general purpose program for assigning sequence reads to genomic features. *Bioinformatics, 30*(7), 923-930. doi:10.1093/bioinformatics/btt656

Lim, K. H., O'Hayer, K., Adam, S. J., Kendall, S. D., Campbell, P. M., Der, C. J., & Counter, C. M. (2006). Divergent roles for RalA and RalB in malignant growth of human pancreatic carcinoma cells. *Curr Biol, 16*(24), 2385-2394. doi:10.1016/j.cub.2006.10.023

Lin, F. M., Yost, S. E., Wen, W., Frankel, P. H., Schmolze, D., Chu, P. G., . . . Yuan, Y. (2019). Differential gene expression and AKT targeting in triple negative breast cancer. *Oncotarget, 10*(43), 4356-4368. doi:10.18632/oncotarget.27026

Lin, J. Z., Wang, Z. J., De, W., Zheng, M., Xu, W. Z., Wu, H. F., . . . Zhu, J. G. (2017). Targeting AXL overcomes resistance to docetaxel therapy in advanced prostate cancer. *Oncotarget, 8*(25), 41064-41077. doi:10.18632/oncotarget.17026

Lin, Y., Dong, C., & Zhou, B. P. (2014). Epigenetic regulation of EMT: the Snail story. *Curr Pharm Des, 20*(11), 1698-1705. Retrieved from https://www.ncbi.nlm.nih.gov/pubmed/23888971

Lindsley, C. W., Zhao, Z., Leister, W. H., Robinson, R. G., Barnett, S. F., Defeo-Jones, D., . . . Duggan, M. E. (2005). Allosteric Akt (PKB) inhibitors: discovery and SAR of isozyme selective inhibitors. *Bioorg Med Chem Lett, 15*(3), 761-764. doi:10.1016/j.bmcl.2004.11.011

Liu, Y., Zhang, N., Wang, Y., Xu, M., Liu, N., Pang, X., . . . Zhang, H. (2012). Zinc finger E-box binding homeobox 1 promotes invasion and bone metastasis of small cell lung cancer in vitro and in vivo. *Cancer Sci, 103*(8), 1420-1428. doi:10.1111/j.1349-7006.2012.02347.x

Ludwig, K. F., Du, W., Sorrelle, N. B., Wnuk-Lipinska, K., Topalovski, M., Toombs, J. E., . . . Brekken, R. A. (2018). Small-Molecule Inhibition of Axl Targets Tumor Immune Suppression and Enhances Chemotherapy in Pancreatic Cancer. *Cancer Res, 78*(1), 246-255. doi:10.1158/0008-5472.CAN-17-1973

Ma, B. B., Goh, B. C., Lim, W. T., Hui, E. P., Tan, E. H., Lopes Gde, L., . . . Chan, A. T. (2015). Multicenter phase II study of the AKT inhibitor MK-2206 in recurrent or metastatic nasopharyngeal carcinoma from patients in the mayo phase II consortium and the cancer therapeutics research group (MC1079). *Invest New Drugs, 33*(4), 985-991. doi:10.1007/s10637-015-0264-0

Makohon-Moore, A. P., Zhang, M., Reiter, J. G., Bozic, I., Allen, B., Kundu, D., . . . Iacobuzio-Donahue, C. A. (2017). Limited heterogeneity of known driver gene mutations among the metastases of individual patients with pancreatic cancer. *Nat Genet, 49*(3), 358-366. doi:10.1038/ng.3764

Malanchi, I., Santamaria-Martinez, A., Susanto, E., Peng, H., Lehr, H. A., Delaloye, J. F., & Huelsken, J. (2011). Interactions between cancer stem cells and their niche govern metastatic colonization. *Nature, 481*(7379), 85-89. doi:10.1038/nature10694

Mani, S. A., Guo, W., Liao, M. J., Eaton, E. N., Ayyanan, A., Zhou, A. Y., . . . Weinberg, R. A. (2008). The epithelial-mesenchymal transition generates cells with properties of stem cells. *Cell, 133*(4), 704-715. doi:10.1016/j.cell.2008.03.027

Marchlik, E., Thakker, P., Carlson, T., Jiang, Z., Ryan, M., Marusic, S., . . . Hall, J. P. (2010). Mice lacking Tbk1 activity exhibit immune cell infiltrates in multiple tissues and increased susceptibility to LPS-induced lethality. *J Leukoc Biol, 88*(6), 1171-1180. doi:10.1189/jlb.0210071

McCarthy, D. J., Chen, Y., & Smyth, G. K. (2012). Differential expression analysis of multifactor RNA-Seq experiments with respect to biological variation. *Nucleic Acids Res, 40*(10), 4288-4297. doi:10.1093/nar/gks042

Meric-Bernstam, F., Frampton, G. M., Ferrer-Lozano, J., Yelensky, R., Perez-Fidalgo, J. A., Wang, Y., . . . Gonzalez-Angulo, A. M. (2014). Concordance of genomic alterations between primary and recurrent breast cancer. *Mol Cancer Ther, 13*(5), 1382-1389. doi:10.1158/1535-7163.MCT-13-0482

Mueller, S., Engleitner, T., Maresch, R., Zukowska, M., Lange, S., Kaltenbacher, T., . . . Rad, R. (2018). Evolutionary routes and KRAS dosage define pancreatic cancer phenotypes. *Nature, 554*(7690), 62-68. doi:10.1038/nature25459

Mure, H., Matsuzaki, K., Kitazato, K. T., Mizobuchi, Y., Kuwayama, K., Kageji, T., & Nagahiro, S. (2010). Akt2 and Akt3 play a pivotal role in malignant gliomas. *Neuro Oncol, 12*(3), 221-232. doi:10.1093/neuonc/nop026

Myers, S. H., Brunton, V. G., & Unciti-Broceta, A. (2016). AXL Inhibitors in Cancer: A Medicinal Chemistry Perspective. *J Med Chem, 59*(8), 3593-3608. doi:10.1021/acs.jmedchem.5b01273

Nakatani, K., Sakaue, H., Thompson, D. A., Weigel, R. J., & Roth, R. A. (1999). Identification of a human Akt3 (protein kinase B gamma) which contains the regulatory serine phosphorylation site. *Biochem Biophys Res Commun, 257*(3), 906-910. doi:10.1006/bbrc.1999.0559

Nakatani, K., Thompson, D. A., Barthel, A., Sakaue, H., Liu, W., Weigel, R. J., & Roth, R. A. (1999). Up-regulation of Akt3 in estrogen receptor-deficient breast cancers and androgen-independent prostate cancer lines. *J Biol Chem, 274*(31), 21528-21532. doi:10.1074/jbc.274.31.21528

Neel, N. F., Martin, T. D., Stratford, J. K., Zand, T. P., Reiner, D. J., & Der, C. J. (2011). The RalGEF-Ral Effector Signaling Network: The Road Less Traveled for Anti-Ras Drug Discovery. *Genes Cancer, 2*(3), 275-287. doi:10.1177/1947601911407329

Nieto, M. A., Huang, R. Y., Jackson, R. A., & Thiery, J. P. (2016). Emt: 2016. *Cell, 166*(1), 21-45. doi:10.1016/j.cell.2016.06.028

Notta, F., Chan-Seng-Yue, M., Lemire, M., Li, Y., Wilson, G. W., Connor, A. A., . . . Gallinger, S. (2016). A renewed model of pancreatic cancer evolution based on

genomic rearrangement patterns. *Nature, 538*(7625), 378-382. doi:10.1038/nature19823

Ocana, O. H., Corcoles, R., Fabra, A., Moreno-Bueno, G., Acloque, H., Vega, S., . . . Nieto, M. A. (2012). Metastatic colonization requires the repression of the epithelial-mesenchymal transition inducer Prrx1. *Cancer Cell, 22*(6), 709-724. doi:10.1016/j.ccr.2012.10.012

Oliveras-Ferraros, C., Corominas-Faja, B., Cufi, S., Vazquez-Martin, A., Martin-Castillo, B., Iglesias, J. M., . . . Menendez, J. A. (2012). Epithelial-to-mesenchymal transition (EMT) confers primary resistance to trastuzumab (Herceptin). *Cell Cycle, 11*(21), 4020-4032. doi:10.4161/cc.22225

Ostapoff, K. T., Cenik, B. K., Wang, M., Ye, R., Xu, X., Nugent, D., . . . Brekken, R. A. (2014). Neutralizing murine TGFbetaR2 promotes a differentiated tumor cell phenotype and inhibits pancreatic cancer metastasis. *Cancer Res, 74*(18), 4996-5007. doi:10.1158/0008-5472.CAN-13-1807

Ou, Y. H., Torres, M., Ram, R., Formstecher, E., Roland, C., Cheng, T., . . . White, M. A. (2011). TBK1 directly engages Akt/PKB survival signaling to support oncogenic transformation. *Mol Cell, 41*(4), 458-470. doi:10.1016/j.molcel.2011.01.019

Ouchida, A. T., Kacal, M., Zheng, A., Ambroise, G., Zhang, B., Norberg, E., & Vakifahmetoglu-Norberg, H. (2018). USP10 regulates the stability of the EMT-transcription factor Slug/SNAI2. *Biochem Biophys Res Commun, 502*(4), 429-434. doi:10.1016/j.bbrc.2018.05.156

Palisoul, M. L., Quinn, J. M., Schepers, E., Hagemann, I. S., Guo, L., Reger, K., . . . Fuh, K. C. (2017). Inhibition of the Receptor Tyrosine Kinase AXL Restores Paclitaxel Chemosensitivity in Uterine Serous Cancer. *Mol Cancer Ther, 16*(12), 2881-2891. doi:10.1158/1535-7163.MCT-17-0587

Park, I. K., Mundy-Bosse, B., Whitman, S. P., Zhang, X., Warner, S. L., Bearss, D. J., . . . Caligiuri, M. A. (2015). Receptor tyrosine kinase Axl is required for resistance of leukemic cells to FLT3-targeted therapy in acute myeloid leukemia. *Leukemia, 29*(12), 2382-2389. doi:10.1038/leu.2015.147

Parker, J. S., Mullins, M., Cheang, M. C., Leung, S., Voduc, D., Vickery, T., . . . Bernard, P. S. (2009). Supervised risk predictor of breast cancer based on intrinsic subtypes. *J Clin Oncol, 27*(8), 1160-1167. doi:10.1200/JCO.2008.18.1370

Pavelka, N., Rancati, G., Zhu, J., Bradford, W. D., Saraf, A., Florens, L., . . . Li, R. (2010). Aneuploidy confers quantitative proteome changes and phenotypic variation in budding yeast. *Nature, 468*(7321), 321-325. doi:10.1038/nature09529

Pearson, G. W., & Hunter, T. (2007). Real-time imaging reveals that noninvasive mammary epithelial acini can contain motile cells. *J Cell Biol, 179*(7), 1555-1567. doi:10.1083/jcb.200706099

Perrais, M., Chen, X., Perez-Moreno, M., & Gumbiner, B. M. (2007). E-cadherin homophilic ligation inhibits cell growth and epidermal growth factor receptor signaling independently of other cell interactions. *Mol Biol Cell, 18*(6), 2013-2025. doi:10.1091/mbc.e06-04-0348

Perry, A. K., Chow, E. K., Goodnough, J. B., Yeh, W. C., & Cheng, G. (2004). Differential requirement for TANK-binding kinase-1 in type I interferon

responses to toll-like receptor activation and viral infection. *J Exp Med, 199*(12), 1651-1658. doi:10.1084/jem.20040528

Pillai, S., Nguyen, J., Johnson, J., Haura, E., Coppola, D., & Chellappan, S. (2015). Tank binding kinase 1 is a centrosome-associated kinase necessary for microtubule dynamics and mitosis. *Nat Commun, 6*, 10072. doi:10.1038/ncomms10072

Potapova, T. A., Zhu, J., & Li, R. (2013). Aneuploidy and chromosomal instability: a vicious cycle driving cellular evolution and cancer genome chaos. *Cancer Metastasis Rev, 32*(3-4), 377-389. doi:10.1007/s10555-013-9436-6

Prior, I. A., Lewis, P. D., & Mattos, C. (2012). A comprehensive survey of Ras mutations in cancer. *Cancer Res, 72*(10), 2457-2467. doi:10.1158/0008-5472.CAN-11-2612

Puls, T. J., Tan, X., Whittington, C. F., & Voytik-Harbin, S. L. (2017). 3D collagen fibrillar microstructure guides pancreatic cancer cell phenotype and serves as a critical design parameter for phenotypic models of EMT. *PLoS One, 12*(11), e0188870. doi:10.1371/journal.pone.0188870

Qian, X., Karpova, T., Sheppard, A. M., McNally, J., & Lowy, D. R. (2004). E-cadherin-mediated adhesion inhibits ligand-dependent activation of diverse receptor tyrosine kinases. *EMBO J, 23*(8), 1739-1748. doi:10.1038/sj.emboj.7600136

Radtke, A. L., Delbridge, L. M., Balachandran, S., Barber, G. N., & O'Riordan, M. X. (2007). TBK1 protects vacuolar integrity during intracellular bacterial infection. *PLoS Pathog, 3*(3), e29. doi:10.1371/journal.ppat.0030029

Rangarajan, A., Hong, S. J., Gifford, A., & Weinberg, R. A. (2004). Species- and cell type-specific requirements for cellular transformation. *Cancer Cell, 6*(2), 171-183. doi:10.1016/j.ccr.2004.07.009

Reichert, M., & Rustgi, A. K. (2011). Pancreatic ductal cells in development, regeneration, and neoplasia. *J Clin Invest, 121*(12), 4572-4578. doi:10.1172/JCI57131

Rhim, A. D., Mirek, E. T., Aiello, N. M., Maitra, A., Bailey, J. M., McAllister, F., . . . Stanger, B. Z. (2012). EMT and dissemination precede pancreatic tumor formation. *Cell, 148*(1-2), 349-361. doi:10.1016/j.cell.2011.11.025

Roberts, A. B., Lamb, L. C., Newton, D. L., Sporn, M. B., De Larco, J. E., & Todaro, G. J. (1980). Transforming growth factors: isolation of polypeptides from virally and chemically transformed cells by acid/ethanol extraction. *Proc Natl Acad Sci U S A, 77*(6), 3494-3498. doi:10.1073/pnas.77.6.3494

Robinson, M. D., McCarthy, D. J., & Smyth, G. K. (2010). edgeR: a Bioconductor package for differential expression analysis of digital gene expression data. *Bioinformatics, 26*(1), 139-140. doi:10.1093/bioinformatics/btp616

Ryseck, R. P., Weih, F., Carrasco, D., & Bravo, R. (1996). RelB, a member of the Rel/NF-kappa B family of transcription factors. *Braz J Med Biol Res, 29*(7), 895-903. Retrieved from https://www.ncbi.nlm.nih.gov/pubmed/9070378

Sadahiro, H., Kang, K. D., Gibson, J. T., Minata, M., Yu, H., Shi, J., . . . Nakano, I. (2018). Activation of the Receptor Tyrosine Kinase AXL Regulates the Immune Microenvironment in Glioblastoma. *Cancer Res, 78*(11), 3002-3013. doi:10.1158/0008-5472.CAN-17-2433

Sale, M. J., Balmanno, K., Saxena, J., Ozono, E., Wojdyla, K., McIntyre, R. E., . . . Cook, S. J. (2019). MEK1/2 inhibitor withdrawal reverses acquired resistance driven by BRAF(V600E) amplification whereas KRAS(G13D) amplification promotes EMT-chemoresistance. *Nat Commun, 10*(1), 2030. doi:10.1038/s41467-019-09438-w

Sanidas, I., Polytarchou, C., Hatziapostolou, M., Ezell, S. A., Kottakis, F., Hu, L., . . . Tsichlis, P. N. (2014). Phosphoproteomics screen reveals akt isoform-specific signals linking RNA processing to lung cancer. *Mol Cell, 53*(4), 577-590. doi:10.1016/j.molcel.2013.12.018

Santi, S. A., & Lee, H. (2010). The Akt isoforms are present at distinct subcellular locations. *Am J Physiol Cell Physiol, 298*(3), C580-591. doi:10.1152/ajpcell.00375.2009

Santi, S. A., & Lee, H. (2011). Ablation of Akt2 induces autophagy through cell cycle arrest, the downregulation of p70S6K, and the deregulation of mitochondria in MDA-MB231 cells. *PLoS One, 6*(1), e14614. doi:10.1371/journal.pone.0014614

Savagner, P. (2001). Leaving the neighborhood: molecular mechanisms involved during epithelial-mesenchymal transition. *Bioessays, 23*(10), 912-923. doi:10.1002/bies.1132

Sekiya, S., & Suzuki, A. (2012). Intrahepatic cholangiocarcinoma can arise from Notch-mediated conversion of hepatocytes. *J Clin Invest, 122*(11), 3914-3918. doi:10.1172/JCI63065

Sequist, L. V., Waltman, B. A., Dias-Santagata, D., Digumarthy, S., Turke, A. B., Fidias, P., . . . Engelman, J. A. (2011). Genotypic and histological evolution of lung cancers acquiring resistance to EGFR inhibitors. *Sci Transl Med, 3*(75), 75ra26. doi:10.1126/scitranslmed.3002003

Seyfried, T. N., & Huysentruyt, L. C. (2013). On the origin of cancer metastasis. *Crit Rev Oncog, 18*(1-2), 43-73. Retrieved from https://www.ncbi.nlm.nih.gov/pubmed/23237552

Shao, D. D., Xue, W., Krall, E. B., Bhutkar, A., Piccioni, F., Wang, X., . . . Hahn, W. C. (2014). KRAS and YAP1 converge to regulate EMT and tumor survival. *Cell, 158*(1), 171-184. doi:10.1016/j.cell.2014.06.004

Sharma, S., tenOever, B. R., Grandvaux, N., Zhou, G. P., Lin, R., & Hiscott, J. (2003). Triggering the interferon antiviral response through an IKK-related pathway. *Science, 300*(5622), 1148-1151. doi:10.1126/science.1081315

Shen, R. R., & Hahn, W. C. (2011). Emerging roles for the non-canonical IKKs in cancer. *Oncogene, 30*(6), 631-641. doi:10.1038/onc.2010.493

Shintani, Y., Fukumoto, Y., Chaika, N., Svoboda, R., Wheelock, M. J., & Johnson, K. R. (2008). Collagen I-mediated up-regulation of N-cadherin requires cooperative signals from integrins and discoidin domain receptor 1. *J Cell Biol, 180*(6), 1277-1289. doi:10.1083/jcb.200708137

Singh, A., Greninger, P., Rhodes, D., Koopman, L., Violette, S., Bardeesy, N., & Settleman, J. (2009). A gene expression signature associated with "K-Ras addiction" reveals regulators of EMT and tumor cell survival. *Cancer Cell, 15*(6), 489-500. doi:10.1016/j.ccr.2009.03.022

Singh, A., & Settleman, J. (2010). EMT, cancer stem cells and drug resistance: an emerging axis of evil in the war on cancer. *Oncogene, 29*(34), 4741-4751. doi:10.1038/onc.2010.215

Sinha, S., Boysen, J. C., Chaffee, K. G., Kabat, B. F., Slager, S. L., Parikh, S. A., . . . Kay, N. E. (2018). Chronic lymphocytic leukemia cells from ibrutinib treated patients are sensitive to Axl receptor tyrosine kinase inhibitor therapy. *Oncotarget, 9*(98), 37173-37184. doi:10.18632/oncotarget.26444

Song, X., Wang, H., Logsdon, C. D., Rashid, A., Fleming, J. B., Abbruzzese, J. L., . . . Wang, H. (2011). Overexpression of receptor tyrosine kinase Axl promotes tumor cell invasion and survival in pancreatic ductal adenocarcinoma. *Cancer, 117*(4), 734-743. doi:10.1002/cncr.25483

Sorrelle, N., Ganguly, D., Dominguez, A. T. A., Zhang, Y., Huang, H., Dahal, L. N., . . . Brekken, R. A. (2019). Improved Multiplex Immunohistochemistry for Immune Microenvironment Evaluation of Mouse Formalin-Fixed, Paraffin-Embedded Tissues. *J Immunol, 202*(1), 292-299. doi:10.4049/jimmunol.1800878

Stahl, J. M., Sharma, A., Cheung, M., Zimmerman, M., Cheng, J. Q., Bosenberg, M. W., . . . Robertson, G. P. (2004). Deregulated Akt3 activity promotes development of malignant melanoma. *Cancer Res, 64*(19), 7002-7010. doi:10.1158/0008-5472.CAN-04-1399

Stottrup, C., Tsang, T., & Chin, Y. R. (2016). Upregulation of AKT3 Confers Resistance to the AKT Inhibitor MK2206 in Breast Cancer. *Mol Cancer Ther, 15*(8), 1964-1974. doi:10.1158/1535-7163.MCT-15-0748

Strobel, O., Dor, Y., Alsina, J., Stirman, A., Lauwers, G., Trainor, A., . . . Thayer, S. P. (2007). In vivo lineage tracing defines the role of acinar-to-ductal transdifferentiation in inflammatory ductal metaplasia. *Gastroenterology, 133*(6), 1999-2009. doi:10.1053/j.gastro.2007.09.009

Suyama, K., Yao, J., Liang, H., Benard, O., Loudig, O. D., Amgalan, D., . . . Hazan, R. B. (2018). An Akt3 Splice Variant Lacking the Serine 472 Phosphorylation Site Promotes Apoptosis and Suppresses Mammary Tumorigenesis. *Cancer Res, 78*(1), 103-114. doi:10.1158/0008-5472.CAN-15-1462

Swift, S., Lorens, J., Achacoso, P., & Nolan, G. P. (2001). Rapid production of retroviruses for efficient gene delivery to mammalian cells using 293T cell-based systems. *Curr Protoc Immunol, Chapter 10*, Unit 10 17C. doi:10.1002/0471142735.im1017cs31

Takahashi, A., Loo, T. M., Okada, R., Kamachi, F., Watanabe, Y., Wakita, M., . . . Hara, E. (2018). Downregulation of cytoplasmic DNases is implicated in cytoplasmic DNA accumulation and SASP in senescent cells. *Nat Commun, 9*(1), 1249. doi:10.1038/s41467-018-03555-8

Takeyama, Y., Sato, M., Horio, M., Hase, T., Yoshida, K., Yokoyama, T., . . . Hasegawa, Y. (2010). Knockdown of ZEB1, a master epithelial-to-mesenchymal transition (EMT) gene, suppresses anchorage-independent cell growth of lung cancer cells. *Cancer Lett, 296*(2), 216-224. doi:10.1016/j.canlet.2010.04.008

Tam, W. L., & Weinberg, R. A. (2013). The epigenetics of epithelial-mesenchymal plasticity in cancer. *Nat Med, 19*(11), 1438-1449. doi:10.1038/nm.3336

Tang, Z., Li, C., Kang, B., Gao, G., Li, C., & Zhang, Z. (2017). GEPIA: a web server for cancer and normal gene expression profiling and interactive analyses. *Nucleic Acids Res, 45*(W1), W98-W102. doi:10.1093/nar/gkx247

Taparra, K., Wang, H., Malek, R., Lafargue, A., Barbhuiya, M. A., Wang, X., . . . Tran, P. T. (2018). O-GlcNAcylation is required for mutant KRAS-induced lung tumorigenesis. *J Clin Invest, 128*(11), 4924-4937. doi:10.1172/JCI94844

Tarin, D., Thompson, E. W., & Newgreen, D. F. (2005). The fallacy of epithelial mesenchymal transition in neoplasia. *Cancer Res, 65*(14), 5996-6000; discussion 6000-5991. doi:10.1158/0008-5472.CAN-05-0699

Terry, S., Savagner, P., Ortiz-Cuaran, S., Mahjoubi, L., Saintigny, P., Thiery, J. P., & Chouaib, S. (2017). New insights into the role of EMT in tumor immune escape. *Mol Oncol, 11*(7), 824-846. doi:10.1002/1878-0261.12093

Thiery, J. P. (2002). Epithelial-mesenchymal transitions in tumour progression. *Nat Rev Cancer, 2*(6), 442-454. doi:10.1038/nrc822

Thiery, J. P., Acloque, H., Huang, R. Y., & Nieto, M. A. (2009). Epithelial-mesenchymal transitions in development and disease. *Cell, 139*(5), 871-890. doi:10.1016/j.cell.2009.11.007

Tiwari, N., Tiwari, V. K., Waldmeier, L., Balwierz, P. J., Arnold, P., Pachkov, M., . . . Christofori, G. (2013). Sox4 is a master regulator of epithelial-mesenchymal transition by controlling Ezh2 expression and epigenetic reprogramming. *Cancer Cell, 23*(6), 768-783. doi:10.1016/j.ccr.2013.04.020

Toulany, M., Maier, J., Iida, M., Rebholz, S., Holler, M., Grottke, A., . . . Rodemann, H. P. (2017). Akt1 and Akt3 but not Akt2 through interaction with DNA-PKcs stimulate proliferation and post-irradiation cell survival of K-RAS-mutated cancer cells. *Cell Death Discov, 3*, 17072. doi:10.1038/cddiscovery.2017.72

Tran, D. D., Corsa, C. A., Biswas, H., Aft, R. L., & Longmore, G. D. (2011). Temporal and spatial cooperation of Snail1 and Twist1 during epithelial-mesenchymal transition predicts for human breast cancer recurrence. *Mol Cancer Res, 9*(12), 1644-1657. doi:10.1158/1541-7786.MCR-11-0371

Tran, H. D., Luitel, K., Kim, M., Zhang, K., Longmore, G. D., & Tran, D. D. (2014). Transient SNAIL1 expression is necessary for metastatic competence in breast cancer. *Cancer Res, 74*(21), 6330-6340. doi:10.1158/0008-5472.CAN-14-0923

Tse, J. C., & Kalluri, R. (2007). Mechanisms of metastasis: epithelial-to-mesenchymal transition and contribution of tumor microenvironment. *J Cell Biochem, 101*(4), 816-829. doi:10.1002/jcb.21215

Turner, K. M., Sun, Y., Ji, P., Granberg, K. J., Bernard, B., Hu, L., . . . Zhang, W. (2015). Genomically amplified Akt3 activates DNA repair pathway and promotes glioma progression. *Proc Natl Acad Sci U S A, 112*(11), 3421-3426. doi:10.1073/pnas.1414573112

Vaziri-Gohar, A., Zarei, M., Brody, J. R., & Winter, J. M. (2018). Metabolic Dependencies in Pancreatic Cancer. *Front Oncol, 8*, 617. doi:10.3389/fonc.2018.00617

Vigil, D., Cherfils, J., Rossman, K. L., & Der, C. J. (2010). Ras superfamily GEFs and GAPs: validated and tractable targets for cancer therapy? *Nat Rev Cancer, 10*(12), 842-857. doi:10.1038/nrc2960

Voon, D. C., Huang, R. Y., Jackson, R. A., & Thiery, J. P. (2017). The EMT spectrum and therapeutic opportunities. *Mol Oncol, 11*(7), 878-891. doi:10.1002/1878-0261.12082

Vouri, M., An, Q., Birt, M., Pilkington, G. J., & Hafizi, S. (2015). Small molecule inhibition of Axl receptor tyrosine kinase potently suppresses multiple malignant properties of glioma cells. *Oncotarget, 6*(18), 16183-16197. doi:10.18632/oncotarget.3952

Vu, H. L., & Aplin, A. E. (2014). Targeting TBK1 inhibits migration and resistance to MEK inhibitors in mutant NRAS melanoma. *Mol Cancer Res, 12*(10), 1509-1519. doi:10.1158/1541-7786.MCR-14-0204

Vuoriluoto, K., Haugen, H., Kiviluoto, S., Mpindi, J. P., Nevo, J., Gjerdrum, C., . . . Ivaska, J. (2011). Vimentin regulates EMT induction by Slug and oncogenic H-Ras and migration by governing Axl expression in breast cancer. *Oncogene, 30*(12), 1436-1448. doi:10.1038/onc.2010.509

Waddell, N., Pajic, M., Patch, A. M., Chang, D. K., Kassahn, K. S., Bailey, P., . . . Grimmond, S. M. (2015). Whole genomes redefine the mutational landscape of pancreatic cancer. *Nature, 518*(7540), 495-501. doi:10.1038/nature14169

Wang, F., Liu, H., Hu, L., Liu, Y., Duan, Y., Cui, R., & Tian, W. (2018). The Warburg effect in human pancreatic cancer cells triggers cachexia in athymic mice carrying the cancer cells. *BMC Cancer, 18*(1), 360. doi:10.1186/s12885-018-4271-3

Wang, M., Topalovski, M., Toombs, J. E., Wright, C. M., Moore, Z. R., Boothman, D. A., . . . Brekken, R. A. (2015). Fibulin-5 Blocks Microenvironmental ROS in Pancreatic Cancer. *Cancer Res, 75*(23), 5058-5069. doi:10.1158/0008-5472.CAN-15-0744

Wang, S., Huang, S., & Sun, Y. L. (2017). Epithelial-Mesenchymal Transition in Pancreatic Cancer: A Review. *Biomed Res Int, 2017*, 2646148. doi:10.1155/2017/2646148

Wang, S. P., Wang, W. L., Chang, Y. L., Wu, C. T., Chao, Y. C., Kao, S. H., . . . Yang, P. C. (2009). p53 controls cancer cell invasion by inducing the MDM2-mediated degradation of Slug. *Nat Cell Biol, 11*(6), 694-704. doi:10.1038/ncb1875

Wang, Z., Li, Y., Ahmad, A., Banerjee, S., Azmi, A. S., Kong, D., & Sarkar, F. H. (2011). Pancreatic cancer: understanding and overcoming chemoresistance. *Nat Rev Gastroenterol Hepatol, 8*(1), 27-33. doi:10.1038/nrgastro.2010.188

Waters, A. M., & Der, C. J. (2018). KRAS: The Critical Driver and Therapeutic Target for Pancreatic Cancer. *Cold Spring Harb Perspect Med, 8*(9). doi:10.1101/cshperspect.a031435

Weinger, J. G., Gohari, P., Yan, Y., Backer, J. M., Varnum, B., & Shafit-Zagardo, B. (2008). In brain, Axl recruits Grb2 and the p85 regulatory subunit of PI3 kinase; in vitro mutagenesis defines the requisite binding sites for downstream Akt activation. *J Neurochem, 106*(1), 134-146. doi:10.1111/j.1471-4159.2008.05343.x

Wente, S. R., & Rout, M. P. (2010). The nuclear pore complex and nuclear transport. *Cold Spring Harb Perspect Biol, 2*(10), a000562. doi:10.1101/cshperspect.a000562

Westcott, J. M., Prechtl, A. M., Maine, E. A., Dang, T. T., Esparza, M. A., Sun, H., . . . Pearson, G. W. (2015). An epigenetically distinct breast cancer cell subpopulation promotes collective invasion. *J Clin Invest, 125*(5), 1927-1943. doi:10.1172/JCI77767

Wild, P., Farhan, H., McEwan, D. G., Wagner, S., Rogov, V. V., Brady, N. R., . . . Dikic, I. (2011). Phosphorylation of the autophagy receptor optineurin restricts Salmonella growth. *Science, 333*(6039), 228-233. doi:10.1126/science.1205405

Witkiewicz, A. K., McMillan, E. A., Balaji, U., Baek, G., Lin, W. C., Mansour, J., . . . Knudsen, E. S. (2015). Whole-exome sequencing of pancreatic cancer defines genetic diversity and therapeutic targets. *Nat Commun, 6*, 6744. doi:10.1038/ncomms7744

Wong, T. S., Gao, W., & Chan, J. Y. (2014). Transcription regulation of E-cadherin by zinc finger E-box binding homeobox proteins in solid tumors. *Biomed Res Int, 2014*, 921564. doi:10.1155/2014/921564

Woodgett, J. R. (2005). Recent advances in the protein kinase B signaling pathway. *Curr Opin Cell Biol, 17*(2), 150-157. doi:10.1016/j.ceb.2005.02.010

Wu, F., Li, J., Jang, C., Wang, J., & Xiong, J. (2014). The role of Axl in drug resistance and epithelial-to-mesenchymal transition of non-small cell lung carcinoma. *Int J Clin Exp Pathol, 7*(10), 6653-6661. Retrieved from https://www.ncbi.nlm.nih.gov/pubmed/25400744

Wu, W. I., Voegtli, W. C., Sturgis, H. L., Dizon, F. P., Vigers, G. P., & Brandhuber, B. J. (2010). Crystal structure of human AKT1 with an allosteric inhibitor reveals a new mode of kinase inhibition. *PLoS One, 5*(9), e12913. doi:10.1371/journal.pone.0012913

Xiao, G., Li, Y., Wang, M., Li, X., Qin, S., Sun, X., . . . Liu, D. (2018). FBXW7 suppresses epithelial-mesenchymal transition and chemo-resistance of non-small-cell lung cancer cells by targeting snai1 for ubiquitin-dependent degradation. *Cell Prolif, 51*(5), e12473. doi:10.1111/cpr.12473

Xiao, J., Li, W., Zheng, X., Qi, L., Wang, H., Zhang, C., . . . Wang, H. (2020). Targeting 7-Dehydrocholesterol Reductase Integrates Cholesterol Metabolism and IRF3 Activation to Eliminate Infection. *Immunity, 52*(1), 109-122 e106. doi:10.1016/j.immuni.2019.11.015

Xiao, Y., Zou, Q., Xie, X., Liu, T., Li, H. S., Jie, Z., . . . Sun, S. C. (2017). The kinase TBK1 functions in dendritic cells to regulate T cell homeostasis, autoimmunity, and antitumor immunity. *J Exp Med, 214*(5), 1493-1507. doi:10.1084/jem.20161524

Xu, W., Yang, Z., & Lu, N. (2015). A new role for the PI3K/Akt signaling pathway in the epithelial-mesenchymal transition. *Cell Adh Migr, 9*(4), 317-324. doi:10.1080/19336918.2015.1016686

Yamaguchi, J., Yokoyama, Y., Kokuryo, T., Ebata, T., & Nagino, M. (2018). Cells of origin of pancreatic neoplasms. *Surg Today, 48*(1), 9-17. doi:10.1007/s00595-017-1501-2

Yang, H., Lu, X., Liu, Z., Chen, L., Xu, Y., Wang, Y., . . . Chen, Y. (2015). FBXW7 suppresses epithelial-mesenchymal transition, stemness and metastatic potential of cholangiocarcinoma cells. *Oncotarget, 6*(8), 6310-6325. doi:10.18632/oncotarget.3355

Yang, K. M., Jung, Y., Lee, J. M., Kim, W., Cho, J. K., Jeong, J., & Kim, S. J. (2013). Loss of TBK1 induces epithelial-mesenchymal transition in the breast cancer cells by ERalpha downregulation. *Cancer Res, 73*(22), 6679-6689. doi:10.1158/0008-5472.CAN-13-0891

Yang, S., Imamura, Y., Jenkins, R. W., Canadas, I., Kitajima, S., Aref, A., . . . Barbie, D. A. (2016). Autophagy Inhibition Dysregulates TBK1 Signaling and Promotes Pancreatic Inflammation. *Cancer Immunol Res, 4*(6), 520-530. doi:10.1158/2326-6066.CIR-15-0235

Yang, Y., Ahn, Y. H., Chen, Y., Tan, X., Guo, L., Gibbons, D. L., . . . Kurie, J. M. (2014). ZEB1 sensitizes lung adenocarcinoma to metastasis suppression by PI3K antagonism. *J Clin Invest, 124*(6), 2696-2708. doi:10.1172/JCI72171

Yap, T. A., Yan, L., Patnaik, A., Tunariu, N., Biondo, A., Fearen, I., . . . Tolcher, A. W. (2014). Interrogating two schedules of the AKT inhibitor MK-2206 in patients with advanced solid tumors incorporating novel pharmacodynamic and functional imaging biomarkers. *Clin Cancer Res, 20*(22), 5672-5685. doi:10.1158/1078-0432.CCR-14-0868

Ye, X., Tam, W. L., Shibue, T., Kaygusuz, Y., Reinhardt, F., Ng Eaton, E., & Weinberg, R. A. (2015). Distinct EMT programs control normal mammary stem cells and tumour-initiating cells. *Nature, 525*(7568), 256-260. doi:10.1038/nature14897

Ye, X., & Weinberg, R. A. (2015). Epithelial-Mesenchymal Plasticity: A Central Regulator of Cancer Progression. *Trends Cell Biol, 25*(11), 675-686. doi:10.1016/j.tcb.2015.07.012

Yi, W., Clark, P. M., Mason, D. E., Keenan, M. C., Hill, C., Goddard, W. A., 3rd, . . . Hsieh-Wilson, L. C. (2012). Phosphofructokinase 1 glycosylation regulates cell growth and metabolism. *Science, 337*(6097), 975-980. doi:10.1126/science.1222278

Yu, Q., Zhou, B. P., & Wu, Y. (2017). The regulation of snail: on the ubiquitin edge. *Cancer Cell Microenviron, 4*(2). Retrieved from https://www.ncbi.nlm.nih.gov/pubmed/29147673

Yuan, M., Cottrell, C. A., Ozorowski, G., van Gils, M. J., Kumar, S., Wu, N. C., . . . Wilson, I. A. (2019). Conformational Plasticity in the HIV-1 Fusion Peptide Facilitates Recognition by Broadly Neutralizing Antibodies. *Cell Host Microbe, 25*(6), 873-883 e875. doi:10.1016/j.chom.2019.04.011

Yuen, A., & Diaz, B. (2014). The impact of hypoxia in pancreatic cancer invasion and metastasis. *Hypoxia (Auckl), 2*, 91-106. doi:10.2147/HP.S52636

Zagorska, A., Traves, P. G., Lew, E. D., Dransfield, I., & Lemke, G. (2014). Diversification of TAM receptor tyrosine kinase function. *Nat Immunol, 15*(10), 920-928. doi:10.1038/ni.2986

Zhang, Z., Lee, J. C., Lin, L., Olivas, V., Au, V., LaFramboise, T., . . . Bivona, T. G. (2012). Activation of the AXL kinase causes resistance to EGFR-targeted therapy in lung cancer. *Nat Genet, 44*(8), 852-860. doi:10.1038/ng.2330

Zhao, X., Gao, S., Ren, H., Sun, W., Zhang, H., Sun, J., . . . Hao, J. (2014). Hypoxia-inducible factor-1 promotes pancreatic ductal adenocarcinoma invasion and metastasis by activating transcription of the actin-bundling protein fascin. *Cancer Res, 74*(9), 2455-2464. doi:10.1158/0008-5472.CAN-13-3009

Zhao, Z., Zhu, X., Cui, K., Mancuso, J., Federley, R., Fischer, K., . . . Wong, S. T. (2016). In Vivo Visualization and Characterization of Epithelial-Mesenchymal Transition in Breast Tumors. *Cancer Res, 76*(8), 2094-2104. doi:10.1158/0008-5472.CAN-15-2662

Zheng, X., Carstens, J. L., Kim, J., Scheible, M., Kaye, J., Sugimoto, H., . . . Kalluri, R. (2015). Epithelial-to-mesenchymal transition is dispensable for metastasis but induces chemoresistance in pancreatic cancer. *Nature, 527*(7579), 525-530. doi:10.1038/nature16064

Zhu, G. H., Huang, C., Feng, Z. Z., Lv, X. H., & Qiu, Z. J. (2013). Hypoxia-induced snail expression through transcriptional regulation by HIF-1alpha in pancreatic cancer cells. *Dig Dis Sci, 58*(12), 3503-3515. doi:10.1007/s10620-013-2841-4

Zhu, Z., Aref, A. R., Cohoon, T. J., Barbie, T. U., Imamura, Y., Yang, S., . . . Barbie, D. A. (2014). Inhibition of KRAS-driven tumorigenicity by interruption of an autocrine cytokine circuit. *Cancer Discov, 4*(4), 452-465. doi:10.1158/2159-8290.CD-13-0646

Zolghadri, Y., Pal Choudhuri, S., Ocal, O., Layeghi-Ghalehsoukhteh, S., Berhe, F., Hale, M. A., & Wilkie, T. M. (2018). Malnutrition in Pancreatic Ductal Adenocarcinoma (PDA): Dietary Pancreatic Enzymes Improve Short-Term Health but Stimulate Tumor Growth. *Am J Pathol, 188*(3), 616-626. doi:10.1016/j.ajpath.2017.11.014